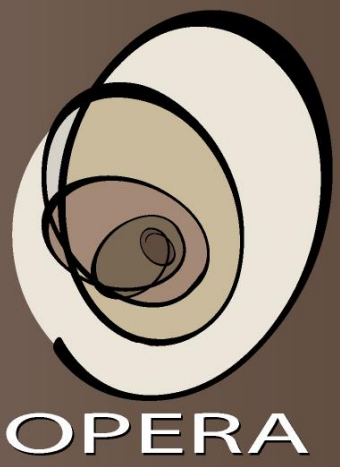

Assessment of the uniform corrosion behaviour of carbon steel radioactive waste packages with respect to the disposal concept in the geological Dutch Boom Clay formation

Bruno Kursten[*], Frank Druyts[*]
[*] The Belgian Nuclear Research Centre, SCK•CEN

OPERA-PU-SCK513

Radioactive substances and ionizing radiation are used in medicine, industry, agriculture, research, education and electricity production. This generates radioactive waste. In the Netherlands, this waste is collected, treated and stored by COVRA (Centrale Organisatie Voor Radioactief Afval). After interim storage for a period of at least 100 years radioactive waste is intended for disposal. There is a world-wide scientific and technical consensus that geological disposal represents the safest long-term option for radioactive waste.

Geological disposal is emplacement of radioactive waste in deep underground formations. The goal of geological disposal is long-term isolation of radioactive waste from our living environment in order to avoid exposure of future generations to ionising radiation from the waste. OPERA (OnderzoeksProgramma Eindberging Radioactief Afval) is the Dutch research programme on geological disposal of radioactive waste.

Within OPERA, researchers of different organisations in different areas of expertise will cooperate on the initial, conditional Safety Cases for the host rocks Boom Clay and Zechstein rock salt. As the radioactive waste disposal process in the Netherlands is at an early, conceptual phase and the previous research programme has ended more than a decade ago, in OPERA a first preliminary or initial safety case will be developed to structure the research necessary for the eventual development of a repository in the Netherlands. The safety case is conditional since only the long-term safety of a generic repository will be assessed. OPERA is financed by the Dutch Ministry of Economic Affairs and the public limited liability company Electriciteits-Produktiemaatschappij Zuid-Nederland (EPZ) and coordinated by COVRA. Further details on OPERA and its outcomes can be accessed at www.covra.nl.

OPERA-PU-SCK513
Title: Assessment of the uniform corrosion behaviour of carbon steel radioactive waste packages with respect to the disposal concept in the geological Dutch Boom Clay formation
Authors: Bruno Kursten, Frank Druyts
Date of publication: May 2015
Keywords: uniform corrosion, corrosion rate, concrete, alkaline, carbon steel

Table of Contents

Summary

The OPERA disposal concept for the final management of Dutch radioactive waste in the 'Rupel' Clay formation is based on the current Belgian Supercontainer concept. In this concept, the radioactive waste is packed in a carbon steel container (i.e. the overpack), which is entirely surrounded by a concrete buffer. In this high alkaline environment (pH ~ 13.6) and under normal conditions (i.e. without the ingress of aggressive species), carbon steel is protected by a passive oxide film, which is believed to result in very low uniform corrosion rates. Considering the long time scales involved in geological disposal, an accurate estimation of the uniform corrosion rate is a crucial part in the safety study. This report provides a best estimate of the uniform corrosion rate of carbon steel exposed to the concrete buffer material. The reported corrosion rate data are based on a state-of-the-art database, which was build on an extensive review of the published literature. This database was composed in the framework of the Belgian disposal programme. Also included is a brief description of the corrosion processes under aerobic and anerobic conditions, the integrated scientific approach that is adopted within the RD&D corrosion studies and the various methods reported in the literature to measure the corrosion rate of carbon steel in alkaline media. The outcome of preliminary geochemical calculations to gain a first level of understanding of the long-term evolution of the environmental conditions surrounding the carbon steel overpack is discussed.

Samenvatting

Het OPERA concept voor de berging van Nederlands radioactief afval in de 'Rupel' kleiformatie is gebaseerd op het huidige Belgische Supercontainer concept. In dit concept wordt het radioactief afval omgeven door een koolstofstalen afvalcontainer (de 'oververpakking'), dewelke op zijn beurt volledig is omsloten door een betonnen buffer. In deze hoog alkaliene omgeving (pH ~ 13.6) en onder normale condities (m.a.w. zonder aanvoer van aggressieve species) wordt koolstofstaal verondersteld beschermd te worden door een passieve oxidefilm waardoor het zéér langzaam zal aangetast worden. Gezien de zéér lange geologische tijdschalen is een zo accuraat mogelijke afschatting van de corrosiesnelheid van de koolstofstalen oververpakking een cruciale parameter in de veiligheidsstudie. In dit rapport wordt de afschatting van de corrosiesnelheid van koolstofstaal, dat is blootgesteld aan hoog alkaliene media, toegelicht. De gerapporteerde corrosiesnelheden zijn gebaseerd op een state-of-the-art database, dewelke is ontstaan uit een grondige review van de beschikbare literatuur. Deze database werd opgesteld in het kader van het Belgische bergingsprogramma. De corrosieprocessen die optreden onder aerobe en anaerobe omstandigheden werden besproken, alsook de geïntegreerde methodologie die gebruikt wordt binnen de RD&D corrosiestudies en de verschillende methodes die in de literatuur gebruikt worden voor het meten van de corrosiesnelheid van koolstofstaal in alkaliene media. Geochemische berekeningen werden uitgevoerd om een eerste inzicht te verwerven in de langetermijn evolutie van de omgevingscondities rond de koolstofstalen overpack.

1. Introduction

1.1.Background

The five-year research programme for the geological disposal of radioactive waste – OPERA - started on 7 July 2011 with an open invitation for research proposals. In these proposals, research was proposed for the tasks described in the OPERA Research Plan. In this report, the execution and results of the research proposed for task 5.1.3 with the following title in the Research Plan: *Metal Corrosion Processes* is described (Verhoef and Schröder, 2011).

The disposal concept envisaged in The Netherlands is based on the current Belgian Supercontainer concept. Radioactive waste is disposed of in a Boom Clay formation (*i.e.* Rupel Clay formations) with a thickness of about 100 metres at a depth of ~500 metres. The Rupel Clay formations mainly differ from the Belgian Boom Clay formation in chloride content. Chloride concentrations up to 0.546 mol/L (~19 400 mg/L) have been measured (Behrends, et al, 2015). This could have serious repercussions on the corrosion behaviour of carbon steel, which is considered as reference material to fabricate the metallic engineered barrier.
Therefore, it is imperative to evaluate the impact of the geochemical conditions, imposed by the Rupel Clay formation, on the corrosion behaviour of the carbon steel overpack. This report only covers the uniform corrosion behaviour of carbon steel exposed to high alkaline conditions. The effect on localised corrosion phenomena (such as pitting corrosion and stress corrosion cracking) should form part of another study.

1.2.Objectives

The main objective of work package 5.1.3 is to provide an estimation of the corrosion rate of the carbon steel overpack related to the Supercontainer (*i.e.* interaction of the carbon steel overpack with OPC concrete buffer) and taking into account the geochemical boundary conditions imposed by the Dutch Boom Clay host rock formation. In the current OPERA safety strategy, it is assumed that the safety function *'engineered containment'* covers the thermal phase of the system design (ONDRAF/NIRAS, 2013), but the chemistry of the Supercontainer may result in longer lifetimes of the overpack.

In order to meet the general requirements of work package 5.1.3, SCK•CEN originally proposed to address the requirements methodically through the following two tasks:

- To predict the corrosion evolutionary path (CEP). On the basis of input on the geochemistry of the Boom Clay, relevant for the OPERA reference design, geochemical simulations are performed to predict the long-term evolution of the major corrosion-related parameters (temperature, water saturation of the concrete buffer, pH, transport of aggressive species);
- To estimate the corrosion rate of the overpack for the different phases established in the CEP, based on an extensive literature study;

1.3.Realization

The literature study and the geochemical simulations presented in this report have been performed by SCK•CEN, Belgium.

The integrated RD&D methodology that is adopted in the corrosion studies, was developed within the framework of the Belgian disposal programme. Our methodology was already

presented at several international fora, reviewed and internationally accepted (Kursten and Druyts, 2008; Kursten, et al, 2011; Kursten, et al, 2013).

The Corrosion Evolutionary Path (CEP) was also developed with respect to the Belgian Supercontainer design. It is believed to be applicable here, for the disposal concept adopted in OPERA (Verhoef, et al, 2014) (for the disposal of radioactive waste), because it is based on a similar concept (*i.e.* Supercontainer concept with a similar OPC based concrete buffer; the Opera concept differs in the repository layout – smaller containers, shorter disposal drifts).

The corrosion data provided in this report originate from studies performed in the framework of the Belgian disposal programme. A more extensive compilation of corrosion rate data is available (Kursten, to be published) but cannot be incorporated in this report as it forms part of a confidentiality clause (and is yet unpublished).

1.4.Explanation contents

Chapter 2 introduces the concept of electrochemical processes leading to and controlling corrosion: the general terminology used in aqueous corrosion, such as anodic oxidation and cathodic reduction, is introduced and the difference between the mechanisms governing aerobic (in the presence of oxygen) and anaerobic (in the absence of oxygen) corrosion in alkaline media is explained. Further, the mechanism of what makes steel passive in concrete is discussed.

Chapter 3 explains the methodology that is adopted within the RD&D corrosion studies to provide confidence that the integrity of the carbon steel overpack will not be jeopordized at least for the duration of the thermal phase. The integrated scientific approach consists of three consecutive steps: (1) Developing the Corrosion Evolutionary Path (CEP); (2) Determining scientifically well-founded estimates of uniform corrosion rates for the different phases established during the CEP; and (3) Proving the validity of the 'exclusion principle'.

The Corrosion Evolutionary Path (CEP) describes the changing environmental conditions the overpack is subjected to in a repository during the entire disposal period. It is therefore closely linked to the evolution of the environmental conditions surrounding the overpack. Details of the numerical models used to predict the long-term evolution of the major corrosion-related parameters (temperature, water saturation of the concrete buffer, pH, transport of aggressive species) are given and their output is discussed in chapter 4.

Chapter 5 describes the various methods reported in the literature to measure or calculate the corrosion rate of carbon steel in alkaline media. These methods are based on either one of the following three principles: (1) gravimetric-based weight loss measurements; (2) electrochemical measurement techniques; or (3) quantification of hydrogen gas evolving from the corrosion of steel. Additionally, some novel methods were reported in the literature that use archaeological artefacts to estimate uniform corrosion rates.

Chapter 6 summarizes the corrosion rate data reported in the literature for carbon steel in high alkaline media. These data originate from studies in the framework of various national nuclear waste management programmes and studies for industrial applications. The corrosion rate data are classified into aerobic and anaerobic media because the aerobic and anaerobic period have been identified as the two major periods in the course of the Corrosion Evolutionary Path (CEP).

Chapter 7 contains a critical review of the uniform corrosion rate data of carbon steel in alkaline media that have been reported in the literature based on eight criteria, which have been developed in the framework of the Belgian disposal programme. The corrosion rate data were divided into two ranges, *viz.* a source and an expert range.

2. Corrosion processes affecting carbon steel

This chapter is not intended to address every possible aspect related to corrosion phenomena of metallic corrosion. The aim is to provide the reader, who is less familiar with the science of corrosion, with a better understanding in the processes involved in the corrosion of iron (being the major constituent of carbon steel) exposed to high pH environments (such as *e.g.* the concrete buffer considered in the Supercontainer, pH ~ 13.5). The overview of the corrosion theory provided in this section is based on standard literature (Bertolini, et al, 2004; Bentur, et al, 1997; Broomfield, 2007; Crossland, 2006; Davis, 2000; Evans, 1981; Hansson, 1984; Hansson, 1987; King, 2007; Preece, 1982; Sedriks, 1996; Shreir, et al, 1994; Stansbury and Buchanan, 2000; Uhlig, 1971).

Because of the electrochemical nature of aqueous corrosion, this section begins with a concise description of the electrochemical processes leading to and controlling corrosion: the general terminology used in aqueous corrosion, such as anodic oxidation and cathodic reduction, is introduced (section 2.1.1.) and the difference between the mechanisms governing aerobic (in the presence of oxygen) and anaerobic (in the absence of oxygen) corrosion is explained (section 2.1.2.). Further, the mechanism of what makes steel passive in concrete is discussed (section 2.2.).

2.1. Corrosion processes affecting carbon steel

2.1.1. Electrochemical considerations

Steel corrosion in any aqueous environment, and therefore also in concrete, is an electrochemical process involving two separate, but coupled, chemical reactions proceeding simultaneously at two different sites on the steel surface and the transfer of electrons resulting in the flow of electrical current: one reaction is capable of producing electrons (the *anodic* reaction) and one is capable of consuming electrons (the *cathodic* reaction); the areas on which these reactions take place in the steel are called anodes and cathodes, respectively.

The actual corrosion process takes place at the anodic site and it involves a process of converting solid metal into metal ions, which dissolve in the surrounding aqueous solution, with the liberation of electrons (*oxidation reaction*). This process results in weight loss or thinning of the solid material. The electrons created in the anodic reaction must be consumed elsewhere on the steel surface to preserve electrical neutrality because large amounts of electrical charge cannot be build up at one place of the steel. Therefore, another reaction must be occurring that consumes the electrons (*reduction reaction*). For the electrons to become available at the cathodic areas to participate in the reduction reactions, they have to be transported from the anode to the cathode (*electron flow*), resulting in an electrical current within the metal. An external current also flows through the solution (through the pores of the concrete surrounding the steel) carried by the movement of charged ions. This external current consists of positively charged ions moving from the anode to the cathode, and also negatively charged ions moving from the cathode to the anode (*ionic flow*).

The flow of electrons from the anodic areas where they are produced by the anodic reaction to the cathodic areas where they are used in the cathodic reaction, and its counter-current ionic flow in the external concrete pore solution constitute the corrosion current. Because there is no net current, it is not possible to measure the current due to corrosion directly but it can be determined indirectly as described later (section 5.).

In summary, for corrosion of steel in concrete to take place, the simultaneous occurrence of the following four processes are required (Bertolini, et al, 2004):

- an oxidation reaction, taking place at the anode, that liberates electrons;
- a reduction reaction, taking place at the cathode, that consumes these electrons;
- an electrical current flowing within the metal as a result of electron flow from the anodic areas, where they become available, towards the cathodic areas, where they are consumed; and
- an electrical current flowing through the pores of the concrete surrounding the steel, carried by the movement of charged ions;

The corrosion rate will thus be determined by the slowest of these four partial processes. In reality, the electrical resistance of the reinforcement is always negligible with respect to that of the concrete. Therefore, the transport of current within the reinforcement is never a slow process and thus never contributes to reducing the rate of corrosion. Instead, under particular conditions inside the concrete, each of the other three processes can take place at negligible rate and thus become the kinetically controlling one. More precisely, the corrosion rate is negligible when one of the following conditions exists (Bertolini, et al, 2004):

- the anodic process is slow because the reinforcement is passive, as when the concrete is not carbonated and does not contain chlorides;
- the cathodic process is slow because *e.g.* the rate at which oxygen reaches the surface of the reinforcement is low, as in the case of water-saturated concrete;
- the electrical resistance of the concrete is high, as in the case of structures exposed to environments which are dry or low in relative humidity. In this respect, it is important to realise that the 'water' in the concrete pores is actually a dilute solution of alkali and calcium hydroxides; it is this fluid that serves as a vehicle for ionic flow. If the pores are dried out, or if the structure of the concrete is so dense that the pores are not very well interconnected, the flow of ions through the pores becomes difficult. Under such circumstances the ionic current will flow only with difficulty, and the corrosion process will slow down or stop;

On the other hand, the corrosion rate is high in those cases where the three following conditions are present simultaneously:

- the reinforcement is no longer in the condition of passivity;
- oxygen can reach the surface of steel; and
- the electrical resistance of the concrete is low.

The two half cell reactions, one capable of producing electrons (the anodic reaction) and one capable of consuming electrons (the cathodic reaction), occurring during the corrosion of steel in aqueous media at high pH (in the absence of an external electrical source), are described below:

❑ *anodic reaction* (oxidation of metal)

The anodic reaction for the dissolution of iron can be written as follows in its simplified chemical form:

$$Fe \rightarrow Fe^{2+} + 2e^{-} \qquad \text{(eq. 2-1)}$$

However, instead of direct transfer of two electrons as implied, in reality there is a single electron transfer sequence. The exact nature of this sequence is still a matter of debate (the exact nature of this sequence is still unkown) (or there still exists some uncertainties as to the exact nature of this sequence (Smart, et al, 2004):

- one possible reaction sequence, involving two single-electron transfer reactions, is

$$Fe + H_2O \rightarrow FeOH_{ads} + H^+ + e^- \quad \text{(eq. 2-2)}$$

$$FeOH_{ads} \rightarrow FeOH^+ + e^- \quad \text{(eq. 2-3)}$$

$$FeOH^+ + H^+ \rightarrow Fe^{2+} + H_2O \quad \text{(eq. 2-4)}$$

  where the subscript '*ads*' denotes an adsorbed species. Reaction 2-4 is the rate determining step. This sequence was identified as the most probable mechanism as the reaction rate is known to increase with hydroxyl concentration.

- an alternative to reactions 2-3 and 2-4, involving deprotonation rather than protonation, is:

$$FeOH_{ads} \rightarrow FeO + H^+ + e^- \quad \text{(eq. 2-5)}$$

  The hydrated form of FeO is the $Fe(OH)_2$. Whether or not reaction 2-5 proceeds in preference to reactions 2-3 and 2-4 depends on such factors as pH, temperature and potential.

- an alternative reaction that could be envisaged for alkaline conditions following reaction 2-3, would be:

$$FeOH^+ + OH^- \rightarrow Fe(OH)_2 \quad \text{(eq. 2-6)}$$

Regardless of which of the mechanisms is followed, the overall anodic reaction in alkaline conditions is (Smart, et al, 2004):

$$Fe + 2H_2O \rightarrow Fe(OH)_2 + 2H^+ + 2e^- \quad \text{(eq. 2-7)}$$

$Fe(OH)_2$ is highly insoluble in moderately alkaline conditions and therefore forms a film on the surface of the iron.

- *cathodic reaction* (reduction)

In alkaline environments, the cathodic reaction can be written as follows depending on the oxygen availability:

- under oxic, alkaline conditions, the balancing cathodic reaction is the reduction of oxygen:

$$2H_2O + O_2 + 4e^- \rightarrow 4OH^- \quad (\textit{oxic conditions}) \quad \text{(eq. 2-8)}$$

- under anoxic, alkaline conditions, the balancing cathodic reaction is the reduction of water:

$$2H_2O + 2e^- \rightarrow 2OH^- + H_2 \quad (\textit{anoxic conditions}) \qquad \text{(eq. 2-9)}$$

This reaction is referred to as either the water reduction or the hydrogen evolution reaction.

2.1.2. Corrosion mechanisms of carbon steel under aerobic and anaerobic conditions

During the initial period after closure of the repository, the environment will be oxygenated as large volumes of air will be trapped in pores and voids due to the excavation works and the construction of the repository. Oxygen, initially present in the repository, will be consumed by a number of mechanisms, including metal corrosion and microbial activity. The environmental conditions in the repository will therefore change progressively and become anoxic. The reactions involved in steel corrosion in aqueous media at high pH under oxic and anoxic conditions are described below:

- *oxic conditions* ('aerobic' corrosion)

The two half cell reactions contributing to the aerobic corrosion of steel under alkaline conditions are:

$$Fe + 2H_2O \rightarrow Fe(OH)_2 + 2H^+ + 2e^- \quad (\textit{anodic reaction}) \qquad \text{(eq. 2-7)}$$

$$2H_2O + O_2 + 4e^- \rightarrow 4OH^- \quad (\textit{cathodic reaction}) \qquad \text{(eq. 2-8)}$$

giving the following overall reaction:

$$2Fe + O_2 + 2H_2O \rightarrow 2Fe(OH)_2 \qquad \text{(eq. 2-10)}$$

In the presence of oxygen, the colourless ferrous hydroxide, $Fe(OH)_2$, readily oxidises to brown ferric hydroxide, $Fe(OH)_3$, via the reaction:

$$4Fe(OH)_2 + 2H_2O + O_2 \rightarrow 4Fe(OH)_3 \qquad \text{(eq. 2-11)}$$

giving an overall reaction (Agg, 1993; Smart, et al, 2002):

$$4Fe + 6H_2O + 3O_2 \rightarrow 4Fe(OH)_3 \qquad \text{(eq. 2-12)}$$

Solid $Fe(OH)_3$ spontaneously loses water (dehydration) according to the following reaction:

$$Fe(OH)_3 \rightarrow FeOOH + H_2O \qquad \text{(eq. 2-13)}$$

giving an overall reaction (King, 2007):

$$4Fe + 2H_2O + 3O_2 \rightarrow 4FeOOH \qquad \text{(eq. 2-14)}$$

The species "*FeOOH*" is used to describe a generic term for a hydrated ferric oxy-hydroxide species. It may also be written as $Fe_2O_3.xH_2O$, where 'x' denotes an unspecified number of water molecules (Crossland, 2006; King, 2007). The principal forms of hydrated ferric oxy-hydroxide that are encountered as corrosion products of

iron are α-Fe_2O_3 (hematite), γ-Fe_2O_3 (maghemite), α-FeOOH (goethite) and γ-FeOOH (lepidocrocite).

The corrosion process of steel in concrete in the presence of oxygen (oxic conditions) is schematically illustrated in Figure 2-1. The actual loss of metal involved in the corrosion process takes place at the anodic site. The iron atoms are ionized (oxidized) to ferrous (Fe^{2+}) ions which dissolve in the aqueous solution around the steel (*oxidation reaction*). The electrons that are generated at the anode by oxidation of iron then flow through or along the steel to the cathode (*electrical current* within the steel as a result of *electron flow*). Here, the electrons combine with dissolved oxygen molecules and water to form hydroxyl ions (OH^-) (*reduction reaction*). Since the electrons carry a negative charge this gives rise to a nominal electrical current flowing in the opposite direction, *i.e.* from the cathode to the anode (because current is, by convention, the flow of positively charged particles).
In order for the corrosion process to continue, the number of electrons accepted at the cathodic site must be equal to the number of electrons donated at the anodic site. Thus, for every dissolved oxygen molecule that reacts at the cathodic site, two iron atoms must be dissolved at the anodic site.
The ferrous (Fe^{2+}) and hydroxyl (OH^-) ions move away from the surface and flow toward one another (external *electrical current* as a result of ionic flow). When they meet, they react to form ferrous hydroxide, $Fe(OH)_2$. In the presence of dissolved oxygen, this is quickly oxidised further to ferric hydroxide, $Fe(OH)_3$.
The porous $Fe(OH)_3$ rust can slowly disintegrate into the insoluble product Fe_2O_3, which is the familiar red-brown rust.

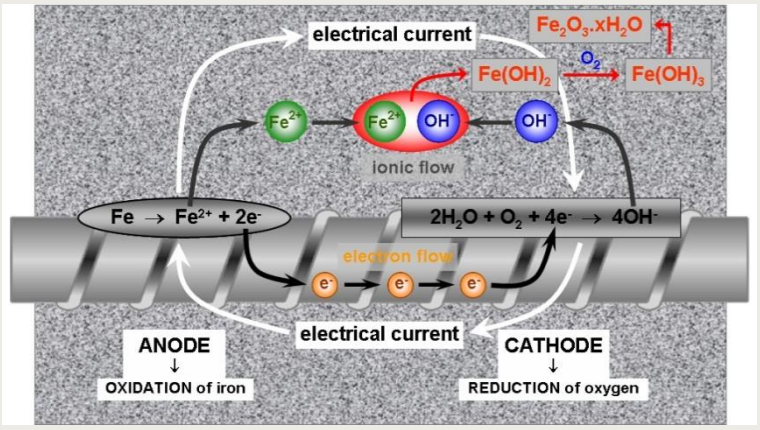

Figure 2-1. The anodic (dissolution of steel) and cathodic reactions for corroding steel in concrete under oxic conditions. Since the electrons carry a negative charge, this gives rise to a nominal electrical current flowing in the opposite direction (the positive direction of the current is, by accepted sign convention, the direction of flow of positivily charged particles).

- *anoxic conditions* ('anaerobic' corrosion)

The two half cell reactions contributing to the anaerobic corrosion of steel under alkaline conditions are:

$$Fe + 2H_2O \rightarrow Fe(OH)_2 + 2H^+ + 2e^- \quad (\textit{anodic reaction}) \qquad \text{(eq. 2-7)}$$

$$2H_2O + 2e^- \rightarrow 2OH^- + H_2 \quad (\textit{cathodic reaction}) \qquad \text{(eq. 2-9)}$$

giving the following overall reaction:

$$Fe + 2H_2O \rightarrow Fe(OH)_2 + H_2 \uparrow \quad \text{(eq. 2-15)}$$

Depending on the temperature and pH of the surrounding environment, the ferrous hydroxide may transform, via the following reaction, known as the Schikorr reaction, into magnetite, leading to the evolution of additional hydrogen:

$$3Fe(OH)_2 \rightarrow Fe_3O_4 + 2H_2O + H_2 \uparrow \quad \text{(eq. 2-16)}$$

giving an overall reaction:

$$3Fe + 4H_2O \rightarrow Fe_3O_4 + 4H_2 \uparrow \quad \text{(eq. 2-17)}$$

Reaction 2-16 is favoured by increasing temperature because magnetite is thermodynamically more stable than ferrous hydroxide at higher temperature. This is shown by the fact that iron corroding in deaerated water at 25°C produces an $Fe(OH)_2$ film, but that magnetite is formed at 60°C. The presence of certain impurities, such as nickel, copper and cobalt, either in solutions or from the metal, can catalyse the Schikorr reaction. However, even with high amounts of impurities, only 10-20% of the initial oxide is transformed to magnetite. On the other hand, increased alkalinity has been shown to inhibit the Schikorr reaction (Blackwood, et al, 1995; Grauer, et al, 1991a; Linnenbom, 1958; Naish, et al, 2001; Smart, et al, 2004).

The corrosion process of steel in concrete in the absence of oxygen (anoxic conditions) is schematically illustrated in Figure 2-2. The reaction taking place at the anodic site (*oxidation* of metal iron to ferrous ions, Fe^{2+}) is identical as under oxic conditions. The electrons that are generated at the anode will flow, through or along the steel, to the cathode (*electrical current* within the steel as a result of *electron flow*) where they combine with water to form hydroxyl ions (OH^-) and hydrogen gas (*reduction reaction*).
The number of electrons accepted at the cathodic site must be equal to the number of electrons donated at the anodic site to satisfy a charge balance. Thus, for every hydrogen molecule that escapes at the cathodic site, one iron atom must be dissolved at the anodic site.
The ferrous (Fe^{2+}) and hydroxyl (OH^-) ions move away from the surface and flow toward one another (external *electrical current* as a result of ionic flow). When they meet, they react to form ferrous hydroxide, $Fe(OH)_2$. In the absencene of oxygen, $Fe(OH)_2$ may not be the stable corrosion product, especially at higher temperatures (>60°C), and can decompose to magnetite (Fe_3O_4).

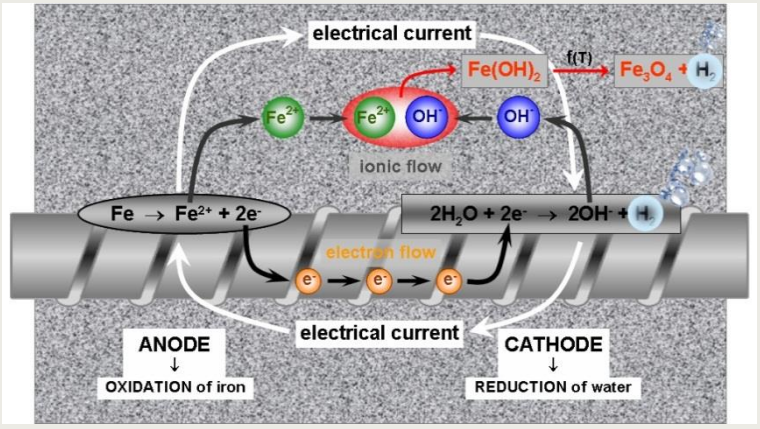

Figure 2-2. The anodic (dissolution of steel) and cathodic reactions for corroding steel in concrete under anoxic conditions. Since the electrons carry a negative charge, this gives rise to a nominal electrical current flowing in the opposite direction (the positive direction of the current is, by accepted sign convention, the direction of flow of positivily charged particles).

2.1.3. Corrosion mechanisms of carbon steel under disposal conditions

Both the aerobic and anaerobic corrosion processes, as described earlier in this section, have been explained starting from a bare steel surface. In reality, however, it is more realistic to assume that, under disposal conditions, an aerobically formed corrosion product layer will be present on the surface of the steel before anaerobic corrosion will commence. Thus, the following reaction sequence can be given to describe the evolution of the corrosion processes taking place at the steel overpack surface embedded in concrete in the course of the disposal period, with respect to the Supercontainer design:

1. during the initial period after fabrication of the Supercontainer, the concrete environment surrounding the steel overpack will be oxygenated and corrosion of the steel overpack will proceed, with the formation of ferric (Fe(III)) corrosion products, according to the following reaction (King, 2007):

$$4Fe + 2H_2O + 3O_2 \rightarrow 4FeOOH \qquad \text{(eq. 2-14)}$$

   As long as oxygen is available, this protective film will continue to grow.

2. as the environment becomes anoxic, the Fe(III) corrosion products will be converted to Fe(II) via (King, 2007):

$$2FeOOH + Fe + 2H_2O \rightarrow 3Fe(OH)_2 \qquad \text{(eq. 2-18)}$$

3. under anaerobic conditions, $Fe(OH)_2$ may not be the stable corrosion product, especially at higher temperatures (>60°C), and can decompose to magnetite (Fe_3O_4) with the liberation of hydrogen according to the following reaction (King, 2007):

$$3Fe(OH)_2 \rightarrow Fe_3O_4 + 2H_2O + H_2\uparrow \qquad \text{(eq. 2-16)}$$

2.2. Corrosion protection provided by concrete

The electrochemical behaviour of steel in contact with cementitious materials (concrete and mortar) is generally governed by the properties of the Portland cement. Cement hydration reactions result in highly alkaline concrete pore solutions: pH values well in

excess of 13 are frequently recorded for Portland cement pastes of water/cement ratios such as are commonly used in practice. In these highly alkaline environments, the potential-pH diagram indicates that iron may remain passive over a wide range of potentials (see red zone in Figure 2-3) and a very limited supply of oxygen is sufficient to provide the necessary degree of anodic polarisation to maintain conditions within this range (Bertolini, et al, 2004; Page and Treadaway, 1982). The steel will be in a passive condition because of the formation of a thin film of oxide – generally considered to be γ-FeOOH – that reduces significantly the corrosion rate (Andrade, et al, 1995; Arup, 1983; Bentur, et al, 1997; Bertolini, et al, 2004; Broomfield, 2007; Hausmann, 1967; Preece, 1982; Roberge, 2000; Slater, 2006; Tuuti, 1982).

In conclusion, the primary mechanism of corrosion protection in concrete involves passivation of embedded steel resulting from the chemically inhibitive influence of the hydroxyl ions (Page and Treadaway, 1982).

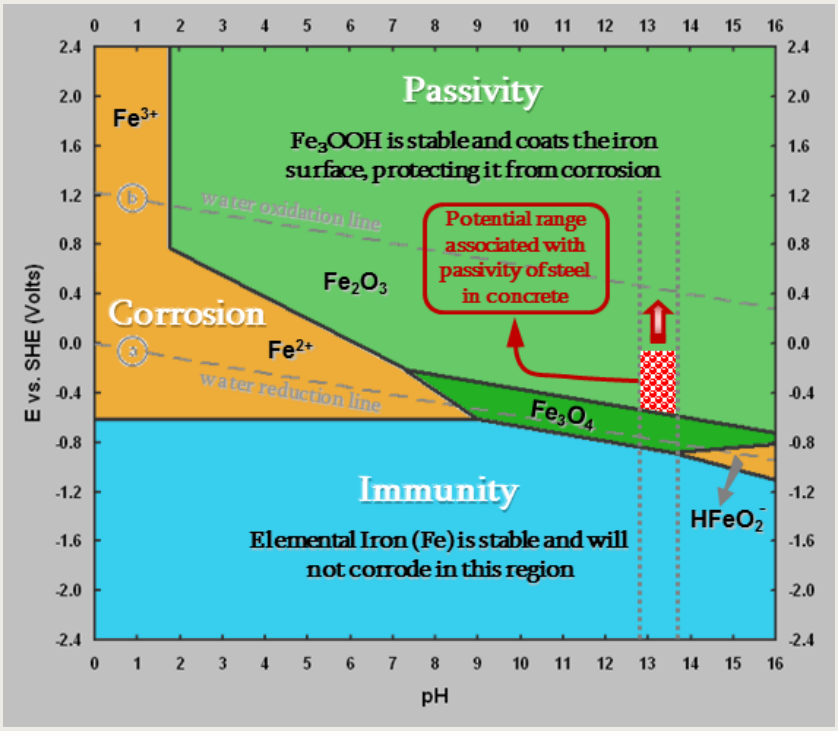

Figure 2-3. Potential-pH equilibrium diagram (Pourbaix diagram) for Fe in H_2O at 25°C, considering as solid substances only Fe, Fe_3O_4 and Fe_2O_3 (FeOOH) (source: adapted from [Roberge, 2000; Gonzalez, et al, 1996]).

From the above, it is clear that the high alkalinity of the concrete pore solution is the driving force behind the protection of steel embedded in concrete. Therefore, a more profound discussion on why the concrete pore solution rapidly acquires such a high pH value seems appropriate:

- immediately after mixing cement with water, free lime (CaO), the alkali sulphates (potassium and sodium sulphate – Na_2SO_4 and K_2SO_4) and gypsum ($CaSO_4 \cdot 2H_2O$) dissolve almost completely resulting in the precipitation of portlandite ($Ca(OH)_2$). Considering the large availability of $Ca(OH)_2$ and the limited pore volume, the concrete pore solution is rapidly saturated with $Ca(OH)_2$ (Li and Sagüés, 2001; Nam, 2004; Reardon, 1992).
  The pH expresses the degree of acidity of an aqueous solution and is defined as minus the decimal logarithm of the hydrogen ion concentration, c_{H^+} (Mortimer, 1986; Nam, 2004; Roberge, 2000; Stumm and Morgan, 1996):

$$pH = -\log_{10}\left(c_{H^+}\right) \qquad \text{(eq. 2-19)}$$

The concentration of hydroxyl ions in water is related to the concentration of hydrogen ions by the following relation (Mortimer, 1986; Skoog, et al, 1992; Stumm and Morgan, 1996)

$$K_w = c_{H^+} \cdot c_{OH^-} \quad \rightarrow \quad c_{H^+} = \frac{K_w}{c_{OH^-}} \qquad \text{(eq. 2-20)}$$

where K_w is the dissociation constant of water (= 10^{-14}) (Mortimer, 1986; Skoog, et al, 1992; Stumm and Morgan, 1996].

Substituting equation 2-20 into equation 2-19 gives:

$$pH = -\log_{10}\left(\frac{K_w}{c_{OH^-}}\right) = -\log_{10}\left(\frac{10^{-14}}{c_{OH^-}}\right) = 14 + \log_{10}\left(c_{OH^-}\right) \qquad \text{(eq. 2-21)}$$

Equation 2-21 is, however, only valid for ideal solutions (dilute solutions, i.e. if the concentration of charged ions present in the solution is below 0.001 M). For real solutions, ion activities rather than concentrations should be used for calculations (Skoog, et al, 1992; Stumm and Morgan, 1996):

$$pH = 14 + \log_{10}\left(a_{OH^-}\right) \qquad \text{(eq. 2-22)}$$

where, a_{OH^-} equals the hydroxyl ion activity.

The activity of a compound in a liquid solution can be defined as (Skoog, et al, 1992):

$$a_{OH^-} = \gamma_{OH^-} \cdot c_{OH^-} \qquad \text{(eq. 2-23)}$$

where γ_{OH^-} is the activity coefficient of OH^- (dimensionless) and c_{OH^-} is the molar concentration of OH^-.

Substituting equation 2-23 into equation 2-22 gives:

$$pH = 14 + \log_{10}\left(\gamma_{OH^-} \cdot c_{OH^-}\right) \qquad \text{(eq. 2-24)}$$

The hydroxyl ion concentration of saturated $Ca(OH)_2$ can be deduced from Figure 2-4, which shows the influence of temperature on the solubility of $Ca(OH)_2$ in water: at 25°C, the solubility of $Ca(OH)_2$ is 1.5 $g.L^{-1}$ solution[a] (Linke and Seidell, 1958; WIKI1).

[a] because calcium hydroxide is only sparsely soluble, there is no visible distinction to clear water and the solubility expressed in $g.kg^{-1}$ may be replaced by the solubility expressed in $g.L^{-1}$ without introducing a significant error (WIKI1).

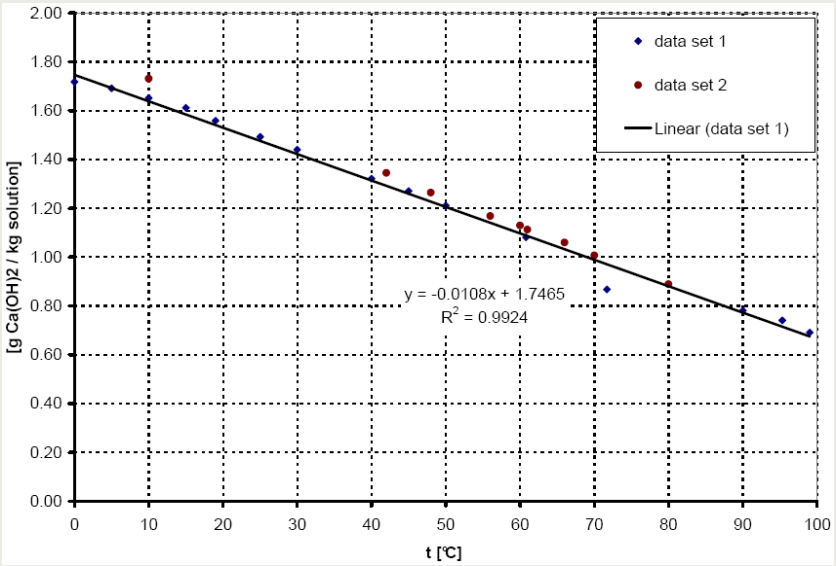

Figure 2-4. Solubility of calcium hydroxide, $Ca(OH)_2$, in water (WIKI1).

The molar concentration of OH^- in a saturated $Ca(OH)_2$ solution can thus be calculated (molecular weight of $Ca(OH)_2$ = 74.09 $g.mol^{-1}$):

$$c_{OH^-,\ sat.Ca(OH)_2} = 2 \times \left(\frac{1.5\ g.L^{-1}}{74.09\ g.mol^{-1}} \right) = 0.0405\ mol.L^{-1}$$

The mathematical model proposed by Samson and co-workers (Samson, et al, 1999), which is essentially a modified version of the Davies equation, can be used to accurately calculate single activity coefficients of concentrated electrolytic solutions: the activity coefficient of OH^- is assumed to be ~0.78 and ~0.70 when $c_{OH^-} \leq 0.1$ mol.L^{-1} and $c_{OH^-} > 0.1$ mol.L^{-1}, respectively.

The pH of a saturated $Ca(OH)_2$ solution can then be calculated by substituting the values for c_{OH^-} and γ_{OH^-} into equation 2-24.

$$pH\ (sat.Ca(OH)_2) = 14 + \log_{10}(0.78 \times 0.0405) = 12.5$$

- the pore water pH of a cement paste is most often not determined by $Ca(OH)_2$, but by the small quantity (normally less than 1%) of alkalis present in the cement clinker. Although the alkalis are expressed analytically in terms as K_2O and Na_2O, they are actually present as alkali sulphates (K_2SO_4 and Na_2SO_4). Much of the alkali content is readily soluble in the mixing water leading to the release of high amounts of Na^+ and K^+ ions into the pore solution. From charge balance considerations, their concentrations must be balanced by an equivalent concentration of anions, the most dominant being OH^- (Bentur, et al, 1997; Li and Sagüés, 2001; Nam, 2004; Reardon, 1992). The reactions of the alkalis during cement hydration can be expressed as (Li and Sagüés, 2001)

$$Na_2SO_4 + Ca(OH)_2 \rightarrow CaSO_4 + 2NaOH \qquad \text{(eq. 2-25)}$$

$$K_2SO_4 + Ca(OH)_2 \rightarrow CaSO_4 + 2KOH \qquad \text{(eq. 2-26)}$$

Stochiometrically, the reaction of each mole of cement alkali oxide produces two moles of hydroxide. Also, the solubility of the alkali hydroxides, NaOH and KOH, is significantly higher compared to that of $Ca(OH)_2$, which results in a relatively large amount of OH^- ions being dissolved into the cement pore solution. Figure 2-5 presents a compilation of data from the literature showing the relative importance of the cement alkali content on the hydroxide concentration of the cement pore solution (Arya, et al, 1995; Constantiner, 1997; Diamond, 1981; Diamond, 1983; Duchesne, 1994; Kawamura, 1988; Kayyali, et al, 1990; Larbi, et al, 1990; Li, 2000; Nam, 2004; Page and Vennesland, 1983; Tritthart, 1989). Regardless of the scatter, the data show a common trend in that $[OH^-]$ increases with increasing equivalent cement alkali content (Nam, 2004; Reardon, 1992).

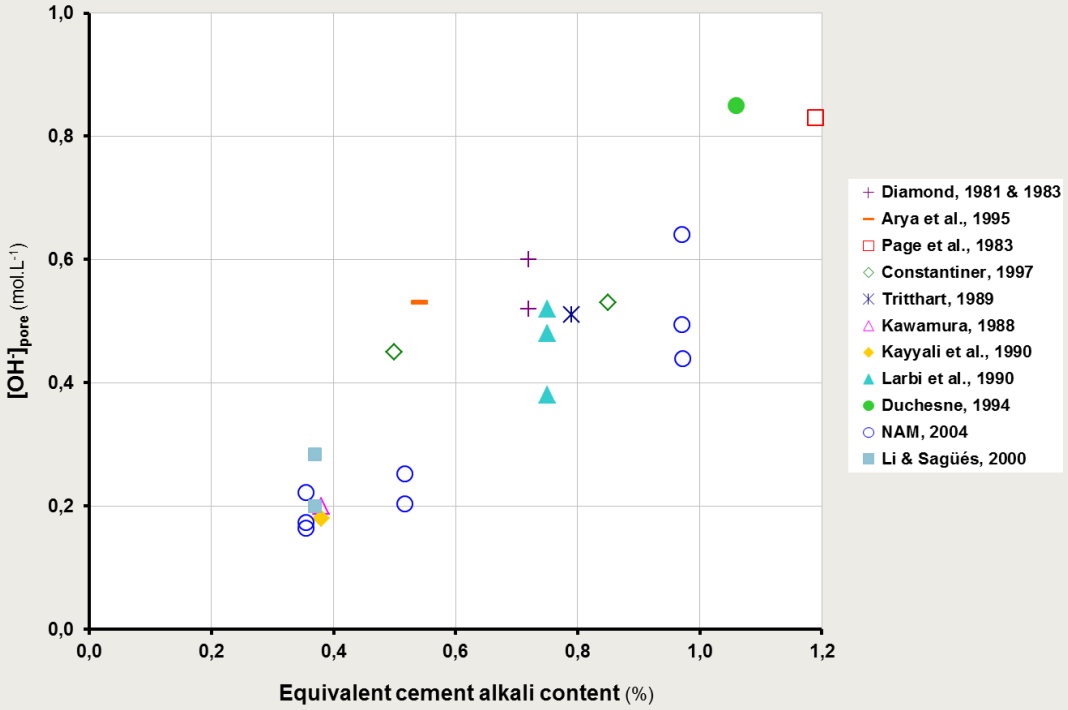

Figure 2-5. Relationship between the cement alkali content and the hydroxide concentration of the pore solution of the cement paste, $[OH^-]_{pore}$ (source: adapted from [Li and Sagüés, 2001; Nam, 2004]).

Table 2-1 shows the ionic concentrations measured by different researchers in the pore solution of cement pastes, mortars and concretes, obtained with Portland cements (OPC). Measurements were carried out by chemical analysis of the liquid extracted under pressure. From hydroxyl ion concentrations, values of pH in the range of 13.2-13.8 can be calculated for Portland cement (Bertolini, et al, 2004).

Table 2-1. Ionic concentration (in mmol/L) measured in the pore solution extracted from cement pastes, mortars and concrete made with ordinary Portland cement (OPC) (source: adapted from [Bertolini, et al, 2004]).

Cement	w/c	Cl^- [(a)] (%)	Age (days)	Sample	Ionic concentration (in mmole/L)						pH[(b)]	Source
					$[Na^+]$	$[K^+]$	$[Ca^{2+}]$	$[Cl^-]$	$[SO_4^{2-}]$	$[OH^-]$		
OPC	0.45	-	28	paste	130	380	1	n.a.	n.a.	470	13.52	Larbi, et al, 1990
OPC	0.50	-	28	mortar	90	288	<1	3	<0.3	391	13.44	Polder, 1986
OPC	0.50	-	28	paste	271	629	1	n.a.	31	834	13.77	Page, et al, 1983
OPC	0.50	-	192	mortar	38	241	<1	n.a.	8	251	13.25	Bürchler et al, 1996
OPC	0.50	-	-	paste	85	228	n.a.	1	n.a.	288	13.30	Sergi, 1986
OPC[(c)]	0.50	-	84	paste	n.a.	n.a.	n.a.	2	n.a.	589	13.62	Holden et al, 1983
OPC[(d)]	0.50	-	84	paste	n.a.	n.a.	n.a.	3	n.a.	479	13.53	Holden et al, 1983
OPC[(c)]	0.50	0.4	84	paste	n.a.	n.a.	n.a.	84	n.a.	741	13.71	Holden et al, 1983
OPC[(d)]	0.50	0.4	84	paste	n.a.	n.a.	n.a.	42	n.a.	661	13.67	Holden et al, 1983
OPC	0.50	0.4	28	mortar	90	161	<1	104	5	62	12.69	Polder, 1986
OPC	0.50	0.4	35	paste	546	630	2	146	41	835	13.77	Page et al, 1983
OPC	0.50	1	-	paste	580	208	n.a.	227	n.a.	458	13.51	Sergi, 1986

n.a. : concentration not available.
[(a)] chloride added by mass of cement.
[(b)] calculated pH-value: $pH = 14 + \log_{10}(\gamma_{OH^-}\cdot[OH^-])$, where γ_{OH} is the activity coefficient of OH^-, which is assumed to be 0.7 when $[OH^-] > 100$ mmole/L and 0.78 when $[OH^-] \leq 100$ mmole/L (Samson, et al, 1999).
[(c)] low C_3A content (7.7%).
[(d)] high C_3A content (14.3%).

3. Methodology of the corrosion studies

The main goal of the ongoing RD&D corrosion studies is to provide confidence that the integrity of the carbon steel overpack will not be jeopordized at least for the duration of the thermal phase. In terms of a geological repository, the thermal phase is defined as the time frame during which the temperature of the host formation is expected to lie above the range of temperatures within which nominal migration properties can be relied upon (e.g. for the Belgian reference disposal design, the time scales vary between 200 years for vitrified high-level nuclear waste and ~3 000 years for spent fuel (MOX) (ONDRAF/NIRAS, 2013)).

An integrated scientific approach was developed consisting of the following three steps:

- Step 1 – Development of the Corrosion Evolutionary Path (CEP);
- Step 2 – Determination of scientifically well-founded estimates of uniform corrosion rates for the different phases established during the CEP; and
- Step 3 – Proving the validity of the 'exclusion principle';

3.1.Development of the Corrosion Evolutionary Path (CEP)

In nuclear waste management, the Corrosion Evolutionary Path (CEP) describes the changing environmental conditions the overpack is subjected to in a repository during the entire disposal period. The CEP defines the time dependent corrosion behaviour of the carbon steel overpack and is therefore closely linked to the evolution of the environmental conditions surrounding the overpack.

The environmental conditions surrounding the supercontainer will gradually evolve over time from hot, oxic and relatively dry to cool, anoxic and fully saturated:

- Temperature will decrease as heat production of the radioactive waste decreases;
- Oxidising conditions will gradually change to reducing conditions following repository closure. Oxygen, initially trapped in the free spaces of the disposal galleries during its construction, will be consumed through chemical reactions, corrosion processes and microbial activity;
- The geochemistry of the environment surrounding the overpack, initially governed by the Ordinary Portland Cement (OPC)-based buffer chemistry, will gradually be modified as Boom Clay pore water penetrates the concrete lining of the disposal galleries and the concrete buffer of the supercontainer;

The development of the CEP is represented in Figure 3-1. Based on the evolution of the environmental conditions, the CEP has been divided in several phases. And the various corrosion processes and parameters that could potentially influence the lifetime of the carbon steel overpack during the different phases have been identified.
The corrosion processes that can affect the lifetime of the overpack in all phases are uniform corrosion and several forms of localised corrosion (such as pitting corrosion, crevice corrosion, stress corrosion cracking and hydrogen embrittlement). And under anoxic conditions, the effect of Sulphate Reducing Bacteria (SRB) and the associated Microbially Induced Corrosion (MIC) also becomes a potential mechanism that should not be ignored.
The various parameters that can influence the corrosion behaviour of the overpack are: temperature, the presence of aggressive species such as chloride, sulphide and thiosulphate, the presence of γ radiation, the presence of welds, etc.

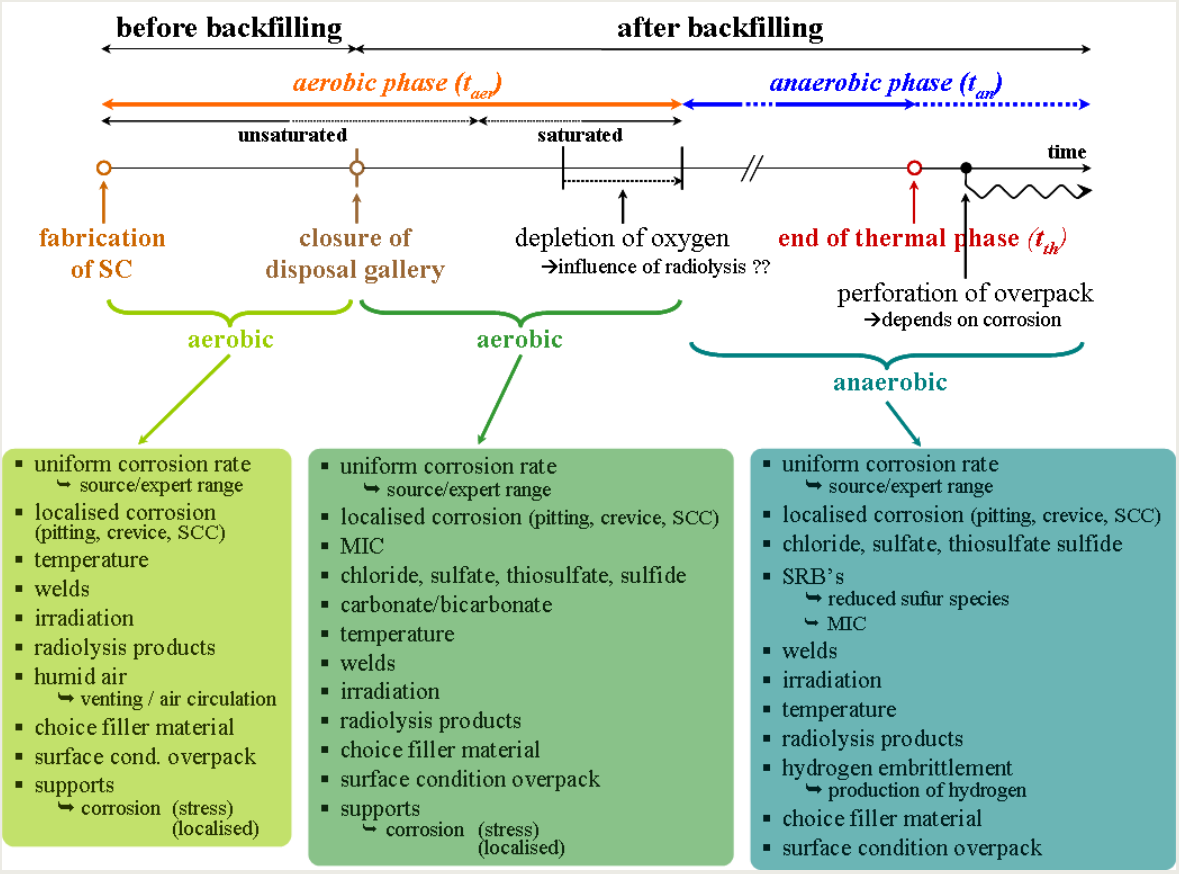

Figure 3-1. Schematic representation of the corrosion evolutionary path (CEP), with indication of the various degradation modes and parameters that could potentially influence the lifetime of the carbon steel overpack during the different phases of the disposal period.

Three phases are identified from the time of fabrication of the supercontainer up to the time of loss of the overpack's integrity (*i.e.* perforation of the carbon steel overpack):

- phase 1 – aerobic unsaturated phase;
- phase 2 – aerobic saturated phase; and
- phase 3 – anaerobic saturated phase (long-term);

Aerobic unsaturated phase 1

The beginning of phase 1 is defined as the time at which the carbon steel overpack is emplaced in the supercontainer, thereby exposing it to the high pH concrete buffer. Corrosion of the carbon steel overpack can commence from the moment it is placed in contact with the precast concrete buffer. This already takes place during the fabrication process of the supercontainer, which is carried out on surface (partly outside and partly inside a radiation shielded hot cell). Although it is intended that emplacement of the supercontainer in the disposal gallery and backfilling, sealing and closing of the disposal gallery should happen in rapid succession, one cannot exclude that a considerable time could elapse between the fabrication of the supercontainer and closing of the disposal gallery.

Corrosion of the outer surface of the carbon steel overpack can only occur through contact with the pore fluid present in the concrete buffer, because it is expected that, at this stage of the disposal period, aggressive species coming from the Boom Clay host rock will not have had sufficient time to penetrate up to the overpack. The oxidising agents present in the supercontainer are oxygen from entrapped air in the concrete buffer and the oxygen

and other oxidising species produced by radiolysis that could have an influence on the redox conditions and on the corrosion reactions at the overpack surface.

Aerobic saturated phase 2

The ingress of Boom Clay pore fluid, in time, will lead to a complete saturation of the concrete buffer and an alteration of the pore water chemistry of the concrete buffer. Ingression of Boom Clay pore fluid will introduce potentially aggressive species into the concrete buffer that could lead to an enhanced corrosion of the carbon steel overpack: chlorides, bicarbonates, thiosulphates and sulphides.

Long-term anaerobic saturated phase 3

The initially trapped oxygen will be consumed by corrosion and microbiological processes (microbial activity is highly unlikely considering the unfavourable conditions close to the overpack owing to the high pH, high temperature and the small size of the pores in the buffer concrete). This phase of saturated anaerobic conditions is expected to persist indefinitely.

Neglecting the effect of radiolysis, the only oxidant available in the system, at this stage of the disposal period, is water. Corrosion under these conditions yields hydrogen gas by reduction of protons and water.

The temperature at the overpack surface will continually decrease until a limiting value of the order of 16°C – *i.e.* the temperature of the undisturbed Boom clay host rock formation – is reached.

The possibility of localised corrosion occurring is much diminished because there is no process by which the anodic and cathodic processes may be spatially separated. Corrosion, therefore, is expected to be uniform in nature, proceeding at a rate determined by the rate of the anodic process. Furthermore, experiments performed by Smart et al. (Smart et al., 2004) demonstrated that carbon steel will repassivate under anoxic and high pH conditions, that is, if damaged, the protective film will reform and the uniform corrosion rate will remain low.

3.2. Determination of scientifically well-founded estimates of uniform corrosion rates

One of the main cornerstones of our methodology is based on the assumption that under the predicted conditions within the supercontainer (i.e. a highly alkaline concrete buffer), the carbon steel overpack is expected to undergo uniform corrosion through the mechanism of passive dissolution (Hausmann, 1967; Preece, 1982; Tuuti, 1982; Bertolini, et al, 2004). The deterministic nature of uniform corrosion makes it possible to provide reliable estimates of the uniform corrosion rate for the different phases of the CEP.

Once the uniform corrosion rate for each of the seperate phases of the CEP has been determined, lifetime prediction (in terms of reduction in wall thickness in µm/year) then becomes very straightforward by simply integrating these corrosion rates over the duration of the different phases on the basis of the following equation:

$$d_{overpack} = \sum v_i \cdot t_i \qquad \text{(eq. 3-1)}$$

where $d_{overpack}$ is the required thickness of the overpack to avoid performation (due to corrosion) during the thermal phase, v_i are the reliable estimates of the uniform corrosion

rate of the different phases (as established from the CEP) and t_i are the durations of the different separate phases.

This calculation only provides an estimation of the corrosion margin on the overpack thickness. The thickness required to withstand mechanical stresses is not taken into account.

3.3.Proving the validity of the exclusion principle

In the high pH environment of the supercontainer (i.e. a concrete-based buffer), the carbon steel overpack is expected to be covered with a protective passive film (Hausmann, 1967; Preece, 1982; Tuuti, 1982; Bertolini, et al, 2004). On the other hand, it is generally recognised (Alonso, et al, 2000; Angst, et al, 2009) that carbon steel exposed to such a high pH environment can undergo depassivation due to for example ingress of aggressive species. This can result in a subsequent localised corrosion attack, such as pitting and crevice corrosion, and/or environmental cracking phenomena, such as stress corrosion cracking (SCC) and hydrogen embrittlement (HE), that can lead to locally very rapid penetration of the overpack. The stochastic nature of these local corrosion phenomena increases the difficulty of making reliable predictions concerning the lifetime of the overpack.

Our proposed integrated approach is based on providing a sound argumentation to defend that each corrosion mechanism (i.e. localised corrosion phenomena such as e.g. pitting corrosion, crevice corrosion, SCC, HE), other than uniform corrosion, cannot take place under the geochemical conditions prevailing within the supercontainer and described in the CEP. Or, if they can occur that we can prove that the effect will be negligible. This is called the 'exclusion principle'.

One possible way to tackle this is the following: it is commonly known that a threshold concentration of aggressive species (e.g. chloride, thiosulphate, sulphide, etc.) exists above which the initiation of the different potential forms of localised corrosion and SCC/HE can occur. The exclusion principle is based on proving that the predicted reference concentrations that can be expected within the supercontainer (at the outer surface of the overpack) are situated well below the threshold concentrations. These threshold concentrations can often be found in the literature (such as e.g. for chloride). And for those aggressive species that we do not know the threshold concentration, this has to be determined experimentally. The occurrence of localised corrosion can be predicted by comparing the critical potentials at which these corrosion modes occur (determined, if available, from literature or experimentally) with the free corrosion potential.

4. Expected evolution of the near-field environment surrounding the carbon steel overpack

The Dutch reference design for geological disposal of heat generating high-level radioactive waste (OPERA-A) involves a multi-barrier system of which the man-made (engineered) barriers are based on the Belgian Supercontainer concept. In this disposal concept, a carbon steel overpack is surrounded by a concrete buffer based on Ordinary Portland Cement (OPC), imposing highly alkaline conditions. As such, containment of the waste (water tightness) should be guaranteed at least during the thermal phase, but possibly much longer. In the RD&D programme, the evaluation of the corrosion resistance of this overpack is crucial, and this requires a good characterization of its chemical and physical environment as well as information about its evolution considering the long timescales involved in geological disposal.

The parameters that can potentially influence corrosion are: temperature, pH of the concrete pore solution, degree of water saturation of the concrete buffer, chemical composition of the concrete pore solution (including the presence of corrosion-aggressive species) and radiation levels. These changing environmental conditions inside the concrete buffer of the Supercontainer are called the Corrosion Evolutionary Path (CEP) (see section 3.1.).

In this chapter, the numerical models used to predict the long-term evolution of the above-mentioned corrosion-related parameters are described and their output is discussed:

- the temperature evolution in the repository near field is calculated using a 2D axisymmetric model. Also, special emphasis is put on the verification of the heat source term;
- the evolution of water saturation in the repository is assessed by means of a 1D radial thermohydraulic simulation;
- a 1D radial chemical diffusive simulation is used to predict the pH evolution;
- 1D axisymmetric transport calculations of the aggressive species, coming from the perturbed host rock formation (Dutch Boom Clay), towards the overpack is carried out using COMSOL Multiphysics 3.5a software;

4.1. Evolution of temperature at the overpack surface

4.1.1. Calculation of thermal power based on inventories

The thermal power calculation is carried out based on calculating the heat output as a function of time for a shortlist of the most heat generating radionuclides in the inventory, taking into account radioactive decay and ingrowth. As a first step, the method for calculating the thermal power is checked using data for HLW provided in the EC RED-IMPACT project, in which both thermal power and radiological inventories per waste canister are given (Cuñado, 2007).

The thermal power (W/canister) provided in the RED-IMPACT report is shown in Figure 4-1 as the red line. The thermal power calculated based on the inventories provided in the report is shown as the green line. The two curves are quite consistent which proves that the method for calculating thermal power based on inventories is correct. More specifically, it proves that the radionuclide shortlist is adequately selected and that the heat production data per disintegration (W/Bq) for these radionuclides are correct.

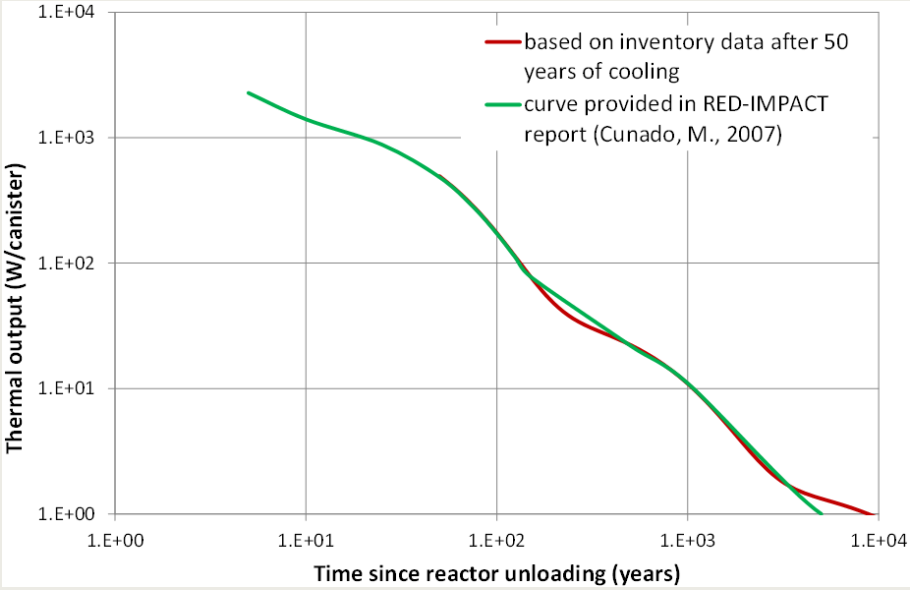

Figure 4-1. Comparison of calculated thermal output based on inventory data with thermal power provided in the RED-IMPACT report.

Next, the thermal power of Belgian HLW has been calculated. NIRAS provides several sets of radiological inventory data (EOL= 10 years):

(1) Inventory data provided by AREVA for already produced canisters (390 canisters);

(2) Inventory data calculated by NIRAS for already produced canisters (390 canisters);

(3) Inventory data calculated by NIRAS for canisters that could be produced in case of future reprocessing, denoted as 'provisions' (2830 canisters).

The evolution of heat production based on these datasets is given in Figure 4-2. The purple curve corresponds to the NIRAS data for produced canisters (2), the dark red curve corresponds to future provisions (3), and the red line corresponds to a weighted average of already existing and potential future canisters. The latter can be considered the reference inventory for Belgian vitrified high-level waste (VHLW) that is generally used in performance assessment calculations.

The green curve in Figure 4-2 corresponds to the heat production of VHLW based on the following formula derived by Put (Put and Henrion, 1992):

$$Q = \sum_i A_i \, e^{-\lambda_i t} \quad \text{(Q in W/tHM)}$$

where the coefficients A_i and λ_i were fitted to heat production data for vitrified waste arising from the reprocessing of spent fuel with a burn-up of 33 GWd/tHM. This heat output has been used in the thermal impact assessments for the near field (Weetjens and Sillen, 2005) and far field (Sillen and Marivoet, 2007) respectively.
The comparisons indicate that the fitted heat output is lower than the one corresponding to the inventory data calculated by NIRAS for existing canisters, especially in the longer term. Indeed, the inventory calculated by NIRAS using the FICAR tool (2) differs significantly in actinide content from the inventory data provided by AREVA (1). The agreement with the data provided in the RED-IMPACT project is rather good (see Figure 4-4).

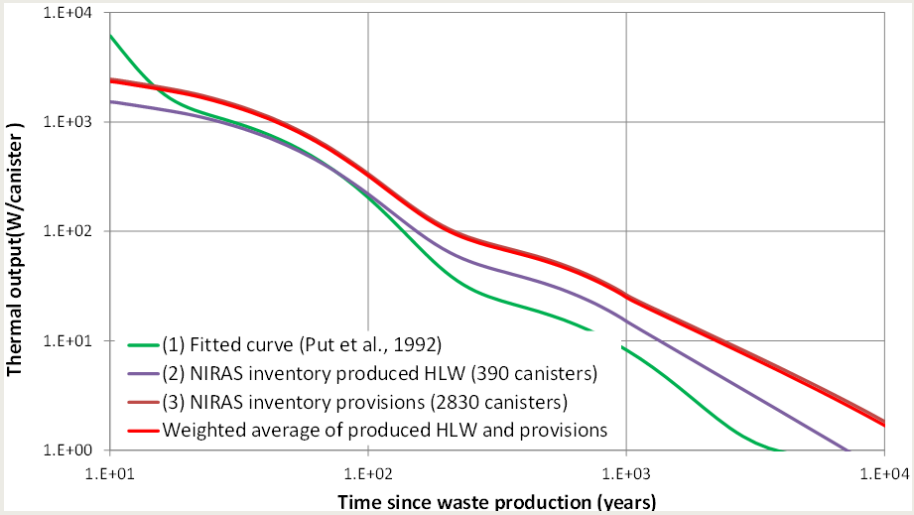

Figure 4-2. Thermal power calculated for Belgian vitrified high-level waste (VHLW).

4.1.2. HLW inventory provided by COVRA

The inventory data used to calculate the heat output for the Dutch VHLW (CSD-V) is based on empirical maximum values at production listed in appendix 6 of the OPERA-PU-NRG1112A report. The radiological inventory of part of the radionuclides is directly provided, while inventories for some isotopes needed to be calculated based on weight/canister (Table 4-1) (without specific information, the reference time of inventory data refers to EOL[b]=0 year).

For actinides, two cases are considered: one corresponding to average data and the other corresponding to average data+stdev. The thermal power for these two cases is compared and differences were found to be very limited. Therefore, in the following calculations, data based on average weights are used.

Table 4-1. Thermal power calculated based on weight.

	AVG.	
	g/canister	Bq/canister
U-234	0.15	3.55E+07
U-235	7.48	5.98E+05
U-236	3.65	8.64E+06
U-238	922.68	1.13E+07
Pu-238	0.28	1.78E+11
Pu-239	8.39	1.93E+10
Pu-240	3.72	3.13E+10
Pu-241	1.37	5.56E+12
Pu-242	0.92	1.33E+08
Cm-244	59	1.78E+14
Am-241	891	1.13E+14
Np-237	910	2.37E+10
Am-243	235	1.74E+12

[b] Reactor end-of-life.

The COVRA inventory of radionuclides relevant for heat production is given in Table 4-2, together with the Belgian reference VHLW inventory (NIRAS) and inventory data from the RED-IMPACT project (Cuñado, 2007).

Table 4-2. Lists of the inventory data used in the thermal power calculation.

	COVRA (EOL+0y)	NIRAS(*) (EOL+10y)	Red-Impact (EOL+50y)
Co-60	3.02E+12	6.37E+13	8.35E+10
Sr-90(+Y-90)	3.97E+15	4.71E+15	1.05E+15
Cs-137(+Ba-137m)	6.18E+15	6.86E+15	1.64E+15
Cm-244	1.78E+14	3.23E+14	3.76E+13
Pu-240	3.13E+10	1.12E+11	4.98E+11
U-236	8.64E+06	2.11E+07	1.25E+07
Am-241	1.13E+14	1.19E+14	4.68E+13
Np-237	2.37E+10	2.92E+10	1.78E+10
Pu-238	1.78E+11	3.17E+11	2.27E+11
U-234	3.55E+07	7.29E+07	6.55E+07
Th-230	0	7.33E+06	2.84E+06
Am-243	1.74E+12	2.72E+12	1.45E+12
Pu-239	1.93E+10	2.28E+10	1.60E+10
U-235	5.98E+05	1.27E+06	5.30E+05

(*) weighted average of produced (2) and potential future canisters (3).

The inventory of those elements which contribute significantly to the thermal power are compared in Figure 4-3.

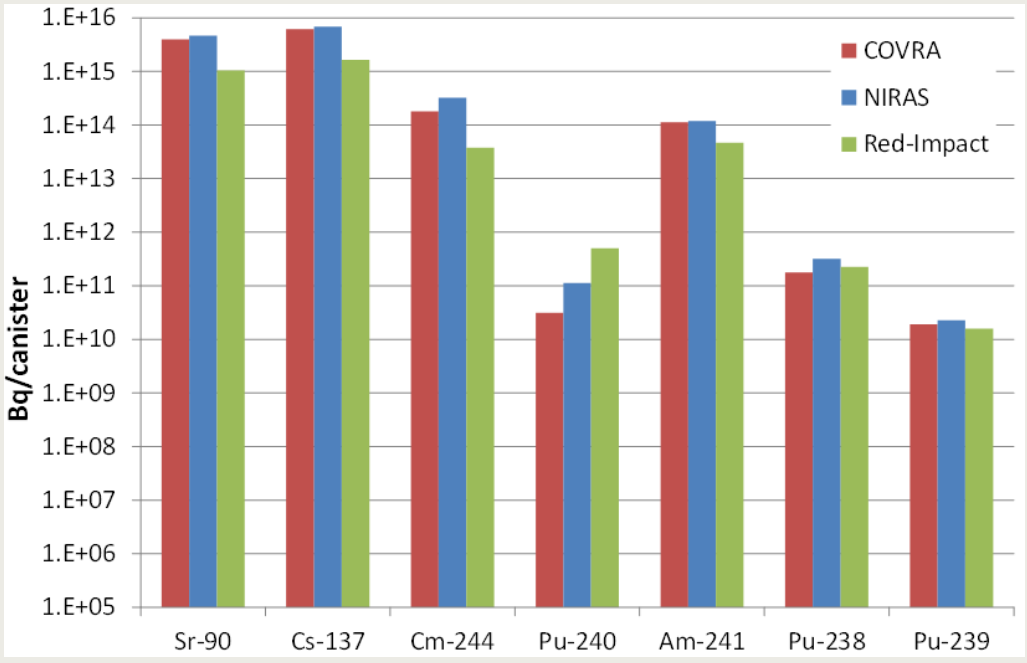

Figure 4-3. Comparisons of the inventory datasets for vitrified HLW from COVRA, NIRAS and the RED-IMPACT project.

The comparison of the power evolution from COVRA (two curves are provided: one is based on inventory calculations based on data in Table 4-2; the other is the heat power directly provided by COVRA); NIRAS (two curves are provided: one is calculated from the reference

inventory in Table 4-2; the other is the fit curve); and RED-IMPACT are illustrated in Figure 4-4.
The thermal power provided by COVRA (blue dashed one) is very consistent to the curve calculated based on the inventory. In the following temperature evolution calculation, the blue solid line is used.

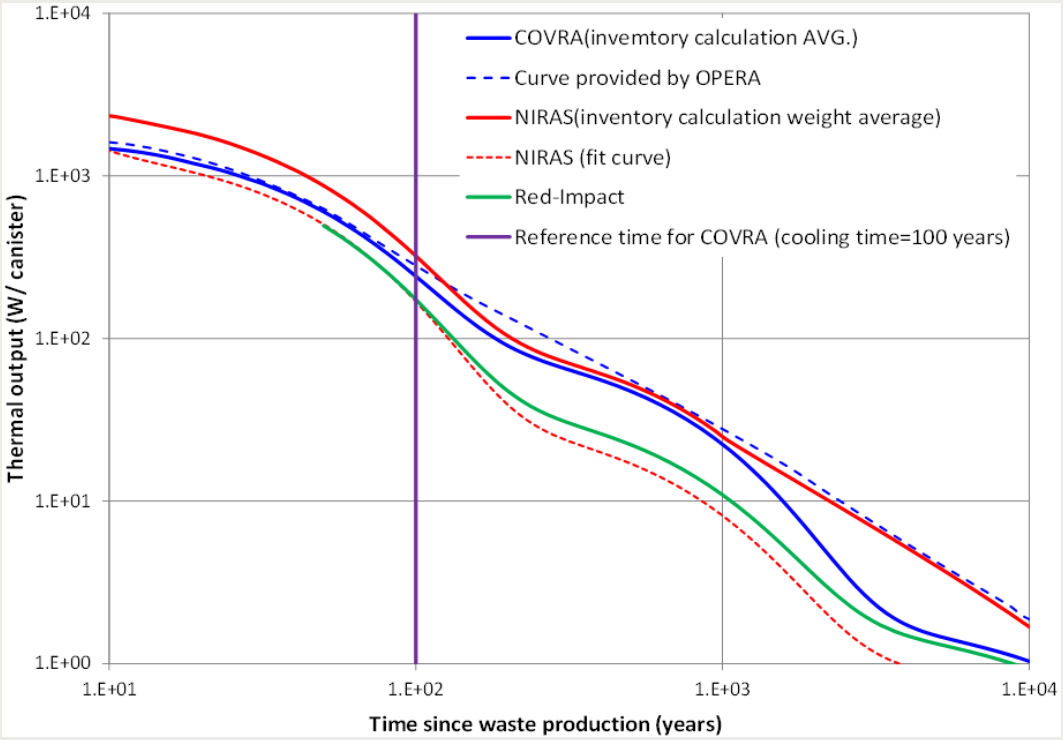

Figure 4-4. Comparisons of the thermal power for VHLW among COVRA, NIRAS and RED-IMPACT (EOL for NIRAS is 10 years, for COVRA and RED-IMPACT 0 and 50 years, respectively).

4.1.3. Temperature evolution calculation in case of HLW disposal in Boom Clay for the Dutch disposal concept

The temperature evolution is calculated using COMSOL Multiphysics 3.5a (COMSOL, 2008). The geometries and material properties are assumed to be the same as for the Belgian disposal design (Weetjens and Sillen, 2005) as depicted in Figure 4-5.
COVRA considers a cooling period of 100 years before disposal. The temperature **increment** evolution at six observation points (distances to the center line of gallery are 0.283, 0.308, 1.014, 1.5 ,1.8, 2.8 m, respectively) are shown in Figure 4-6.

Figure 4-5. Temperature increment (ΔT) field after 6 years since waste disposal. The X axis represents the distance from the gallery into the Boom Clay. 2D axisymmetric COMSOL model is used for temperature calculations. Because of symmetry rules, only half a supercontainer needs to be modelled. Interactions between waste canisters are negelected in the modelling.

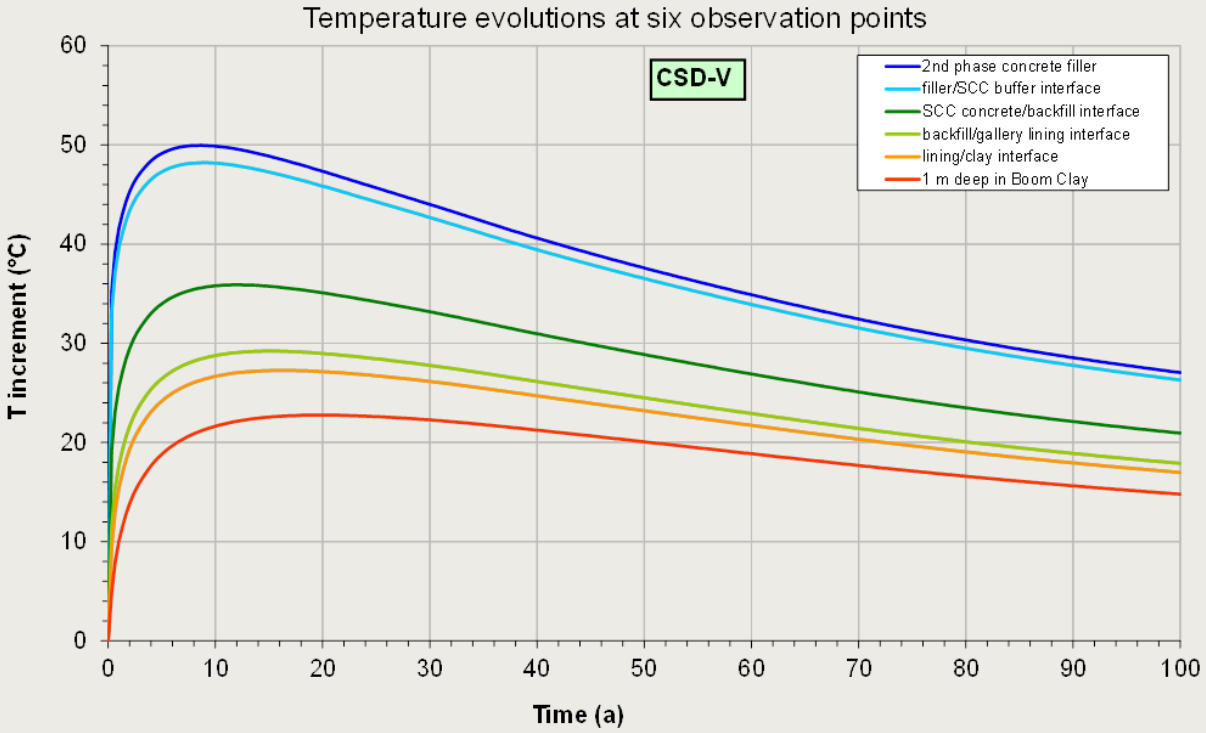

Figure 4-6. Evolution of ΔT at six observation points for CSD-V (cooling time of 100 years).

4.2. Evolution of water saturation of the concrete buffer

The resaturation analysis consists of a non-isothermal hydraulic analysis based on a 1D axial model geometry. The initial saturation degree of the backfill and buffer is assumed to be 80% and the buffer has a low permeability similar to that of the Boom Clay. A detailed description of the system can be found in Weetjens and Sillen (Weetjens and Sillen, 2005). The current analysis is carried out using Code_Bright (Olivella, et al, 1996), which is capable of considering vapour transport which is transformed from pore water under the thermal loading. The simulation considers two years of re-equilibration of water pressure after the excavation. Thereafter, the waste is emplaced and the disposal tunnels are backfilled. The results (shown in Figure 4-7 and Figure 4-8) indicate that the system becomes become fully water-saturated soon after the disposal tunnels are backfilled.

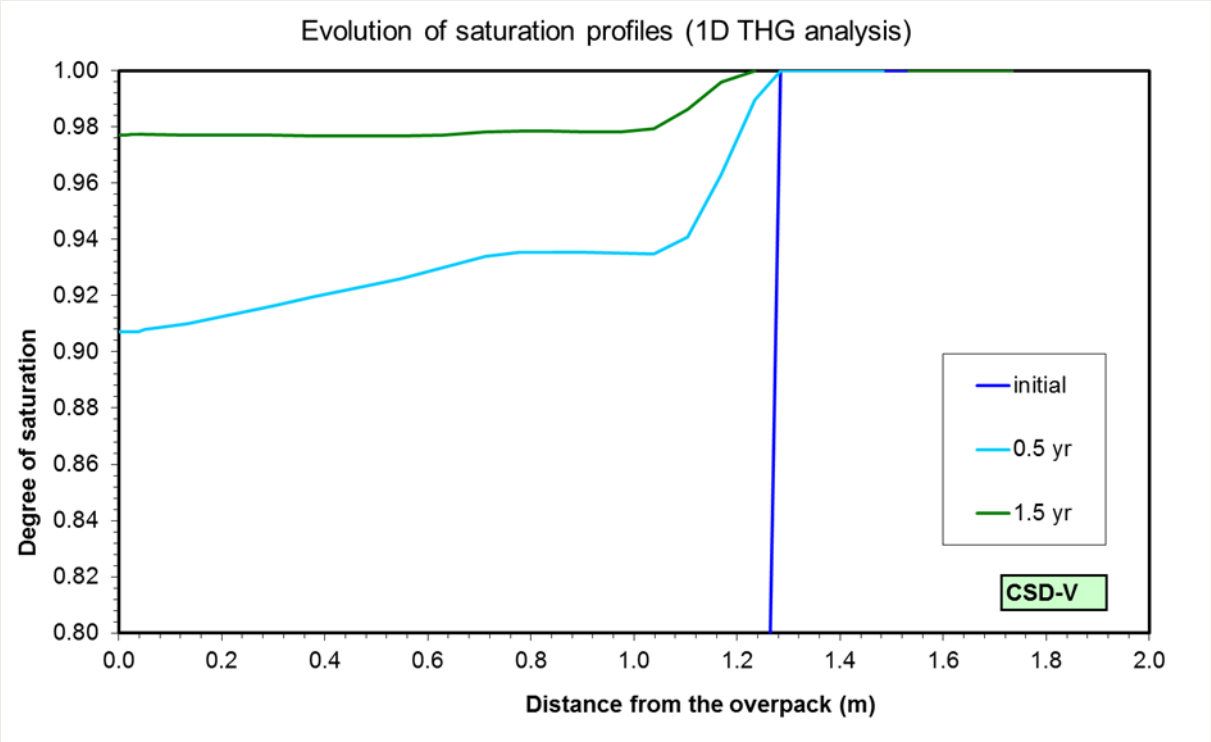

Figure 4-7. Evolution of the saturation profile at different time intervals (initial time refers to two years after excavation and backfilling the disposal tunnels).

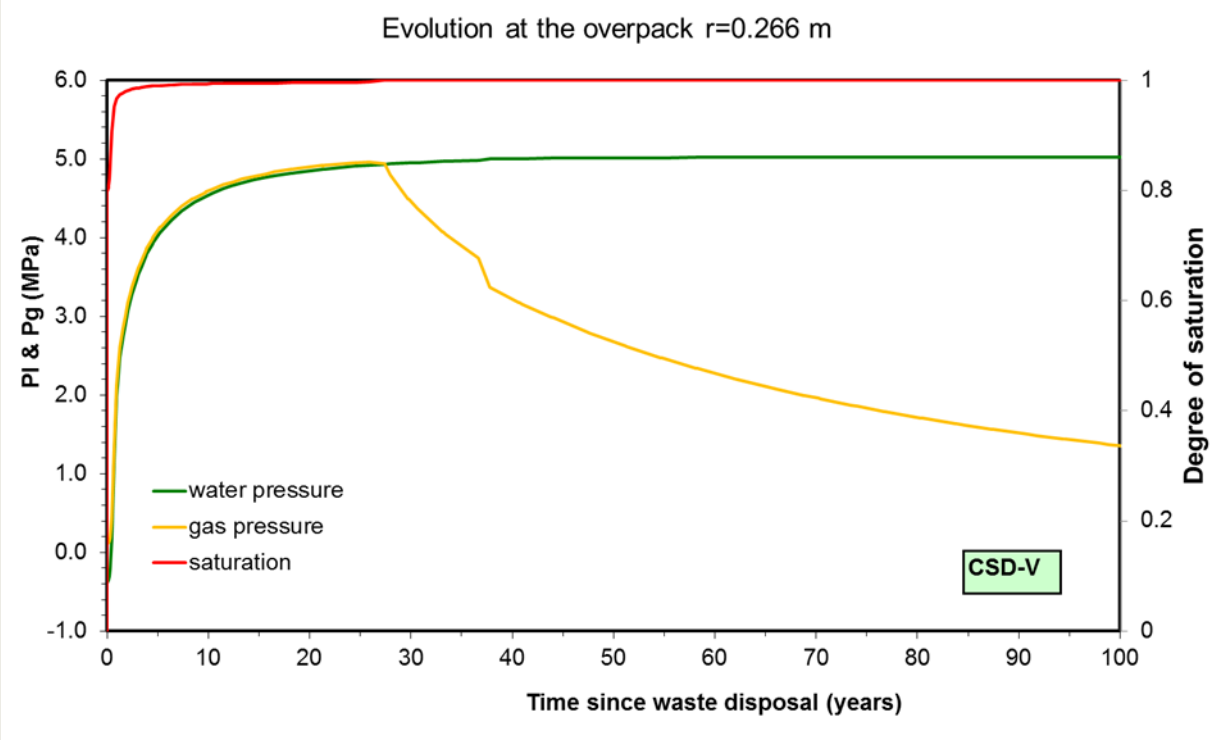

Figure 4-8. Evolution of water pressure, gas pressure and water saturation at the overpack surface.

4.3. Evolution of pH of the concrete pore solution

4.3.1. Reference clay porewater composition

The reference porewater composition of the Boom Clay formation, located in the Netherlands, used in the calculations is based on the data reported in Table 4-1 of the report of Behrends and co-workers (Behrends, et al, 2015). For clarity of this section, we repeat this table in Table 4-3.

Table 4-3. Chemical composition of solution retrieved by mechanical squeezing from core sample 101 (slice 17 and 18), 104 (slice 9 and 11), and 103 (slices 11, 12 and 13). Errors indicate the variation between duplicate measurements. Evaluation of the calibration with independent standards were in the range of ± 5%. Measured concentrations are compared to those reported for Boom Clay pore water in Mol (De Craen, et al, 2004) and in Essen (De Craen, et al, 2006). For comparison, also the seawater composition according to Appelo and Postma (Appelo and Postma, 2005) is listed. This table is a copy of Table 4-1 of the report of Behrends and co-workers (Behrends, et al, 2015).

	Seawater	Sample 104	Sample 101	Sample 103	Boom Clay in Mol	Boom Clay in Essen
Na [mM]	485	443** ± 3	237** ± 4	133.1 ± 0.1	15.6	56
Cl [mM]	566	546** ± 2	408** ± 5	394.0 ± 0.1	0.5	44.1
S [mM]	29	65** ± 2	57** ± 1	3.9 ± 0.1	0.02*	4.2*
K [mM]	11	15.95** ± 0.02	10.4 ± 0.2	3.7 ± 0.2	0.2	0.7
Ca [mM]	11	47.0 ± 0.1	60.4 ± 0.7	69.7 ± 0.1	0.04 – 0.2	0.9
Mg [mM]	55	51.7 ± 0.3	42.3 ± 0.5	58.4 ± 0.1	0.05 – 0.2	2
Fe [µM]		297 ± 1	746 ± 12	3260 ± 0.1	6 - 50	70
pH	7.5 – 8.4	3.05***	3.17***	6.7***	8.3 – 8.6	8.3 – 8.6
Alkalinity [meq/L]	2.47			0.55		

* SO_4^{2-} concentration.
** concentrations exceeded the calibration range and might have an error > 5%.
*** not representative for in situ porewater due to acidification during collection for sample 104 and 101; for sample 103, a thicker rubber stopper was applied and may represent in situ porewater.

Based on the report of Behrends and co-workers (Behrends, et al, 2015), the porewater compositions determined by mechanical squeezing and leaching are very different so it is difficult to decide which to use. We choose to use the compositions from the squeezing experiments because the leaching data are lacking model interpretations with respect to cation exchange reactions. From our experiences, leaching clay samples will unavoidably perturb the original chemistry in terms of cation exchange and mineral solubility so a model interpretation is needed to reconstruct the porewater composition. Also from our experiences, mechanical squeezing is a reliable method to extract porewater composition that is representative for the original conditions. This is especially true for the major ion concentrations. Among the water samples from the three cores used for squeezing, sample 104 and 101 had a very low pH around 3 suggesting a severe acidification which might be due to oxidation of pyrite. The ratio of SO_4^{2-}/Cl in these two samples is above 0.1, which is more than a factor 2 higher than the one in seawater (0.05). This might have been caused by pyrite oxidation and the release of SO_4^{2-}. The porewater of sample 103 has a pH of 6.7, which is still a bit too low but more likely representative for the type of clay water in Boom Clay with a relatively high salinity, for example the water at Essen, Belgium. For this reason, we choose the water of sample 103 as the reference composition. However, it is also noticed that the water of sample 103 has a much lower salinity than that of sample

104. Although the porewater pH of sample 104 is questionable, the chloride content of sample 104 is quite high and as chloride is a conservative anion and an good indicator of water salinity, the water composition of sample 104 might also be representative except for the pH value. We thus also use the porewater composition of sample 104 to test the effect of salinity. As the pH of 3.05 is too low and causes disability of clay minerals, a pH value of 6.7 (the same as the one in the sample 103), is used.

The concentrations of Si, Al, and inorganic carbon (except the water sample 103 where the alkalinity is measured) were estimated by assuming a chemical equilibrium with quartz, kaolinite, and calcite, because the data of these concentrations was lacking at the time of writing the report. In practice, however, the dissolved concentrations of these elements in the porewater are calculated by solubility of these minerals in the porewaters of samples 104 and 103. These data are needed for calculating the cement/clay interactions as these elements are part of the basic constituents of cementitious materials.

4.3.2. Chemical evolution at 25°C controlled by equilibrium reactions and diffusion

At this stage no fully coupled thermal-chemical-transport simulation is performed, but a 1D radial chemical diffusive simulation at 25°C is carried out to scope the status of chemical evolution as a function of time assuming that diffusion at 25°C does not differ significantly from diffusion under higher temperatures (up to 50°C, which is the maximum T increment as given in Figure 4-6). This 1D radial chemical diffusive simulation is similar to that used by Wang (Wang, 2006) in the Belgian concept.
The aim is to see if the duration of the thermal phase is long enough to cause a significant change at the overpack/cement interface, where the pH evolution is required for assessing the corrosion rate. The rationales are: if the duration of the thermal phase is short, and within the time span during which the chemistry of the interface of our interest remains unchanged, then the simulation can be done by decoupling the thermal and chemical processes. If however, a significant change in chemistry is observed at the interface within the considered thermal phase, then a fully coupled simulation is probably needed to accurately assess the pH evolution at the interface. Such fully coupled simulation is possible but more complicated to be implemented.

Figure 4-9 presents the results of pH evolution (as indicator of the chemical characteristics of the interface) as a function of time, assuming a constant concentration of the inlet porewater (103 and 104 respectively) diffusing into the cementitious near field.

It is seen, from Figure 4-9, that the pH at the overpack/cement interface (left side of the plots, which corresponds to ~0.2 meters from the center of the waste canister) is around 13.45 which is very close to the original state I pH of 13.5 suggesting that the chemistry at the interface has not changed significantly, certainly not after 100 years of diffusion. Towards the cement/clay interface (right side of the plots), however, the pH decreases to around 10 because of the effect of the neutralization reactions by the inlet clay porewaters.

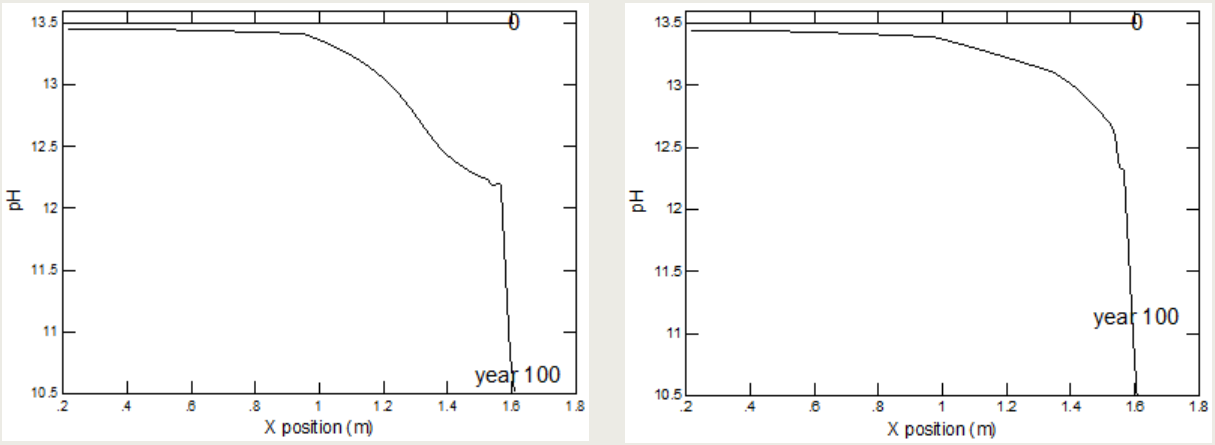

Figure 4-9. Calculated pH in a cementitious near field at 25°C after 100 years diffusion of clay porewaters into the cement buffer (left: porewater composition of sample 103; right: porewater composition of sample 104).

The results of Figure 4-9 demonstrates that after 100 years the cement near the metallic overpack is still intact and not yet degraded to a significantly extent. The chemistry at the overpack/cement interface is still well buffered by the state I cement so the pH evolution can be estimated by calculating the cement chemistry at state I under an elevated temperature. Note that the simulated pH drop in Figure 4-9 should be considered as being much faster than in reality since the model neglects the phenomenon of porosity clogging due to carbonation, i.e., the neo-formation of calcite as the result of clay water/cement interaction. Figure 4-10 shows the saturation indices (SI) of calcite in the near field and as can be seen the SI is significantly larger than 1 in the near field, suggesting the precipitation of calcite. The consequence of neo-calcite formation is a decrease of the porosity resulting in a much slower ingress of clay water into the near field compared to the cases shown in Figure 4-9, where no clogging is considered. Wang (Wang, 2006) predicted that if clogging is taken into account, a completely clogged near field in the case of Boom Clay at Mol, Belgium is formed and in that case diffusion of clay water stopped so the near field would remain intact shortly after the closure of the repository.

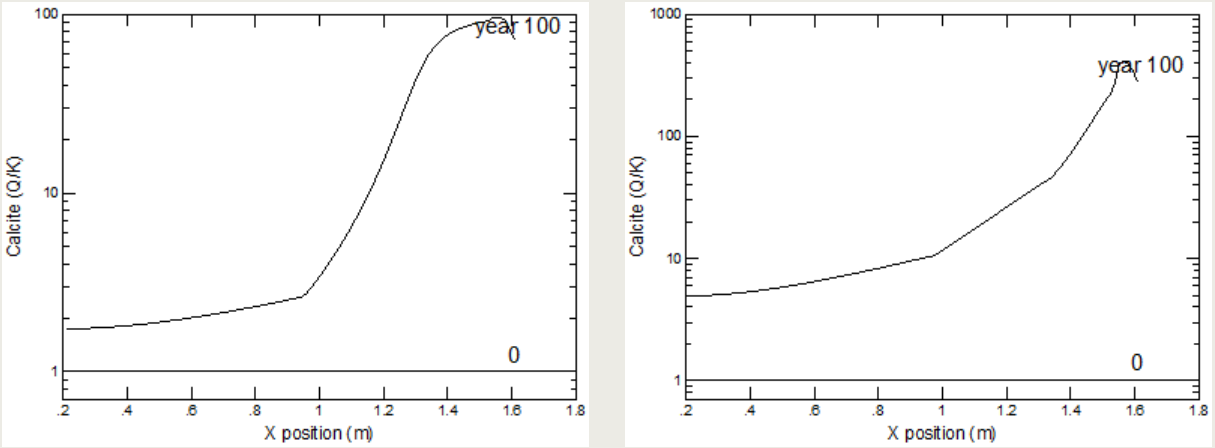

Figure 4-10. Calculated saturation indices for calcite in a cementitious near field at 25°C after 100 years diffusion of clay waters into the cement buffer (left: porewater composition of sample 103; right: porewater composition of sample 104).

4.3.3. Estimated evolution of pH at the overpack/cement interface as a function of temperature and time

The results of the pH evolution calculations at the overpack/cement interface are given in Figure 4-11. Figure 4-11(a) shows the evolution of the pH during the initial thermal phase (short term), where temperature effects may play a role (introduction of the radioactive waste will initially cause a temperature increase and the subsequent decay of the radioactive waste will lead to a decrease of temperature). The results for the long term evolution (10^5 years) are given in Figure 4-11(b).
The pH evolution calculation at the overpack/cement interface is based on the state I cement chemistry calculations, considering the temperature evolution given in Figure 4-6 (only the data of 2nd phase concrete filler are considered). Because the results given in Figure 4-6 are temperature increments, it is necessary to know the original temperature of the clay formation where the cores were drilled. According to Behrends and co-workers (Behrends, et al, 2015), no clear indication about the in situ temperature of the clay is available, but 26°C was given as the temperature for the laboratory leaching experiments. Therefore, 26°C is used as the in situ temperature to calculate the temperature evolution in the near field. The distance between the center of the waste canister and the 2nd phase concrete filler is 0.283 meters (i.e. the position at the overpack/cement interface).

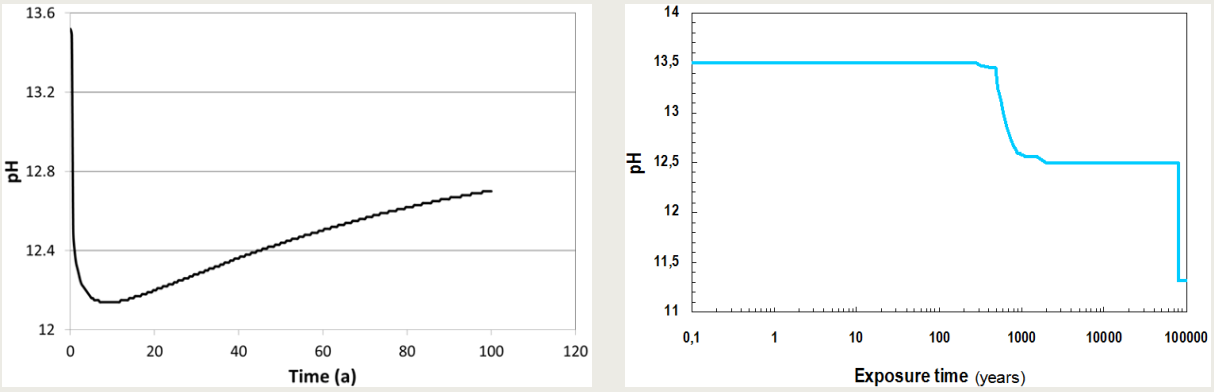

(a) *(b)*

Figure 4-11. pH evolution at the overpack/cement interface as a function of time after closure of the repository: thermal phase (left) and long term (right).

The pH at the overpack/cement interface at the beginning of the thermal phase is around 13.5, controlled by the dissolved alkalis (Na and K) (see Figure 4-11(a)). As temperature increases, according to the results shown in Figure 4-6, the pH decreases and reaches a minimum value of 12.14 after 9 years (when temperature reaches its highest value of 50°C). The process controlling this pH evolution is the dependence of pH on temperature. More precisely, it is due to the dependence of the water hydrolysis constant on temperature. Such dependence is reflected by the change in the value of the water stability constant with temperature. In the present case and in the temperature range concerned, the pH is inversely correlated to temperature, i.e., the higher the temperature the overpack/cement interface becomes, the lower the pH is in the pore water.
One may expect that when the temperature at the interface decreases back to the original one of 26°C, the pH of the interface will become 13.5 again, if the cement is still at the state I. As the thermal phase is quite short in this case, it is highly likely that the cement at the overpack/cement interface remains intact and a high pH condition will be resumed after the thermal phase.

Since then on, the pH of the interface will evolve under an isothermal condition at ambient temperature. When the concrete buffer gets depleted in Na- and K-oxides (after ~1,000 years), portlandite will determine the pH at a value of 12.5 (see Figure 4-11(b)).

The pH of 12.5 is predicted to persist for at least 80,000 years, after which it will drop to a value of 11.3.

The pH evolution calculations are very conservative because of the following two reasons:

- an infinite dilution boundary condition is directly applied at the concrete/clay interface, neglecting transport limitations in the Boom Clay;
- an unrealistically low rate constant is applied to make calcite inert. In reality, however, calcite precipitation is likely to occur as a result of calcium reacting with the in-diffusing dissolved CO_2 from the Boom Clay pore water. Calcite precipitation could lead to pore clogging in the first centimetres of the buffer, so that the time needed for exhausting the alkalis and portlandite would prolong substantially. As such, it is expected that a high pH of 12.5 could be maintained for much longer than 80,000 years;

4.4. Evolution of chemical composition of the concrete pore solution (aggressive species)

4.4.1. Input parameters

4.4.1.1. Porewater composition of Dutch Boom Clay

The chloride and sulphate concentrations of the undisturbed Dutch Boom Clay porewater used in the transport calculations are based on the data reported in Table 4-1 (Sample 103) of the report of Behrends and co-workers (Behrends, et al, 2015). This corresponds to 3.94×10^{-1} and 3.9×10^{-3} mol/L for Cl^- and SO_4^{2-}, respectively. The reasoning for chosing this pore water composition is discussed in detail in section 4.3.1. Thiosulphate and sulphide species are not expected to be present in undisturbed Boom Clay porewater (De Craen, et al, 2004). No reactions of the aggressive species with concrete or clay componennts are included in the calculations.

The expected composition of the perturbed Dutch Boom Clay porewater diffusion towards the overpack's surface is given in Table 4-4. The chloride concentration in the excavation disturbed zone (EDZ) is set to the highest value found in Table 4-1 of the report of Behrends and co-workers (Behrends, et al, 2015). The sulphate and thiosulphate concentrations are chosen based on analysis of *in situ* collected porewater (piezometers) with subsequent laboratory measurements (Van Geet, et al, 2006a; Van Geet, et al, 2006b; Van Geet, et al, 2006c) and scoping calculations (Wang, 2006; Van Geet, et al, 2006a). They correspond to the worst case, which lists all maximum concentrations ever observed in Boom Clay (not necessarily measured in the same water sample).

Table 4-4. Input concentrations of perturbed Dutch Boom Clay porewater (worst ever measured).

Aggressive specie	**Worst conc. ever measured**	
	mol/L	mg/L
Cl^-	5.46E-1	19 328
SO_4^{2-}	2.15E-1	20 600
$S_2O_3^{2-}$	9.50E-3	1 070
HS^-/S^{2-}	4.70E-3	150

Also, two additional sulphide concentrations are used: 500 mg/L (15.7 mmol/L) and a worst case concentration

- for the worst case concentration, it is assumed that all pyrite in the EDZ (a 1 m zone[c] around the concrete gallery lining) will be oxidized into sulphate and that all sulphate will be transformed into sulphide by microbial activity. As Boom clay contains about 1 wt% pyrite and the bulk concentration of clay is 1600 kg/m^3, a sulphide concentration in the liquid phase of the EDZ of 19 420 mg/l (609 mmol/l) is obtained. As sulphide compounds are highly insoluble, it is doubtfull that this concentration will even be possible;
- an arbitrary concentration of 500 mg/L (15.7 mmol/L) is chosen as an intermediate value;

4.4.1.2. Transport parameters (pore diffusion coefficients, effective porosity)

Table 4-5 contains the transport parameters for the four aggressive species used as input for the calculations. The pore diffusion coefficient, D_p, for chloride, sulphide, sulphate and thiosulphate in concrete are set to the value of 3.83E-11 m^2/s. This is the D_p value of Cl for intact concrete that was used in the safety calculations for the Belgian Category A programme (Seetharam, et al, 2011). Another, more pessimistic calculation case assumes that all concrete is in a degraded state, and a higher D_p value of 2.03E-10 m^2/s is used, again in accordance with values from the Belgian Category A programme. The same goes for the porosity values used in both cases, which are also given in Table 4-5.

Best Estimate values for pore diffusion coefficients and effective porosity in Boom Clay are given in Table 4-6. Dp of Selenate[d] in Boom Clay has been used for the transport parameters of the (thio)sulphate species, and iodide has been used for sulphide and chloride.

As some anions (e.g. Cl^- and I^-) are (strongly) retarded by concrete phases by either sorption or precipitation processes (Seetharam, et al, 2011), this could also be the case for sulphide, sulphate and thiosulphate. This could delay the arrival of these species at the overpack with many thousands of years. Sorption and solubility limits in the concrete phases, EDZ and near field clay have been conservatively neglected for all species in the present calculations.

Table 4-5. Transport parameters (pore diffusion coefficient, D_p, and effective porosity) in intact and degraded concrete.

Aggressive specie	Intact concrete		Degraded concrete	
	D_p (m^2/s)	Porosity (-)	D_p (m^2/s)	Porosity (-)
Cl^-	3.83E-11	0.097	2.03E-10	0.31
$SO_4^{2-}/S_2O_3^{2-}$	3.83E-11	0.097	2.03E-10	0.31
HS^-/S^{2-}	3.83E-11	0.097	2.03E-10	0.31

[c] Excavation of the disposal tunnels will lead to fracturing of the Boom Clay host rock formation up to a depth of about 1 meter.
[d] If fact, migration parameters for selenate are determined using sulphate-ions.

Table 4-6. Transport parameters (pore diffusion coefficient, D_p, and effective porosity) in Boom Clay.

Aggressive specie	Boom Clay	
	D_p (m^2/s)	Porosity (-)
Cl^-	1.4E-10	0.16
$SO_4^{2-}/S_2O_3^{2-}$	3.2E-11	0.10
HS^-/S^{2-}	1.4E-10	0.16

4.4.2. Predicted transport calculation of aggressive species through the concrete buffer

The transport calculations of the aggressive species (chloride, sulphate, thiosulphate, sulphide) through the concrete buffer of the Supercontainer are performed with COMSOL Multiphysics 3.5a, Earth science module (COMSOL, 2008). A 1-dimensional axisymmetric geometry is used to simplify the computer simulations. The calculations incorporate diffusive transport and advective flow driven by the pressure gradient at repository depth as potential transport processes. A schematic representation of the computational domain is given in Figure 4-12.

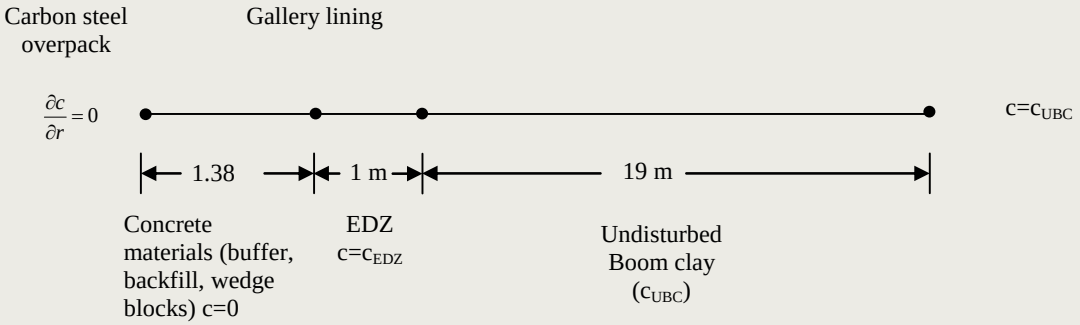

Figure 4-12. Computational domain and boundary conditions.

All cementitious materials (buffer, cementitious backfill material and concrete gallery liner) are considered to have similar properties and will be treated in the same way. This is based on the fact that most relevant concrete compositions for the disposal facility all use ordinary Portland cement (OPC) and calcareous aggregates in similar amounts. The dimensions are based on the models used in the scoping calculations for the Belgian Supercontainer design (Govaerts and Weetjens, 2010).

Because the 1D thermo hydraulic analysis of the resaturation time of the concrete materials pointed out that the concrete will resaturate almost completely (up to 95 – 98%) after already one to five years (see section 4.2., Figure 4-7), the concrete materials are assumed to be completely saturated from the start in order not to unnecessarily complicate the calculations. It could also be concluded from the work of Govaerts and Weetjens (Govaerts and Weetjens, 2010) that because of the fast equilibration and resaturation of the system, there are little differences observed when explicitly including the effect of the resaturation of the concrete on the transport of aggressive species towards the overpack.

The following initial and boundary conditions are considered in the calculations (see Figure 4-12):

- a non-flux condition for concentration is imposed at the overpack;
- all concentrations in the concrete region are set to zero;
- concentrations in the EDZ are initially at the values mentioned in Table 4-4;
- concentrations in the undisturbed Boom Clay are initially equal to the undisturbed Boom clay concentrations (UBC);
- concentrations at the Boom clay outer radial boundary are fixed to the initial undisturbed Boom clay concentrations;

Two cases are calculated:

- Case A: assuming that the concrete materials are intact and the migrations properties are favourable for preventing the ingress of the aggressive anions;
- Case B: assuming that the concrete materials are degraded and the migrations properties are not favourable for preventing the ingress of the aggressive anions;

Case A

Breakthrough curves of chloride, sulphate, thiosulphate and sulphide (with initial low, medium and high concentrations) are shown in Figure 4-13.

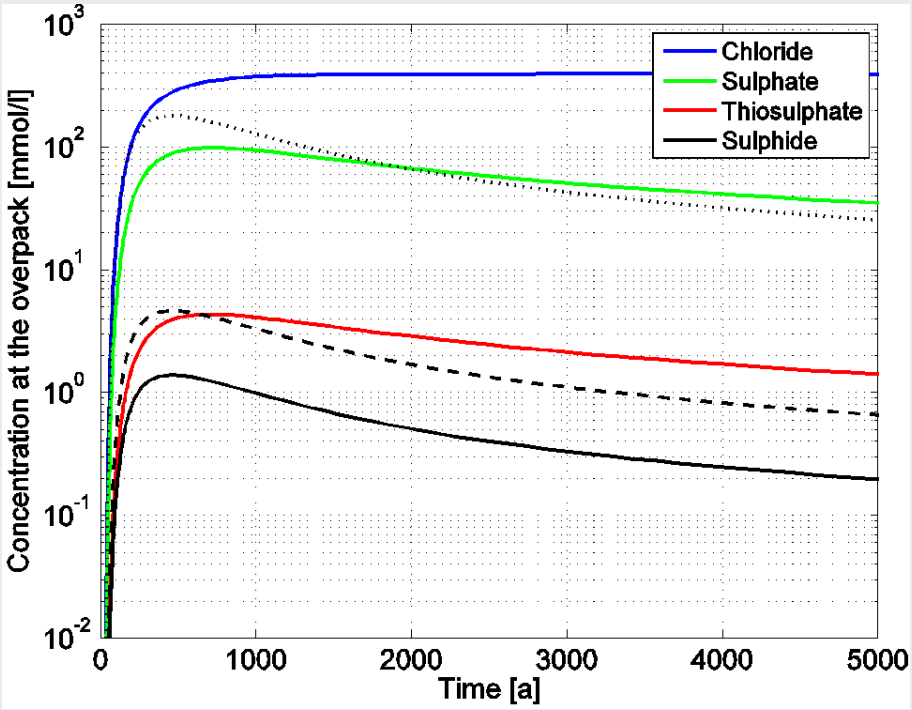

Figure 4-13. Concentration evolution of the aggressive species at the overpack for Case A with (—) low, (— —) mediam and (· · ·) high initial sulphide concentration.

These calculations show that the chlorine concentration at the overpack will approach the Rupelian Clay background concentration after a period of about 2000 years. The maximum sulphide concentrations at the overpack are reached after 500 years due to indiffusion from the EDZ into the concrete and will then slowly decrease due to outdiffusion towards the boundary of the clay. The same behaviour can be observed for sulphate and thiosulphate but the maximum occurs slightly later (700 years) and the decrease after the occurrence of the maximum concentration is less steep due to the lower diffusion coefficient in clay.

Case B

In the second calculation, all concrete materials are assumed to be severely degraded, which is reflected in a higher value of the porosity and the diffusion coefficient. Breakthrough curves of chloride, sulphate, thiosulphate and sulphide (with initial low, medium and high concentrations) are shown in Figure 4-14.

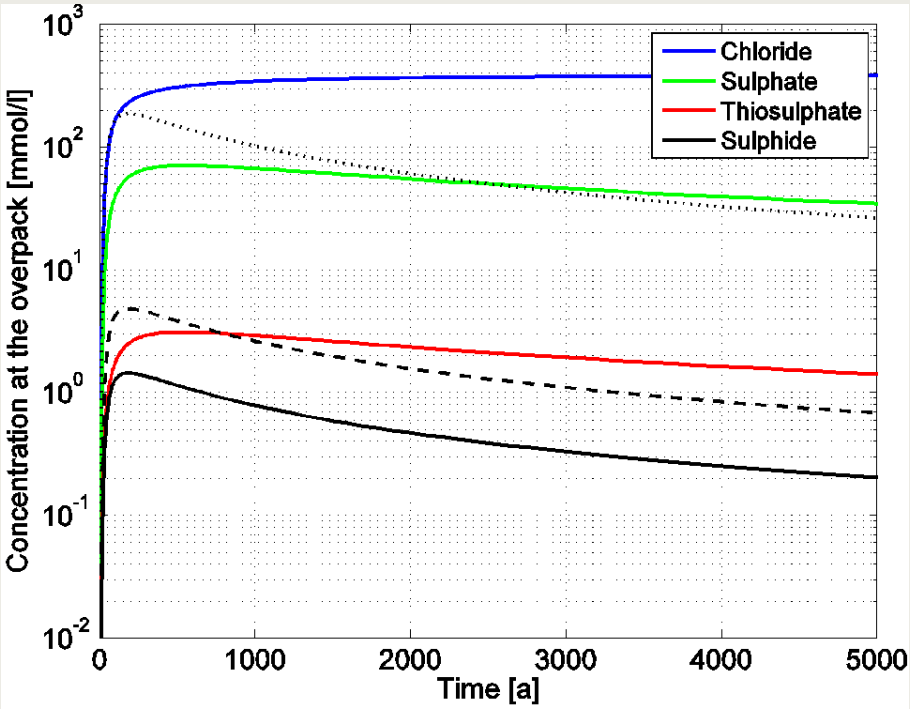

Figure 4-14. Concentration evolution of the aggressive species at the overpack for Case B with (—) low, (— —) mediam and (· · ·) high initial sulphide concentration.

The maximum sulphide concentrations at the overpack are already reached after 185 years due to the higher diffusion coefficient in the concrete and are also slightly higher compared to the ones obtained in case A. Maximum sulphate and thiosulphate also occur at earlier times, but are slightly lower compared to case A. This is due to the larger difference in effective porosities between concrete (0.31) and clay (0.10) in this case, which forces the amount of (thio)sulphate, initially present in the EDZ, to be distruted over a larger pore volume of the concrete. This effect is less important in the case of sulphide due to the larger effective clay porosity (0.16). Chlorine concentrations will reach the level of the background undisturbed, although it will take slightly more time compared to case A, due to the larger pore volume that needs to be filled.

The maximum concentrations and their time of occurrence are summarized in Table 4-7.

Table 4-7. Maximum concentrations and their time of occurrence reached at the overapck.

Aggressieve specie	Case A		Case B	
	Concentration (mmol/L)	**Time** (year)	**Concentration** (mmol)	**Time** (year)
Cl^-	394	>2000	394	>3000
SO_4^{2-}	98.9	700	70.9	540
$S_2O_3^{2-}$	4.3	700	3.1	540
HS^-/S^{2-} (low)	1.4	467	1.4	185
HS^-/S^{2-} (medium)	4.6	467	4.8	185
HS^-/S^{2-} (high)	180	467	187.3	185

5. Corrosion rate data reported in the literature

Since the start of the twentieth century, reinforced concrete has been used extensively for a variety of building and civil engineering applications, thus becoming the most versatile constructional material available. However, with its ever-increasing use, cases of premature collapse of reinforced concrete structures due to the corrosion of the steel reinforcement has increasingly been identified. The number of studies of corrosion of steel reinforcements in concrete rose steadily since the 1970s to meet the demand of the building companies to cope with the corrosive effects of chlorides (used as de-icing salts). This widespread research on corrosion of steel reinforcements has led to a vast amount of uniform corrosion rate data in cementitious environments.

Besides building and civil engineering applications, reinforced concrete is a structural material that is widely used in the nuclear industry:

- in power plants, for components containing iron/concrete interfaces;
- in the context of nuclear waste storage (low level waste, LLW, and intermediate level waste, ILW, waste disposals) for various purposes such as cell structures and some types of radioactive waste containers;

Relevant uniform corrosion rate data reported in the literature originate from studies in the framework of various national nuclear waste management programmes and studies for industrial applications:

- nuclear waste management programmes
  - the UK Nirex Safety Assessment Research Programme (NSARP);
  - the Swiss Nagra's crystalline rock programme;
  - the Swedish SKB's research programme;
  - the Japanese H-12 Project studies;
  - the Spanish ENRESA research programme;
  - the French CIMETAL research programme;
  - the Belgium Ondraf/Niras RD&D programme;
  - miscellaneous nuclear waste management studies (Germany, South Korea);
- non-nuclear waste management literature (industrial applications);

In this report, the uniform corrosion rate data found in the literature are classified according to the change of the environmental conditions, surrounding the carbon steel overpack, in time from oxidising to reducing, *viz*. aerobic alkaline media and anaerobic alkaline media. After all, the aerobic and anaerobic period have been identified as the two major periods in the course of the Corrosion Evolutionary Path (CEP).

A more detailed summary of the corrosion rate data relating to the corrosion of carbon steel in alkaline media is presented elsewhere (Kursten, to be published).

5.1. Aerobic alkaline environments (solutions + concrete)

The corrosion rate data in alkaline media under oxic conditions reported in the literature largely originate from the non-nuclear waste management literature, such as studies initiated by the various State Departments of Transportation (DOTs) of the U.S. in an effort to find improved (*i.e.* better corrosion-resistance to cost ratio) reinforcement alternatives to carbon steel for bridge deck applications (chloride-contaminated concrete from de-icing salts), supplemented with independent studies from other industrial applications. Few data is obtained from studies performed in various national nuclear waste management programmes (LLW and ILW).

Figure 5-1 summarizes the corrosion rate data reported in the non-nuclear industrial and nuclear waste management literature for carbon steel in oxic and alkaline chloride-free solutions. Corrosion rates in the range from 0.1 to ~10 µm/year have been reported for temperatures up to 80°C in environments that are most relevant for the concrete buffer environment inside the Supercontainer (*i.e.* in the pH range 12-13).

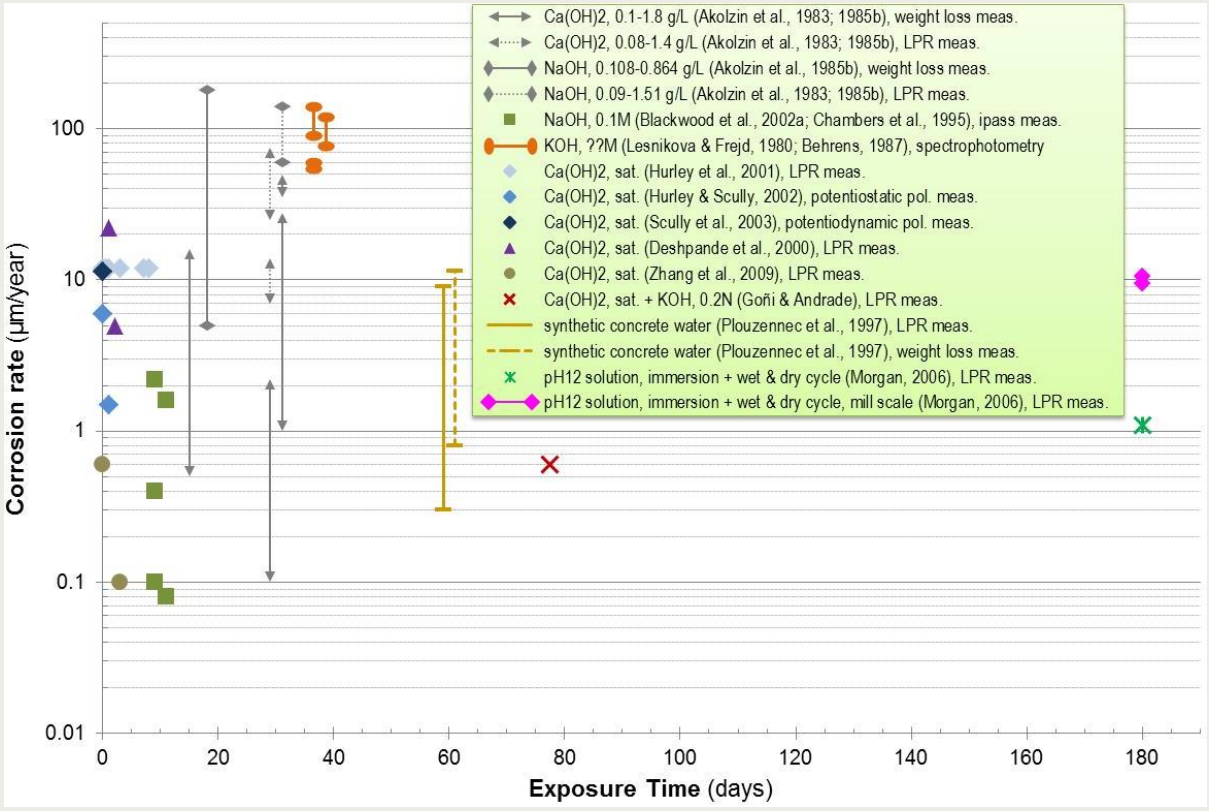

Figure 5-1. Compilation of uniform corrosion rates (reported in the non-nuclear industrial and nuclear waste management literature) for carbon steel in oxic and alkaline chloride-free solutions representative for the Supercontainer (i.e. pH ~ 12–13.5).

Akolzin et al. (Akolzin, et al, 1983; Akolzin, et al, 1985b) reported high corrosion rates up to 180 µm/year. The highest corrosion rates (between ~20 and 180 µm/year) were measured in $Ca(OH)_2$ solutions with a concentration of <0.8 $g{\cdot}L^{-1}$ and in NaOH solutions with a concentration of <0.76 $g{\cdot}L^{-1}$. These high corrosion rates can be directly linked to the composition of the testing solutions, which were too dilute to provide adequate protection of the steel from corrosion and can therefore be considered as corrosion rates under an active corrosion regime. For comparison, concrete pore water is often simulated (in the laboratory) by a saturated $Ca(OH)_2$ solution, which corresponds to a $Ca(OH)_2$ concentration of 1.5 $g{\cdot}L^{-1}$ or higher.

High corrosion rates (50–140 µm/year) were also reported by Lesnikova and Frejd (Lesnikova and Frejd, 1980). However, experimental details (e.g. the concentration of the KOH test solutions) were not given in this reference. And moreover, they used a rather dubious method (the method has not been used by any of the other investigators): the corrosion rate was calculated from the amount of dissolved iron that was measured spectrophotometrically.

Hurley and co-workers (HURLEY, et al, 2001; Hurley and Scully, 2002; Scully, et al, 2003) published a vast amount of corrosion rate data in a saturated $Ca(OH)_2$ solution that were either obtained from potentiostatic or potentiodynamic polarisation measurements or calculated from polarisation resistance data (measured by the linear polarisation resistance method, LPR). The highest reported corrosion rate values (11.5 µm/year) were

calculated from passive current densities that were measured potentiodynamically. Macdonald, however, found that passive current densities measured potentiodynamically can be up to three orders in magnitude higher than those measured potentiostatically under steady-state conditions (Azizi, et al, 2008b; Macdonald, et al, 2009c).

The experimental conditions of the data reported by Byakova and co-workers (Byakova, et al, 1976), Dražić and Hao (Dražić and Hao,1983), Yasuda and co-workers (Yasuda, et al, 1987), Hubbe (Hubbe, 1980), Schwenk (Schwenk, 1983) and Huet (Huet, 2005a) greatly differ from the expected environmental conditions inside the Supercontainer (according to the normal evolution of the repository system):

- Byakova and co-workers (Byakova, et al, 1976) performed experiments in a 30% KOH solution with a calculated pH of 14.7 (at 25°C);
- Dražić and Hao (Dražić and Hao,1983) performed experiments in a 5M KOH solution with a calculated pH of 14.5 (at 25°C);
- Yasuda and co-workers (Yasuda, et al, 1987) recorded corrosion rates of up to 4,000 µm/year. The experiments, however, were performed in caustic soda solutions (either 30% or 50% NaOH with a calculated pH of 14.8 and 15.1, at 25°C, respectively);
- Hubbe (Hubbe, 1980) performed experiments in a NaOH solution of pH 9.8 (at the start of the experiment), which decreased to 7.7 at the end of the exposure period. According to the literature, the pH of these test solutions was too low for maintaining a stable passive film on the surface of the steel samples. Therefore the steel samples probably corroded in an active regime, hence the highly measured corrosion rates. Furthermore, details on the concentration of chlorides added to the test solution were not given in the reference;
- Schwenk (Schwenk, 1983) and Huet (Huet, 2005a) performed experiments in $NaHCO_3$, Na_2CO_3 or $CaCO_3$ solutions with a pH lower than 9.5. These solutions were used to simulate the pore chemistry of carbonated concrete. However, under normal evolution conditions, carbonation of the concrete buffer is not expected to occur;

5.2. Anaerobic alkaline environments (solutions + concrete)

The corrosion rate data in alkaline media under anoxic conditions reported in the literature largely originate from studies performed under the auspices of various national nuclear waste management authorities (LLW and ILW programmes). Despite the widespread industrial use of low alloyed steel as reinforcement in concrete and the corresponding extensive literature, there are relatively few published studies of corrosion rates under anaerobic conditions in this field. Furthermore, the studies in the literature related to industrial applications, are performed under aerated and carbonated conditions.

Figure 5-2 summarizes the corrosion rate data reported in the nuclear waste management and non-nuclear industrial literature for mild steel in anoxic and alkaline chloride-free solutions. The data in Figure 5-2 clearly exhibit a decreasing tendency of the uniform corrosion rate with increasing time of exposure towards a constant and very low value. Long-term corrosion rates (> 365 days) in the range of 0.1 µm/year or lower have been reported for temperatures up to 80°C in chloride-free solutions that are most relevant for the concrete buffer environment inside the Supercontainer (i.e. in the pH range 11.8–13.5).

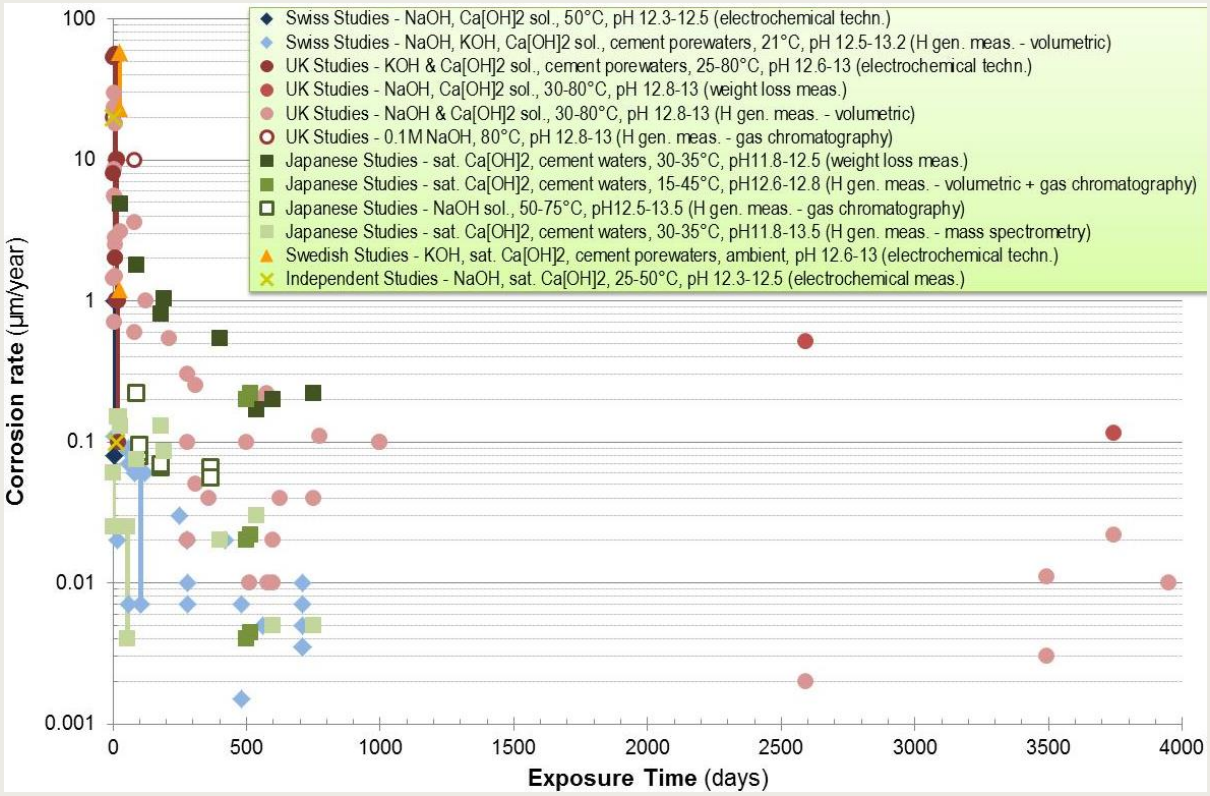

Figure 5-2. Compilation of uniform corrosion rates (reported in the non-nuclear industrial and nuclear waste management literature) of carbon steel in anoxic and alkaline chloride-free solutions representative for the Supercontainer (i.e. pH ~ 12—13.5).

The graph is compliled from data reported in the following REFERENCES:

- ◆ (Grauer, 1988);
- ◆ (Grauer, et al, 1991a; Grauer, et al, 1991b; Kreis, 1991; Kreis and Simpson, 1992; Kreis, 1993);
- ● (Naish, 1993; Smart, et al, 2004; Smart, 2008; Smart, 2009);
- ● (Smart, et al, 2004; Smart, 2008; Smart, 2009);
- ● (Naish, 1993; Naish, et al, 1995; Naish, et al, 2001; Smart, et al, 2004; Smart, 2008; Smart, 2009);
- ○ (Naish, et al, 2001);
- ■ (RWMC, 1998; Fujiwara, 2002; Kaneko, et al, 2004);
- ■ (Fujisawa, et al, 1997);
- □ (Honda, et al, 2006; Honda, et al, 2009);
- ■ (RWMC, 1998; Fujiwara , 2002; Kaneko, et al, 2004);
- ▲ (Hansson, 1984c; Hansson, 1985; Hansson, 1985a; Hansson, 1987);
- × (Heusler, et al, 1958; Kaesche, 1965; Grubitsch, et al, 1970; Grubitsch, et al, 1979);

The highest corrosion rates were obtained either

- from electrochemical experiments;
- from weight loss measurements; or
- from H_2-generation rates measured during the first initial period of the experiment. Increased instantaneous corrosion rates were initially measured (on pickled samples), which was attributed to the build up of a protective corrosion product layer;

The H_2-generation derived corrosion rates measured by Swiss and Japanese workers were consistently about one order of magnitude lower than those reported in the UK studies in similar environments. A possible explanation could be the use of glass test cells in the Japanese studies, resulting in the inhibition of the corrosion process due to the dissolution of glass (Si) at high pH. This assumption seems to be confirmed by the outcome of a study performed by Smart and co-workers (Naish, et al, 2001; Smart, et al, 2004), in which the effect of the use of a polythene insert inside a glass cell on the anaerobic corrosion of

carbon steel was investigated in a highly alkaline environment (0.1M NaOH solution). Tests performed in glass cells without a plastic liner showed a rapid decline of the corrosion rate to very low values (see Figure 5-3). Tests performed in glass cells with a plastic liner to separate the test solution from the glass walls of the test cell showed a very slow decline of the corrosion rate. The authors have, however, not attempted neither to measure the concentration of Si in solution nor to analyse the composition of the corrosion products formed on the surface of the carbon steel specimens.

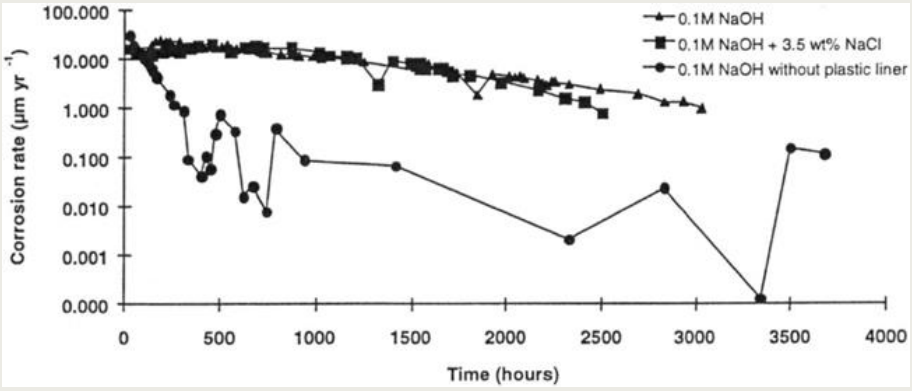

Figure 5-3. Effect of corrosion cell type (glass vs. plastic) on the anaerobic corrosion rate of carbon steel in 0.1M NaOH at 80°C (Naish, et al, 2001).

The experimental conditions of the data reported by Schenk (Schenk, 1988), Simpson and Schenk (Simpson and Schenk, 1989), Yasuda and co-workers (Yasuda, et al, 1987), Schenk and Noack (Schenk and Noack, 1995) and Jelinek and Neufeld (Jelinek and Neufeld, 1982) greatly differ from the expected environmental conditions inside the Supercontainer (according to the normal evolution of the repository system):

- Simpson and Schenk (Schenk, 1988; Simpson and Schenk, 1989) measured the hydrogen generation rate from carbon steel in pure water of pH 7 or in $Na_2CO_3/NaHCO_3$ buffered solutions with pH 8.5 or 10 using gas chromatography methods in the temperature range between 50 and 80°C;
- Yasuda and co-workers (Yasuda, et al, 1987) reported extremely high corrosion rates of 1,500 and 28,000 µm/year determined from weight loss and linear polarisation resistance measurements, respectively. The experiments were performed in caustic soda solutions at 117°C (30% NaOH, with a calculated pH of 14.9 at 25°C). Furthermore, the authors assumed that the high measured corrosion rates were caused by the oxidation of hydrogen instead of corrosion of the steel specimens;
- Schenk and Noack (Schenk and Noack, 1995) conducted volumetric hydrogen generation measurements on pure iron in synthetic cement pore water solutions of pH 9.0 or 10.5 at 50°C. Extremely low corrosion rates of <0.0003 µm/year (at both pH's) were measured after a testing period of 330 days;
- Jelinek and Neufeld (Jelinek and Neufeld, 1982) measured the hydrogen generation rate from carbon steel in 0.1N $NaHCO_3$ solution of pH 8.8 using gas chromatography methods in the temperature range between 60 and 90°C;

5.3. Discussion of the reported data

5.3.1. Criteria for passive/active corrosion

Andrade and co-workers assumed 0.1−0.2 µA/cm² as the boundary i_{CORR} range between active and passive corrosion for carbon steel in concrete (Andrade and González, 1978;

González, et al, 1980; Andrade, et al, 1981; Alonso, et al, 1988; Feliu, et al, 1988; Goñi and Andrade, 1990; Andrade, et al, 1990; Andrade and Alonso, 1994; González, et al, 1995):

- steel embedded in concrete remains in its passive state when the measured i_{CORR} remains below 0.1 to 0.2 µA/cm² (~1.1 to 2.2 µm/year);
- when the measured i_{CORR} value reaches 0.2 µA/cm² (~2.2 µm/year), steel reinforcements are expected to corrode actively;

This assumption is based on a huge amount of i_{CORR} data that originated from a large set of laboratory experiments (Andrade and González, 1978; González, et al, 1980; Andrade, et al, 1981, Alonso, et al, 1988) and measurements in real structures (Feliu, et al, 1988) that were collected over a 20-year period. The recorded i_{CORR} values are calculated using the polarisation resistance technique. Figure 5-4 summarizes the expected values of i_{CORR} for carbon steel in concrete as a function of the ambient aggressivity (e.g. amount of chlorides in the mix, carbonated concrete) and relative humidity of the environment. Furthermore, they concluded that:

- in uncracked concrete, the maximum i_{CORR} measured in aggressive environments is about 100 to 200 µA/cm² (~1 100 to 2 200 µm/year);
- in completely saturated concrete, the maximum corrosion rate is limited to 1 µA/cm² (~10 µm/year), even if carbon steel is corroding actively;

However, it may be worth mentioning that the i_{CORR} values reported by Andrade et al. may be somewhat underestimated because the literature also states (Gepraegs, 2002; Mendoza, 2003; Poursaee, 2007) that these values were obtained with measuring devices that are believed to generally give lower values than other commercial equipment.

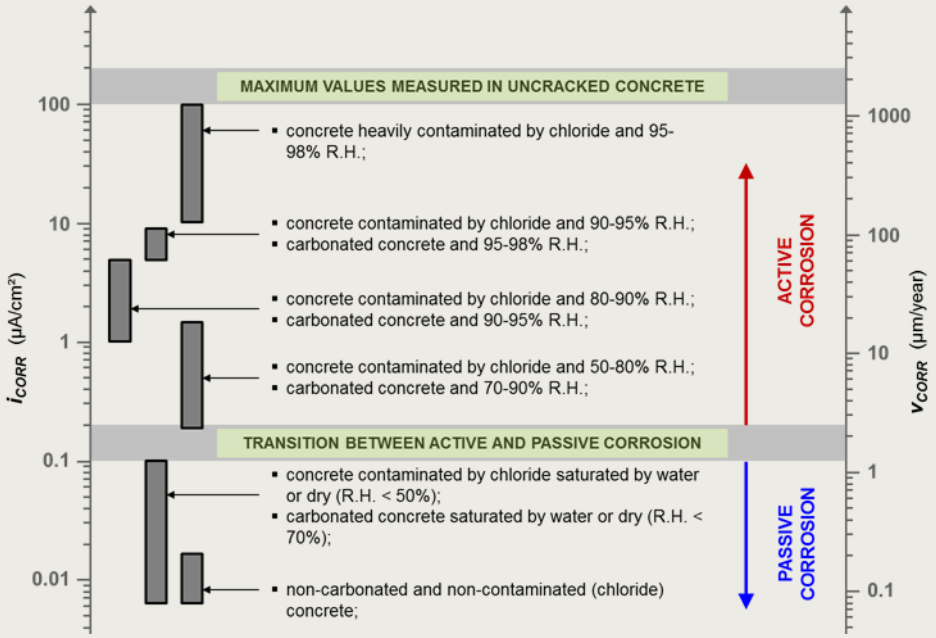

Figure 5-4. Map of ranges of corrosion current density, i_{CORR}, and corrosion rate, v_{CORR}, of steel in different concretes and exposure conditions (source: adapted from [Bertolini, et al, 2004]; original reference: [Andrade and Alonso, 1994]).

5.3.2. Effect of measuring technique

The anaerobic corrosion rates measured either electrochemically or from the weight loss are considerably higher than those obtained from the H_2-generation measurements. This

discrepancy becomes even more apparent when the reported corrosion rate data, determined with the different techniques, are plotted in individual graphs, as illustrated in Figure 5-5, Figure 5-6 and Figure 5-7:

- the corrosion rates derived from electrochemical techniques are summarized in Figure 5-5. Very high corrosion rates of up to ~60 µm/year were measured, with 0.1 µm/year as a lower limit value. The highest reported corrosion rates (~60 µm/year) are not considered representative because they were measured using techniques that are known to give an over-estimation of the instantaneous long-term corrosion rate for several reasons:
  - corrosion rates derived from electrochemical methods are based on the measurement of corrosion currents. Electrochemical measuring systems, however, can not distinguish electric currents generated by the corrosion process from electrical currents coming from other electrochemical processes that can occur at the electrode surface;
  - Macdonald has demonstrated that passive current densities measured potentiodynamically can be up to three orders in magnitude higher than those measured potentiostatically under steady-state conditions (Azizi, et al, 2008b; Macdonald, et al, 2009c);
  - electrochemical techniques in which the corrosion current is determined by extrapolating the polarisation diagram (cathodic and/or anodic branch) to the corrosion potential (such as the graphical polarisation curve extrapolation method, the Tafel extrapolation method and the linear polarisation resistance technique) are more suited to determine the corrosion rate for actively corroding metals. Heitz and Schwenk (Heitz and Schwenk, 1976) found that for very slowly corroding systems, such as for passivating metals (as is the case for carbon steel exposed to concrete), these electrochemical methods do not provide the corrosion current. Instead, the kinetic data of the cathodic half-cell reaction (exchange current density or limiting current density) is found, which results in a too high estimation of the corrosion current;
  - furthermore, it is difficult to properly account for the effects of time-dependent film formation (which is very important in nuclear waste management because of the decrease in rate with time due to film formation) (KING, 2008);

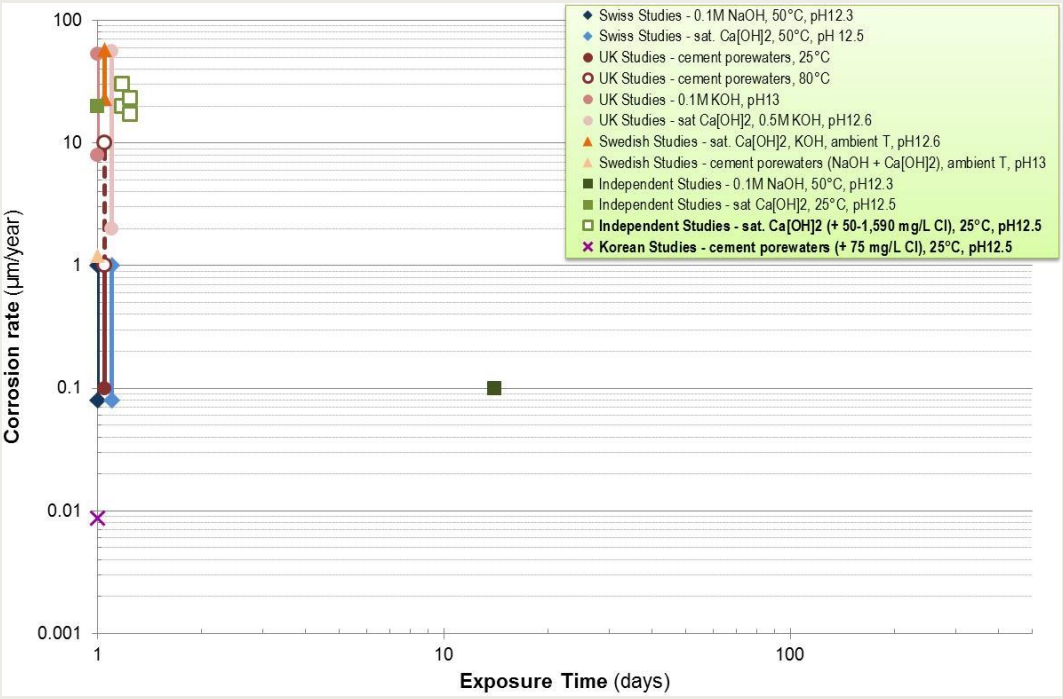

Figure 5-5. Compilation of uniform corrosion rates (reported in the non-nuclear industrial and nuclear waste management literature) of carbon steel in anoxic and alkaline solutions using electrochemical techniques.

The following electrochemical techniques were used in the various national waste management R&D programmes to derive the corrosion rate:

- Swiss studies (◆, ◆): LPR[e], PCD[f] (potentiostatic or potentiodynamic);
- UK studies (●, ●, ●, ○): PC[g] (potentiodynamic), GP[h], EIS[i], PCD[19] (potentiostatic);
- Swedish studies (▲, ▲): PC[20] (potentiostatic), PCD[19] (potentiodynamic);
- independent studies (■, ■, □): PCD[19] (potentiostatic and potentiodynamic);
- Korean studies (×): TP[j];

- the corrosion rates calculated from weight loss are summarized in Figure 5-6. Corrosion rates in the range of 0.1 – ~15 µm/year were measured, with a clear decrease of the corrosion rate in time. Weight loss measurements are also known to give higher corrosion rates than the actual rate at the end of the test, because weight loss corrosion rates are averaged over the entire duration of the exposure period. This is best illustrated by King (King, 2008): if one considers that the corrosion rate decreases according to $t^{-1/2}$, then the time-averaged weight loss corrosion rate is twice the instantaneous rate at any given time. An additional error that can possibly contribute to the over-estimation of weight loss derived corrosion rates is a small amount of metal that can be dissolved when stripping the samples from its corrosion product layer in a cleaning solution;

[e] Linear Polarisation Resistance technique.
[f] Passive Current Density measurements: the passive current densities were derived graphically from the polarisation curves (recorded either potentiostatically or potentiodynamically).
[g] Polarisation Curve measurements: the corrosion current densities were derived graphically from the polarisation curves (recorded either potentiostatically or potentiodynamically) by extrapolating the the linear regions of the cathodic and anodic reactions to the corrosion potential.
[h] Galvanostatic Pulse technique.
[i] Electrochemical Impedance Spectroscopy measurements.
[j] Tafel slope Extrapolation method.

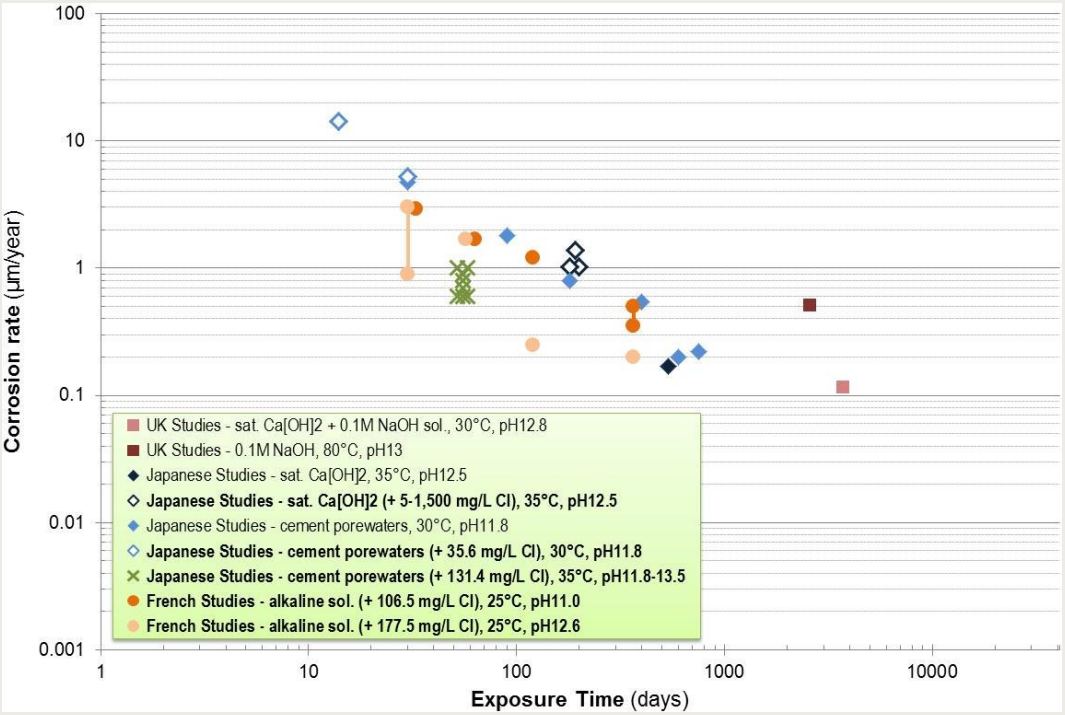

Figure 5-6. Compilation of uniform corrosion rates (reported in the non-nuclear industrial and nuclear waste management literature) of carbon steel in anoxic and alkaline solutions using the weight loss.

- the corrosion rates generated from measurements of the rate of H_2 evolution are summarized in Figure 5-7. Corrosion rates in the range of 0.0015 – ~30 µm/year were reported. The measured corrosion rates were found to decrease with increasing exposure time. This time dependence of the anaerobic corrosion rate can also be clearly demonstrated from the data in Table 5-1. The highest measured corrosion rates were based on short-term experiments (exposure period of < 10 days). These values are not considered to be a reliable estimate because they correspond to the very high initial peak in corrosion rate consistent with the formation of the protective corrosion product layer. However, longer-term studies (e.g. UK Studies have been running for ~4,000 days) suggest an instantaneous long-term corrosion rate of carbon steel of the order of <0.1 µm/year;

Table 5-1. Anaerobic corrosion rates of carbon steel in high pH solutions determined from long-term H_2-generation experiments.

Environment	pH	T (°C)	Test duration (days)	v_{CORR} (µm/year)	R&D programme
0.1M NaOH	12.8	21	initial 60 120 280 710	0.09 – 0.11 0.07 0.06 0.02 0.005	Swiss Studies
KOH	12.8	21	60 280 710	0.09 0.01 0.0035	Swiss Studies
sat. $Ca(OH)_2$	12.8	21	18 280 710	0.02 0.007 0.0035	Swiss Studies
0.1M NaOH	12.8	30	initial 280 625 750 3949	1.5 – 3.11 0.1 0.04 0.04 0.01	UK Studies
0.1M NaOH	12.8	50	initial 80 210 310 600 3492	5.5 – 8.6 0.6 0.54 0.005 0.02 – 0.01 0.011	UK Studies
0.1M NaOH	12.8	80	initial 80 125 311 2591	18 – 29.6 3.6 1 0.25 0.002	UK Studies
sat. $Ca(OH)_2$	12.8	50	initial 360 500 580 3494	5.1 – 5.4 0.84 0.1 0.01 0.003	UK Studies
sat. $Ca(OH)_2$ + 0.1M NaOH	12.8	30	initial 280 510 1000 3743	0.7 – 1.43 0.3 0.2 0.1 0.022	UK Studies
sat. $Ca(OH)_2$ + 0.1M NaOH	12.8	50	initial 510 773 1000	2.5 – 2.8 0.2 0.11 0.1	UK Studies
cement equilibrated water	11.8	30	30 90 400 600 750	0.13 0.075 0.02 0.005 0.005	Japanese Studies

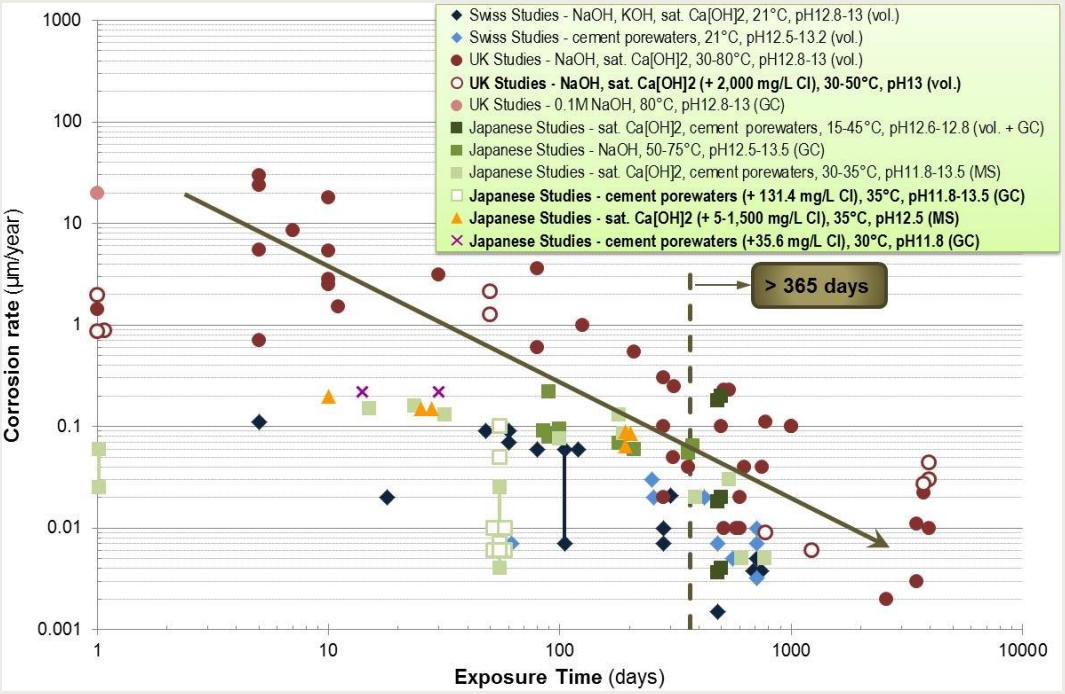

Figure 5-7. Compilation of uniform corrosion rates (reported in the non-nuclear industrial and nuclear waste management literature) of carbon steel in anoxic and alkaline solutions using the rate of hydrogen generation.

Numerous examples of differences between uniform corrosion rates calculated from weight loss and uniform corrosion rates obtained from hydrogen gas measurements have been reported in various national waste management programmes. The weight loss corrosion rates give an average value calculated over the entire testing period, while H_2-generation corrosion rates give an instantaneous value measured at the end of the testing period:

- Smart and co-workers (Smart, et al, 2004) have measured one to two orders of magnitude higher corrosion rates by weight loss relative to H_2-generation measurements in saturated $Ca(OH)_2$ + 0.1M NaOH and 0.1M NaOH solutions (see Table 5-2). The maximum duration of the laboratory experiments was approximately 10 years;

Table 5-2. Comparison of uniform corrosion rates calculated either from weight loss or from hydrogen generation rates (volumetric) of carbon steel in high pH solutions relevant for the UK waste management programme (Smart, et al, 2004).

Test solution	Test duration (days)	v_{CORR} (ΔM) (µm/year)	v_{CORR} (H_2) (µm/year)
sat. Ca(OH)2 + 0.1M NaOH, 30°C	3743	0.115	0.022
0.1M NaOH, 80°C	2591	0.511	0.002

- Fujiwara and co-workers (RWMC, 1998; Fujiware, et al, 2001) investigated the effect of dissolved O_2 concentration on the uniform corrosion rate of carbon steel in synthetic cement pore solutions at 35°C. The corrosion rates calculated from weight loss were approximately 100 times higher compared to those calculated from the amount of H_2 gas generation (see Figure 5-8);

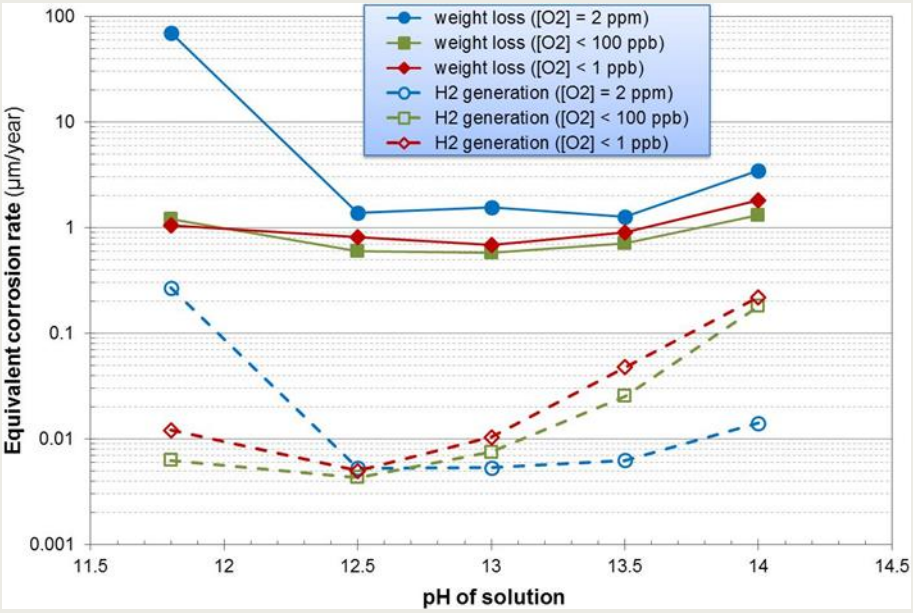

Figure 5-8. Uniform corrosion rates, calculated either from weight loss or from hydrogen generation rates (mass spectrometry), of carbon steel in synthetic cement pore solutions at 35°C as a function of pH and dissolved oxygen concentration (source: adopted from [RMWC, 1998; Fujiware, et al., 2001]).

(the solution containing 2 ppm of dissolved oxygen equals an O_2 concentration in the gaseous phase of 20%, which corresponds to oxic conditions)

- Japanese workers (RWMC, 1998; Kaneko, et al., 2004) measured the corrosion rate in cement-equilibrated water (pH 11.8) by means of the weight loss and the H_2-generation method. The corrosion rates calculated from weight loss were more than 10 times higher compared to those calculated from the amount of H_2 gas generation (see Figure 5-9). The corrosion rate, after a lapse of about 2 years, was as follows:

  – ~0.2 µm/year (calculated from weight loss);

  – ~0.005 µm/year (calculated from the rate of H_2 gas generation);

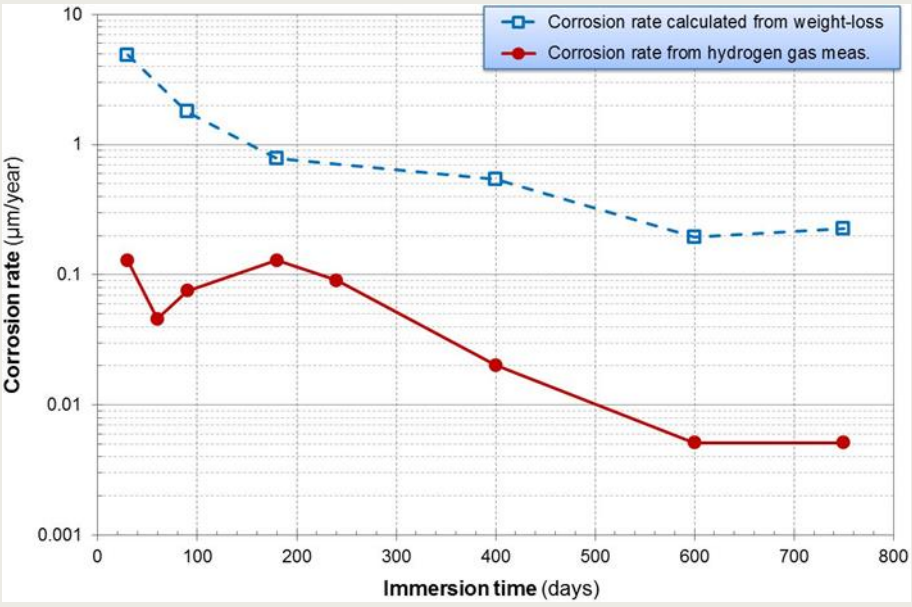

Figure 5-9. Comparison of uniform corrosion rates calculated either from weight loss or from hydrogen generation rates (mass spectrometry) of carbon steel in cement equilibrated water at 30°C (source: adopted from [RWMC, 1998; KANEKO et al., 2004]).

- Kaneko et al. (Kaneko, et al, 2004) investigated the effect of chloride concentration (up to 20,000 mg/L) on the uniform corrosion rate of carbon steel in saturated $Ca(OH)_2$ (pH 12.5) at 35°C. The corrosion rates calculated from weight loss were found to be about one order of magnitude higher than those calculated from the H_2-generation rate for all chloride concentrations (see Figure 5-10);

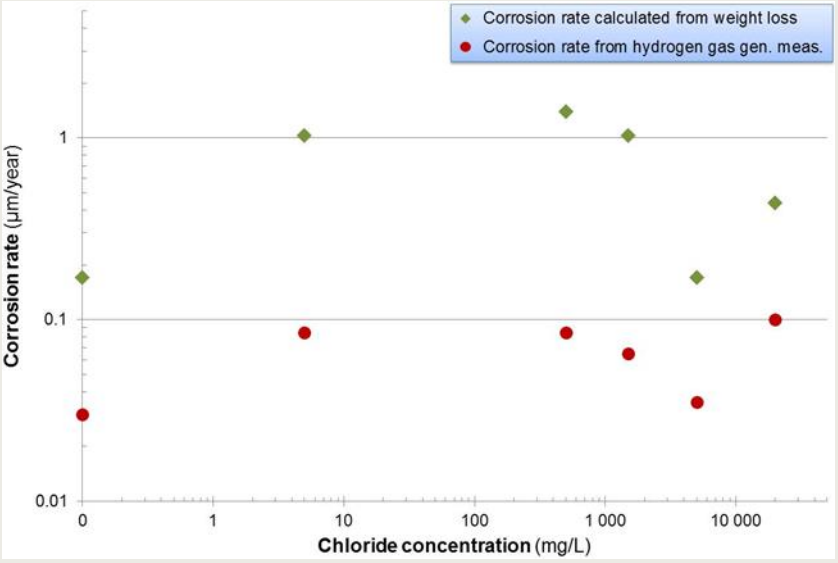

Figure 5-10. Comparison of uniform corrosion rates calculated either from weight loss or from hydrogen generation rates (mass spectrometry) of carbon steel in saturated $Ca(OH)_2$ with varying chloride concentrations at 35°C.

(the graph is compiled from data reported in [Kaneko, et al, 2004]).

- Kaneko et al. (Kaneko, et al, 2004) investigated the effect of pH on the uniform corrosion rate of carbon steel in a saturated $Ca(OH)_2$ solution containing 5,000 mg/L Cl^- at 35°C. The corrosion rates calculated from weight loss were found to be about one order of magnitude higher than those calculated from the H_2-generation rate for all pH's (see Figure 5-11);

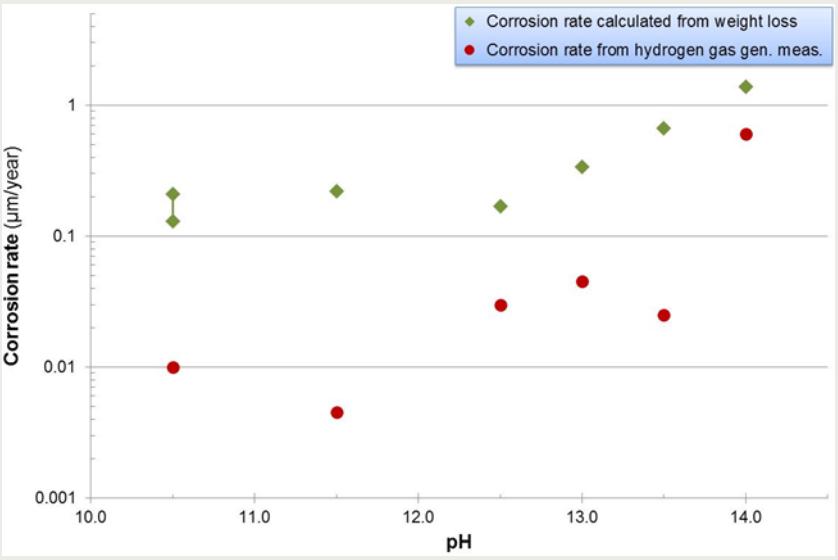

Figure 5-11. Comparison of uniform corrosion rates calculated either from weight loss or from hydrogen generation rates (mass spectrometry) of carbon steel in saturated $Ca(OH)_2$ with 5,000 mg/L Cl^- with varying pH at 35°C.

(the graph is compiled from data reported in [Kaneko, et al, 2004]).

5.3.3. Effect of exposure period

For long-term corrosion prediction, only knowing the corrosion rate is not sufficient. One must also have knowledge on how the corrosion rate varies in time. The rate of corrosion generally decreases with time either because of the depletion of reactants or, more usually, because of the formation and growth of a protective corrosion product film (King, 2007).

A decreasing time dependence towards a constant uniform corrosion rate has been proven in many individual laboratory studies performed in alkaline media (solutions and concrete), which are representative for the environment surrounding the carbon steel overpack within the Supercontainer. Figure 5-12 summarizes the uniform corrosion rate data for carbon steel in alkaline solutions and concrete, representative for the Supercontainer concrete buffer environment, under anaerobic conditions reported in the literature. The data originate from laboratory experiments lasting for more than 10 years performed within the framework of the UK, Swiss, Japanese, Swedish, Spanish and Korean waste management programmes. The data confirms a decrease of the uniform corrosion rate in time, with the largest drop occurring during the first ~400 days. The data also suggests that the long-term (> one year) corrosion rate is of the order of ≤0.1 µm/year.

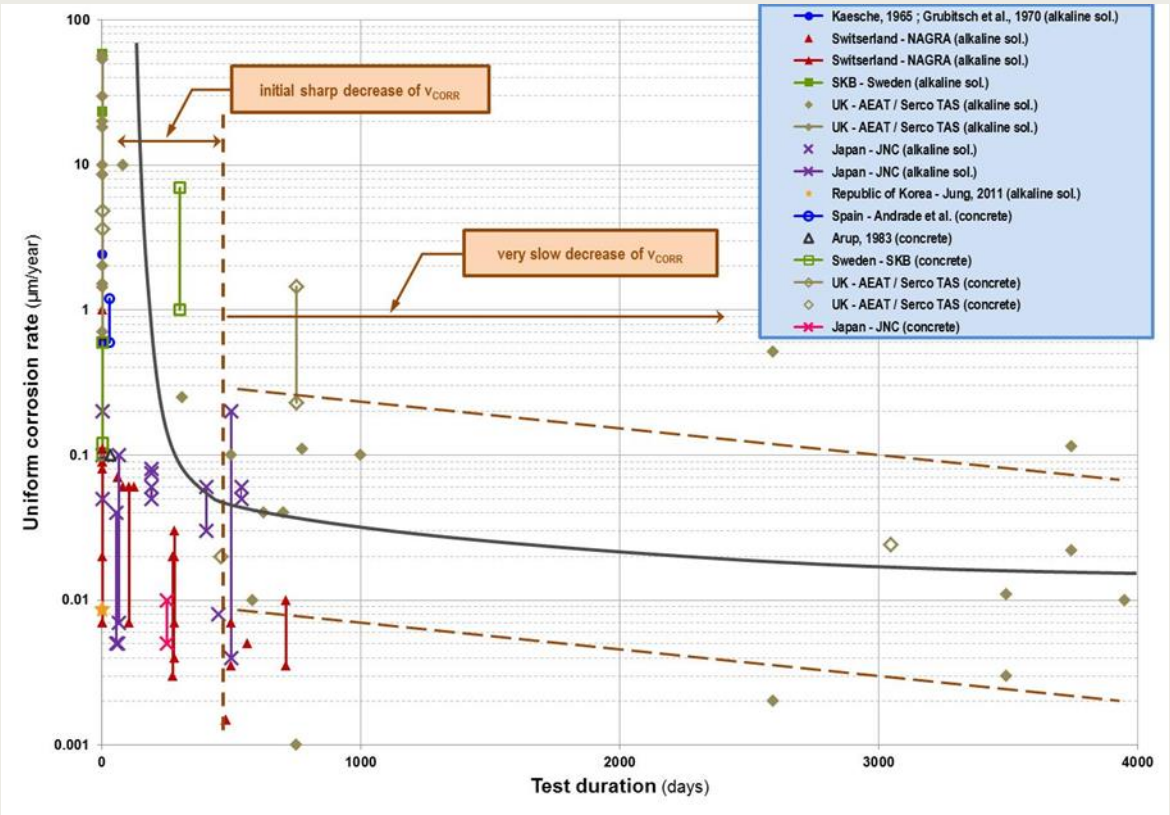

Figure 5-12. Compilation of uniform corrosion rates of carbon steel in alkaline solutions and concrete under anaerobic conditions.

Further evidence for the uniform corrosion rate of carbon steel decreasing in time can be obtained from analogue studies:

- Chitty and co-workers (Chitty, et al, 2005) studied the long-term corrosion resistance of ferrous reinforcements embedded in concrete originating from nine archaeological sites, eight situated in France and one in India, aged from the Gallo-Roman period to the beginning of the 20th century A.D. All the ferrous reinforcements examined in this study were hypoeutectoid steels (carbon content under 0.8 mass%). Average corrosion

rates were calculated using thickness measurements of the corrosion products coupled to a local density correction (see Appendix A2, section A2.4). The calculated average corrosion rate of the studied ferrous analogues originating from nine different sites versus sample age are presented in Figure 5-13. This figure shows that the average corrosion rate roughly decreases from the youngest to the oldest sample. Additionally, the more recent sample (RA01) presents a corrosion system (type of concrete, steel) that is very similar to contemporary ones and therefore the authors concluded that it can be compared to the materials envisaged for the current waste management systems.

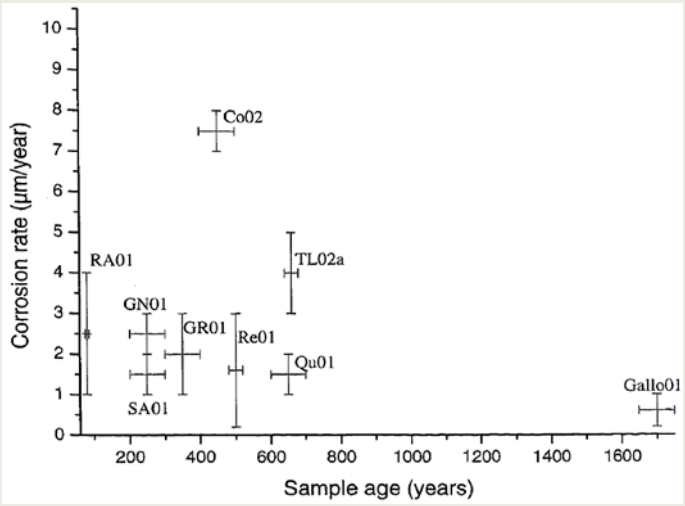

Figure 5-13. Average corrosion rates of the studied ferrous analogues originating from nine different sites versus sample age (Chitty, et al, 2005).

6. Source and expert range for the corrosion rate of carbon steel in high alkaline media

The uniform corrosion rate data that have been found in the literature were critically reviewed considering the following hypotheses:

- under the high pH conditions inside the Supercontainer concrete buffer, the surface of the carbon steel overpack will be passivated and will remain so for the entire disposal period (or at least for the duration of the thermal phase), resulting in very low uniform corrosion rates (through the mechanism of passive dissolution);
- under normal evolution conditions, the carbon steel overpack will only be prone to uniform corrosion. This implies that corrosion processes other than uniform corrosion (such as *e.g.* pitting corrosion, crevice corrosion, stress corrosion cracking, …) cannot occur under the environmental conditions prevailing in the Supercontainer (this is called the 'exclusion principle'). However, the validity of the 'exclusion principle' still needs to be proven;
- under normal evolution conditions, carbonation of the concrete buffer surrounding the carbon steel overpack (which could lead to a drop in pH causing depassivation of the overpack surface) is not expected to occur;
- thermal simulations suggest that a maximum temperature of ~75°C is to be expected at the surface of the carbon steel overpack. More detailed information can be found in section 4.1.;
- pH evolution calculations predict that the pH around the carbon steel overpack will remain higher than 12.5 for at least 80 000 years. More detailed information can be found in section 4.3.;
- transport calculations of aggressive species show that chloride concentrations as high as ~19 000 mg/L (*i.e.* the background concentration of the Rupel Clay host formation) could be reached at the surface of the overpack after a period of about 2 000 years. More detailed information can be found in section 4.4.;
- the potential effect of other aggressive species (such as *e.g.* sulphide and thiosulphate) are currently not considered. The investigation of the influence of these species on the uniform corrosion rate should form part of another study;

Our methodology consisted in evaluating the corrosion rate data reported in the literature as such that the data was divided into two ranges:

- source range, i.e. the range of values outside of which the value of the corrosion rate is very unlikely to lie, considering current knowledge. It includes all theoretical and experimental values of the corrosion rate, except the outliers that are rejected;
- expert range, i.e. the range of values within which experts expect the value of the corrosion rate to lie. It is meant to be a more realistic range of the corrosion rate value than the *source range* and is thus expected to be more narrow;

6.1. Selection criteria applied to derive the source and expert range

Despite the widespread research effort on the corrosion of steel reinforcement in concrete for industrial uses (construction: bridges, road decks, reinforced columns; buildings: garage floors; …), the corresponding extensive literature data is not entirely applicable for our purpose because

- the environment surrounding the steel reinforcements in these industrial applications differs from the Supercontainer concrete buffer environment because the concrete samples are usually carbonated (due to a reaction with the atmospheric environment);
- none of the published studies of corrosion rates refer to anaerobic conditions;

Consequently, the interpretation of the source and expert ranges of the uniform corrosion rate of carbon steel is mainly based on data originating from studies from the nuclear waste management literature. These studies include surface disposal of low level nuclear waste (concrete bunkers) and deep disposal of high level nuclear waste and spent fuel.

The following criteria have been applied in selecting those studies considered to be reliable sources for estimating the *source range* of the uniform corrosion rate of carbon steel in alkaline media:

- ***traceability of the data***.
  - data for which some of the experimental parameters (test duration, experimental technique, environmental conditions, …) are not entirely known;
  - and no cross-references can be found to trace back the information that is lacking;
- ***application of the safety methodology developed within this study***.
  - under normal evolution conditions (and without the presence of aggressive species), it is believed that the surface of the carbon steel overpack will be passivated under the high pH conditions inside the Supercontainer, resulting in very low uniform corrosion rates (through the mechanism of passive dissolution). As pointed out in section 5.3.1., strong evidence exists that, for carbon steel/concrete systems, current densities in the range 0.1-0.2 $\mu A/cm^2$ are considered as a transition zone between passive and active corrosion. This corresponds to a uniform corrosion rate of ~1.1-2.2 µm/year. Therefore, reported uniform corrosion rates higher than ~2-3 µm/year were considered as active corrosion values and were therefore rejected;
  - the cornerstone of our scientific approach is based on proving that corrosion processes other than uniform corrosion (such as e.g. pitting corrosion, crevice corrosion, stress corrosion cracking, …) cannot occur under the environmental conditions prevailing in the Supercontainer (this is called the 'exclusion principle'). Therefore, uniform corrosion rate data originating from studies in which the specimens have suffered from localised corrosion were rejected;
- ***relevant type of material***.
  - In this study, the 'improved' steel grade CarElso 70 SOHIC (P355QL2) has been considered as reference candidate overpack material. This improved steel grade was developed as a result of a CEA-study (Herms, 2009), which reviewed the main metallurgical requirements for carbon steel selection to prevent possible environmentally assisted cracking phenomena (SCC, hydrogen embrittlement). The chemical composition of the 'improved' steel grade CarElso 70 SOHIC is given in Table 6-1;
  - only uniform corrosion rate data reported for low alloyed carbon steel was taken into consideration. But, because of the reduced levels of impurities (the reference carbon steel grade contains less than 2 wt.% of impurities), the data for pure iron was also considered relevant;
  - uniform corrosion rate data for other Fe-containing materials, such as stainless steel and cast iron were rejected;

– and other, non-ferrous, materials, such as Ni-, Ti- or Cu-alloys (some of them are studied in other disposal programmes), were considered irrelevant in this study;

Table 6-1. Chemical composition of the reference carbon steel grade CarElso 70 SOHIC.

Designation		**Chemical composition** (wt. %)							
UNS[(1)]	**W. Nr.**[(2)]	**Fe**	**C**	**Mn**	**P**	**S**	**Si**	**Cu**	**Ni**
P355QL2[(3)]	1.8869	bal	<0.16	<1.0	<0.01	<0.001	<0.45	<0.1	<0.1

UNS	**W. Nr.**	**Cr**	**Mo**	**Al**	**Co**	**Nb**	**V**	**Ti**	**B**
P355QL2[(3)]	1.8869	<0.1	<0.05	<0.05	<0.01	<0.01	<0.01	<0.01	<0.0005

[(1)] Unified Numbering system.
[(2)] Deutsche Werkstoff Nr.
[(3)] QL2 : heat-treatment code (quenched and tempered).

- ***relevant environment***.
  - according to the literature (Grauer, et al, 1991b; Kreis, 1991; Kreis and Simpson, 1992; Kreis, 1993; Naish, 1993; Naish, et al, 1995; Naish, et al, 2001; Fujiwara, 2002; Smart, et al, 2004; Kaneko, et al, 2004; Huet, et al, 2005a), alkaline solutions containing $Ca(OH)_2$, NaOH or KOH are commonly used to simulate the chemical characteristics of the pore solution of unaltered concrete;
  - theory (see section 2.2) shows that the pH of the pore solution of young concrete is fixed by the alkali content (Na^+ and K^+) to a high value of ~13.5. After leaching of the alkali ions, the pH is set by the portlandite equilibrium ($Ca[OH]_{2,(s)} \leftrightarrow Ca^{2+} + 2OH^-$) to a value of ~12.5. It is, therefore, common practice to use a saturated calcium hydroxide ($Ca[OH]_2$) solution (equilibrium pH of 12.5 at 25°C, see section 2.2) as simplified simulated concrete pore solution. Sodium hydroxide (NaOH) and potassium hydroxide (KOH) solutions, in various proportions, are commonly used to simulate higher pH solutions (Huet, et al, 2003; Huet, et al, 2005a; Huet, et al, 2005b; Huet, et al, 2005c);
  - too concentrated NaOH or KOH solutions were not taken into account because of the unrealistically high pH (*e.g.* a 30% NaOH solution has a calculated pH value of 14.9 at 25°C);
  - data gathered from solutions containing $NaCO_3$/$NaHCO_3$ were rejected because these solutions are normally used to simulate the composition of the pore solution of carbonated concrete;
  - numerous studies have also been reported in the literature providing uniform corrosion rate data for carbon steel in concrete. For the estimation of the source range of the corrosion rate, we only focussed on data from uncarbonated OPC-based concrete because
    - the SC concrete buffer will be fabricated from OPC-based cement (blended cements, such as silica fume, fly ash, blast furnace slag, … are not considered); and
    - under normal evolution conditions, carbonation of the SC concrete buffer is not expected to occur;
- ***relevant conditions***.
  - uniform corrosion rate data was limited to studies performed under relevant environmental conditions that are fixed by the reference scenario:

- 12.5 < pH < 13.5;
- T < 75°C;
- [Cl^-] ~ 19,000 mg/L;
- the potential influence of other aggressive species (such as *e.g.* sulphides and thiosulphates) has currently not been included. This should form part of another study;

The following criteria have been applied in selecting those studies considered to be reliable sources for estimating the *expert range* of the uniform corrosion rate of carbon steel in alkaline media:

- ***reliability of the data***. Some of the reported data sets showed strong evidence to question the reliability of the reported uniform corrosion rates:
  - difference between calculated values (*e.g.* from graphs) and reported data (*e.g.* in tables);
  - prove of inconsistency of the reported data sets, such as *e.g.*
    - the integrated uniform corrosion rate data (calculated from weight loss measurements) is higher than the initial uniform corrosion rate data (derived from hydrogen evolution measurements);
    - the hydrogen evolution measuring technique was used to measure corrosion rates under aerobic conditions. Hydrogen can only be produced during the anaerobic corrosion process unless localised corrosion is occurring;
- ***experimental technique applied to measure the uniform corrosion rate***. The experimental techniques providing the most realistic uniform corrosion rate data are:
  - the weight-loss measurement method provides the most reliable data for average corrosion rate determination. However, this technique generally over-estimates the uniform corrosion rate, as a result of which weight-loss corrosion rates are higher than the actual rate at the end of the test. The reason being that weight-loss corrosion rates are calculated as an average value over the entire duration of the exposure period (and thereby the initial much higher corrosion rates are included in the calculations). For example, if the corrosion rate decreases according to $t^{-1/2}$, the time-averaged weight-loss corrosion rate is twice the instantaneous rate at any given time (King, 2008). This is also confirmed by data found in the literature. Corrosion studies within the framework of the UK Nirex Safety Assessment Research Programme (NSARP) showed that uniform corrosion rates of carbon steel in saturated $Ca(OH)_2$ and 0.1M NaOH solutions measured by weight-loss measurements were a factor of 5 to 250 higher than those measured by the hydrogen evolution measurement technique, as illustrated in Table 6-2. Furthermore, the rate of metal dissolution associated with anaerobic corrosion is generally low and weight losses from coupons tend to be small, even after long exposure times. Consequently, under such circumstances, the technique is susceptible to experimental error, which has resulted, on occasions, in weight gains rather than weight losses (Naish, et al, 2001);

Table 6-2. Comparison between long-term uniform corrosion rates coming from weight-loss and hydrogen evolution measurements.

Condition	v_{corr} (weight loss) (µm/year)	v_{corr} (H evol.) (µm/year)
$Ca(OH)_2$ sat., 30°C, 3743 days	0.115	0.022
0.1M NaOH, 80°C, 2591 days	0.511	0.002

- the following techniques were identified to provide the most reliable data for instantaneous corrosion rates:
  - hydrogen gas measurements (volumetric, mass spectrometry, gas chromatography): these experimental techniques are limited to providing corrosion rates under anaerobic conditions;
  - passive current density measurements (at steady-state, potentiostatically): this technique can result in an over-estimation of the corrosion rate in the presence of oxygen (or other active species, such as *e.g.* in sulphur containing environments) due to the contribution of the redox reactions, other than the corrosion reaction, to the passive current;
  - linear polarisation technique (extrapolation to zero sweep rate): no data has been found in the literature using this technique under relevant conditions;
- it should be mentioned in this respect that electrochemical experiments (*e.g.* TP, LPR, GP) generally give an over-estimation of the corrosion rate because often processes other than corrosion are also taken into account in the calculation of the corrosion rate. Furthermore, it is very difficult to account for the effects of time-dependent film formation (King, 2008). Therefore corrosion rate data generated by such electrochemical experiments are considered here as initial corrosion rate data and are only included in the source range (but excluded from the expert range);

• ***test duration***.

- it is generally accepted that the uniform corrosion rate decreases with increasing exposure period due to film formation (King, 2008). This assumption is based on results from both long-term laboratory studies and from archaeological artefact studies, in concrete as well as in other environments (such as clay and granite), under aerobic and anaerobic conditions;
- because of the decrease of the corrosion rate in time, the use of initial high corrosion rates would lead to a significant under-estimation of the lifetime of the overpack. Therefore, and in view of the long timescales that are considered in waste disposal, an accurate estimation of the corrosion rate in the long term is essential to guarantee the robustness of the disposal system;
- an accurate determination of long-term uniform corrosion rates is of major importance for the anaerobic period considering its very long duration (thousands of years). For the aerobic period, it is less important because of its limited duration (several tens of years);
- for the interpretation of the uniform corrosion rate data, a distinction has been made between initial corrosion rates (v_{ini}) and long-term corrosion rates (v_{lt}):
  - initial corrosion rates (studies < 1 year) have been selected to define the source range. Initial corrosion rates are those rates that have been generated by hydrogen evolution measurements (initial high values), short-term passive current density measurements and electrochemical measurements (*e.g.* TP, LPR, GP);

- long-term corrosion rates (studies > 1 year) have been selected to define the expert range. Long-term corrosion rates are those rates that have been generated by hydrogen evolution measurements (long-term data) and long-term passive current density measurements;

– several studies that have been performed in environments relevant for the Supercontainer (such as saturated $Ca(OH)_2$ solution, 0.1M NaOH solution, NRVB cementitious backfill material considered for the geological disposal of intermediate-level and low-level radioactive wastes in the UK), have indicated that the major decline of the corrosion rate occurs during the first ~365 days (see Figure 6-1 and Table 6-3). Therefore, long-term corrosion rates are defined here as corrosion rates generated from studies lasting longer than ~1 year;

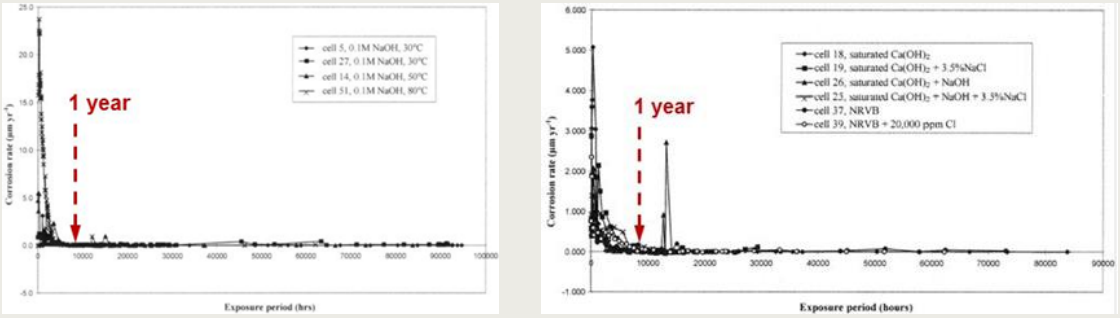

(a) *(b)*

Figure 6-1. Decrease of uniform corrosion rate in time in media relevant for near field environment surrounding the carbon steel overpack in the Supercontainer.

Table 6-3. Decrease of uniform corrosion rate in time in media relevant for the near field environmnet surrounding the carbon steel overpack in the Superconatiner.

Conditions	Test duration	v_{corr} (µm/year)	Reference
0.1M NaOH, 80°C	initial	18.0	Naish et al, 2001
	125	1.0	Naish et al, 2001
	311	0.25	Smart et al, 2004; Smart, 2008; Smart, 2009
	2591	0.002	Smart et al, 2004; Smart, 2008; Smart, 2009
sat. $Ca(OH)_2$, 50°C	initial	5.4	Naish et al, 2001
	500	0.1	Smart et al, 2004;
	3494	0.003	Smart, 2008; Smart, 2009

6.2. Proposed expert ranges for the corrosion rate of carbon steel

The reported corrosion rate data were critically reviewed based on the eight criteria, described in section 6.1., which have been developed in the framework of the Belgian disposal programme. The corrosion rate data were divided into two ranges, *viz.* a source (SR) and an expert range (ER). They were also classified into aerobic and anaerobic media because the aerobic and anaerobic period have been identified as the two major periods in the course of the Corrosion Evolutionary Path (CEP).

The SR and ER of corrosion rates for carbon steel in high alkaline environments (pH ~ 13.6) and under normal conditions (*i.e.* without the ingress of aggressive species) are summarized in the Table 6-4.

Table 6-4. Proposal of the source (SR) and expert range (ER) for the uniform corrosion rate of the carbon steel overpack in high alkaline environments (pH ~ 13.6) and under normal conditions (*i.e.* without the ingress of aggressive species).

Condition	SR	ER
oxic, alkaline media	0.005 – 2.2	0.005 – 2.2
anoxic, alkaline media	0.0015 – 2.4	0.0015 – 0.2

6.3. Effect of chloride concentration on SR and ER

6.3.1. Aerobic alkaline environments

A huge amount of information is available in the literature on the effect of chloride on the corrosion rate of carbon steel in concrete under oxic conditions. This information largely originates from the non-nuclear waste management literature, because for industrial applications (longevity of bridge decks, garage platforms, …), the effect of de-icing salts on the corrosion behaviour of the steel reinforcements is of a major concern. In these studies, specimens are often subjected to repetitive wet-dry cycles in simulated concrete pore solutions with the addition of incrementally increasing concentrations of chloride.

From the literature, a general trend of increasing corrosion rate with increasing chloride concentation could be observed. For the purpose of illustration, we incorporate a couple of examples.

Goñi and Andrade (Goñi and Andrade, 1990) reported corrosion rate data (expressed as a corrosion current density) of carbon steel rebars in synthetic concrete pore solutions (saturated $Ca[OH]_2$ solution) of different pH (ranging from 11.64 to 13.22) and various chloride concentrations at 21°C. The pH was changed by adding 0, 0.2 or 0.5N KOH to the $Ca(OH)_2$ solution. Chloride ions were added either as NaCl or $CaCl_2$. Polarisation resistance measurements were performed to calculate the instantaneous corrosion rate (a B-value of 26 mV was used).
The influence of chloride additions on the corrosion rate of carbon steel in a saturated $Ca(OH)_2$ + 0.2N KOH solution is illustrated in Figure 6-2(a) for NaCl and in Figure 6-2(b) for $CaCl_2$. The boundary i_{CORR} range (~0.1-0.2 µA/cm²) between active and passive corrosion for carbon steel in concrete is also indicated on the graphs (see section 5.3.1.).
In the chloride-free solution, the steel rebars remained passivated during the entire experiment (with a measured corrosion rate of ~0.6 µm/year after about 80 days).
In the NaCl solutions, the addition of 0.1N Cl^- increased the corrosion rate slightly but still remained in the passive region (~1.0 µm/year). The addition of 0.5-1.0N Cl^- showed corrosion rate values in the active domain (13.5-18 µm/year), but without significant differences among them.
The corrosion rate values in the $CaCl_2$ solutions were of the same order of magnitude for 0.5N and 0.75N Cl^-, compared to their corresponding NaCl solutions. However, the addition of 0.1N and 1.0N Cl^- seemed to be much more aggressive in the $CaCl_2$ solutions. A fivefold (for 0.1N Cl^-) to tenfold (for 1.0N Cl^-) increase of the corrosion rate was observed.

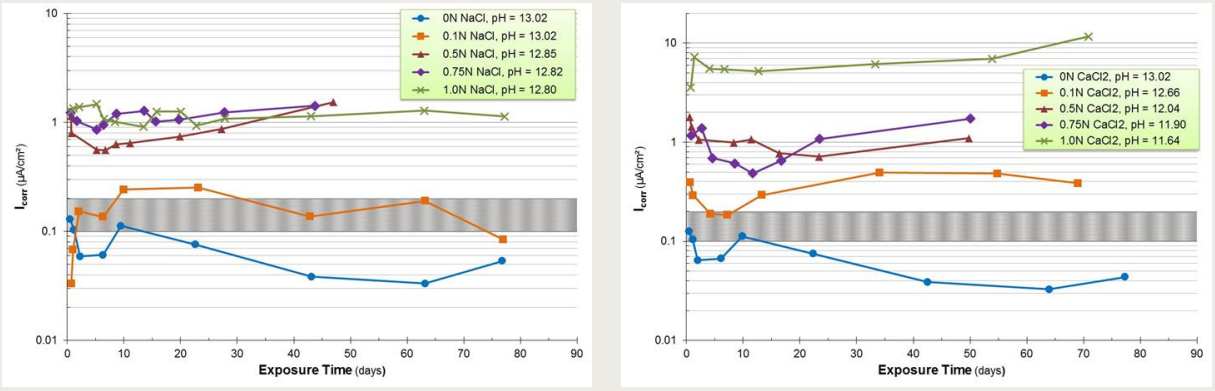

(a) ***(b)***

Figure 6-2. Evolution of the corrosion rate of carbon steel in saturated $Ca(OH)_2$+0.2N KOH solution at 21°C as a function of chloride addition (adapted from [Goñi and Andrade, 1990]).
(a) chlorides added as NaCL salt;
(b) chlorides added as $CaCl_2$ salt;

The Texas Department of Transportation (TxDOT) funded a research project to compare the corrosion resistance of various types of polymer-coated rebars (PVC- and nylon-coated rebars) and metal-clad rebars (stainless steel-clad and galvanized rebars) to conventional carbon steel rebars. Polarisation resistance measurements, from which the corrosion rate was estimated, were conducted in a saturated $Ca(OH)_2$ solution (1.85 g/L $Ca(OH)_2$) for a period of 6 days. During the first 2 days, the specimens were immersed in a choride-free saturated $Ca(OH)_2$ solution. After 2 days, increasing amounts of NaCl were added to the test solution: for the third and fourth day, 0.67 g/L NaCl (0.01146 mol/L) was added; for the fifth and sixth day, the NaCl concentration was increased to a total amount of ~3.5% (0.51334 mol/L). Bent rebar specimens were used (Deshpande, et al, 2000).
Figure 6-3 shows the variation of the corrosion rate in time for carbon steel immersed in a saturated calcium hydroxide solution. The corrosion rate decreased initially during the 2-day exposure period to the chloride-free $Ca(OH)_2$ solution. This initial drop was attributed to the formation of the passive film. On addition of increasing amounts of NaCl, the corrosion rate progressively increased to a value of ~80 µm/year after 6 days.

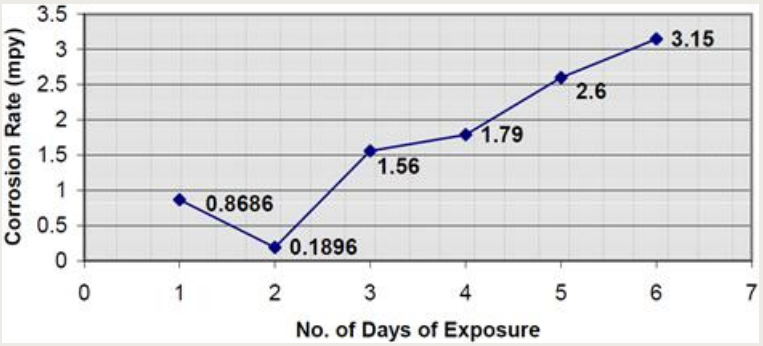

Figure 6-3. Corrosion rate versus exposure time for carbon steel immersed in a 1.85 g/L $Ca(OH)_2$ solution with increasing NaCl concentrations (days 1-2: chloride-free sat. $Ca(OH)_2$; days 3-4: sat. $Ca(OH)_2$ + 0.67 g/L NaCl; days 5-6: sat. $Ca(OH)_2$ + 35 g/L NaCl) (Deshpande, et al, 2000).
(conversion factor: 1 mpy ~ 25.4 µm/year)

Although the literature clearly shows an increasing trend of the corrosion rate with increasing additions of chloride, it is very difficult to assign an absolute value (in terms of corrosion rate expressed in µm/year) to the effect of chloride concentration, because from the data reported in the literature it is impossible to discriminate between the effect of increasing exposure time and the effect of increasing chloride concentration (in these tests,

chloride concentration is gradually increased in time). This is illustrated in Figure 6-4. This figure shows the current density results from potentiostatic polarisation experiments carried out at +200 mV (vs. SCE[k]) in a saturated $Ca(OH)_2$ solution (pH 12.6) (Hurley and Scully, 2002). After a 24-hour stabilisation period (without chloride), chlorides (NaCl) were added incrementally to the test solution in 24-hour cycles.
In chloride-free $Ca(OH)_2$ solutions, the current density decreased from $5 \cdot 10^{-7}$ A/cm² (~6 µm/year) to $1.3 \cdot 10^{-7}$ A/cm² (~1.5 µm/year) over a 1-day period. When chlorides were added to the test solution, the current density increased with time to a value of $2 \cdot 10^{-4}$ A/cm² (~$2.40 \cdot 10^{3}$ µm/year) for 0.0034 M NaCl addition ($[Cl^-]/[OH^-] = 0.14$). According to the authors, the increase of the corrosion rate is to be interpreted as an effect of time rather than an effect of chloride additions because the increase (of i_{CORR}) showed no abrupt changes at the times of chloride additions but occurred at an approximately constant rate.

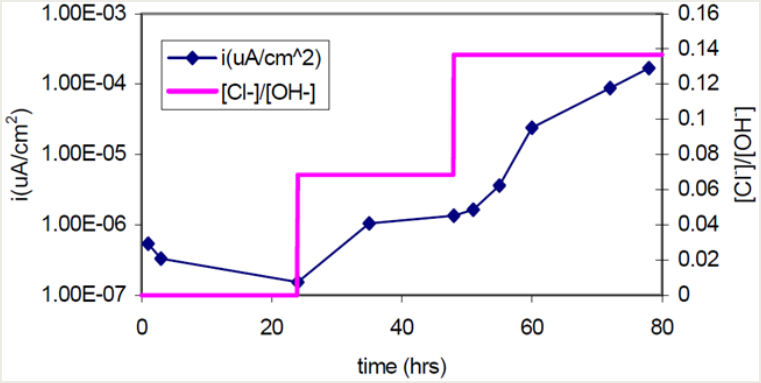

Figure 6-4. Plot of current density (determined potentiostatically) as a function of chloride content versus time for A615 grade carbon steel in saturated $Ca(OH)_2$ solution at 25°C (Hurley and Scully, 2002).

Zhang et al. (Zhang, et al, 2009) studied the chloride threshold concentration at which the corrosion of various types of steel (carbon steel, stainless steel, Cr steel) changed from a passive state to an active state when exposed to a saturated $Ca(OH)_2$ solution (pH=12.6). The corrosion potential and the corrosion rate were monitored in time while adding sodium chloride (NaCl) to the test solution step by step (0%, 0.61%, 1.2%, 1.8%, 2.4%, 3.0%). The linear polarisation resistance technique was used to determine the electrochemical resistance (R_p) and the corrosion rate (expressed as the corrosion current density). The samples were immersed in a saturated $Ca(OH)_2$ solution for 2 days before testing to allow a passive film to be formed at the surface.
This study concluded that the chloride threshold concentration of carbon steel in saturated $Ca(OH)_2$ is about 1.0 wt.% (i.e. ~6000 mg/L Cl^-) (average from 4 replicate experiments), as illustrated in Figure 6-5. This figure shows the evolution of the corrosion potential and the corrosion current density of carbon steel in a saturated $Ca(OH)_2$ solution in time (bottom X-axis) and with chloride concentration (top X-axis).
i_{CORR} decreased sharply from about 0.05 µA/cm² (~0.6 µm/year) (passive state) to 0.01 µA/cm² (~0.1 µm/year) after three days, indicating a continued formation and growth of the passive film on the surface in an environment of pH=12.6. When 0.61 wt.% of chlorides was added to the solution, i_{CORR} showed a relatively large increase from 0.01 µA/cm² (~0.1 µm/year) to 0.1 µA/cm² (~1.2 µm/year) (both were still passive though) before it started to decrease again to a value of 0.035 µA/cm² (~0.4 µm/year) after six days. This clearly showed the interference of chlorides on the passive film formation followed by the recovery of the passive film at this small concentration of chlorides. When the chloride concentration was increased to 1.2 wt.% (i.e. ~7300 mg/L Cl^-), i_{CORR} significantly increased by two orders of magnitude from 0.035 µA/cm² (~0.4 µm/year)

[k] Saturated Calomel Electrode scale.

(passive state) to 3.35 μA/cm² (~40 μm/year) (active state). For chloride concentrations higher than 1.2 wt.%, i_{CORR} remained fairly constant in time.

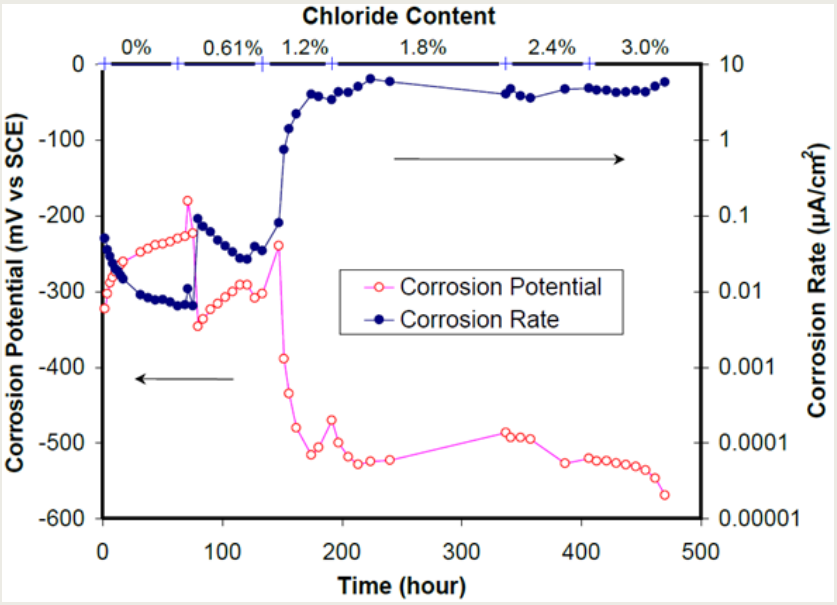

Figure 6-5. Evolution of the corrosion potential and corrosion rate (expressed as a corrosion current density) of carbon steel in saturated $Ca(OH)_2$ solution as a function of chloride addition (Zhang, et al, 2009).

6.3.2. Anaerobic alkaline environments

A number of experiments have been conducted with the addition of chloride:

- in the UK studies, chloride was added up to 20,000 mg/L (Naish, 1993; Naish, et al, 1995; Naish, et al, 2001; Smart, et al, 2004; Smart, 2008; Smart, 2009);
- Fujisawa and co-workers (Fujisawa, et al, 1999) measured the corrosion rate (volumetric hydrogen generation measurements) of carbon steel exposed to $Ca(OH)_2/CaCO_3$ solutions of pH 10.5 or 12.8 with the addition of 19,525 mg/L chloride;
- Mihara and co-workers (Mihara, et al, 2002) performed weight loss and hydrogen generation experiments in NaOH solutions containing 19,000 mg/L chloride at 50°C;
- Nishimura and co-workers (Nishimura, et al, 2003) measured the hydrogen generation rate from carbon steel in saturated $Ca(OH)_2$ solution containing 3,000 mg/L chloride using mass spectrometry at 35°C;
- Fujiware and Kaneko (Fujiwara, 2002; Kaneko, et al, 2004) investigated the effect of chloride concentration (up to 20,000 mg/L) on the hydrogen generation rate (mass spectrometry) of carbon steel in saturated $Ca(OH)_2$ solution. They also studied the effect of pH in saturated $Ca(OH)_2$ solution containing 5,000 mg/L chloride;
- Kaesche and Grubitsch (Kaesche, 1965; Grubitsch, et al, 1970; Grubitsch, et al, 1979) studied the active-passive corrosion behaviour of mild steel by recording potentiodynamic polarisation scans in saturated $Ca(OH)_2$ solutions containing various chloride concentrations in the range from 50 to 12,770 mg/L;

The corrosion rate data reported in the nuclear waste management and non-nuclear industrial literature for mild steel in anoxic and alkaline solutions containing chloride concentrations are summarized in Figure 6-6. The maximum chloride concentration the

surface of the carbon steel overpack is expected to be subjected to has been calculated to be ~19,000 mg/L (after ~2,000 years of exposure) (see section 4.4.).
The data in Figure 6-6 show that the measured corrosion rate decreased with increasing exposure time, even in the presence of chlorides. Comparison of the data in Figure 5-2 (without chloride) with the data shown in Figure 6-6 (with chloride), it can be concluded that the presence of chloride (up to 20,000 mg/L) has no discernible effect on the long-term corrosion rate of carbon steel in anaerobic high pH media.

6.3.3. Considerations

The study of Zhang and co-workers (Zhang, et al, 2009) is of a major importance because it shows that with the addition of ~6,000 mg/L Cl^- (~1 wt.% NaCl) to high alkaline environments (such as the concrete buffer considered in the Supercontainer), the corrosion regime of carbon steel changes from passive to active corrosion (under oxic conditions). This is most likely coupled with the destruction of the protective oxide film.

Considering the high chloride concentrations (~19,000 mg/L) expected at the surface of the carbon steel overpack in the course of the disposal period (see transport calculations of aggressive species, section 4.4.), combined with the potential risk of the passive film being destroyed locally, may result in a significant increased susceptibility to localised corrosion phenomena (such as pitting corrosion, crevice corrosion and stress corrosion cracking).

The effect of this high chloride concentrations of the stability of the protective oxide film should be studied experimentally. Experiments should be performed to evaluate the effect of chloride (19,000 mg/L) on (1) the corrosion rate of carbon steel under oxic conditions and on (2) the occurrence of localised corrosion phenomena.

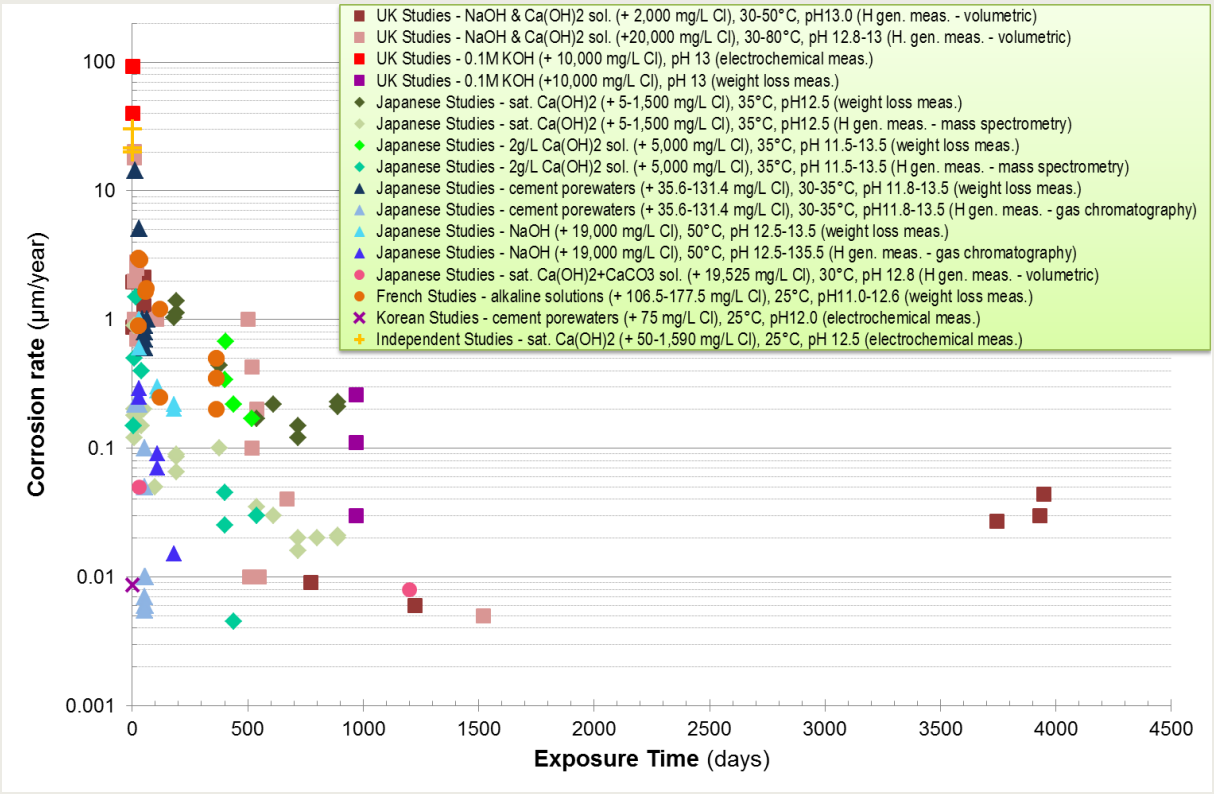

Figure 6-6. Compilation of uniform corrosion rates (reported in the non-nuclear industrial and nuclear waste management literature) of carbon steel in anoxic and alkaline solutions containing chloride concentrations representative for the Supercontainer (i.e. pH ~ 12-13.5). The maximum chloride concentration that is expected to reach the surface of the carbon steel overpack has been calculated to be ~19,000 mg/L.

The following electrochemical techniques were used in the various national waste management R&D programmes:

- Korean studies (×): TP[l];
- independent studies (+): PCD[m] (potentiodynamic);
- UK studies (■):PCD[q] (potentiodynamic);

The graph is compiled from data reported in the following REFERENCES:

- [Smart et al., 2004; Smart, 2008; Smart, 2009];
- [Naish, 1993; Naish, et al, 1995; Naish, et al, 2001; Smart et al., 2004; Smart, 2008; Smart, 2009];
- [Smart et al., 2004; Smart, 2008; Smart, 2009];
- [Smart et al., 2004; Smart, 2008; Smart, 2009];
- [Fujiwara, 2002; Kaneko et al., 2004];
- [Fujiwara, 2002; Kaneko et al., 2004];
- [Fujiwara, 2002; Kaneko et al., 2004];
- [Fujiwara, 2002; Kaneko et al., 2004];
- [Matsuda et al., 1995; RWMC, 1998; Fujiwara et al., 2001];
- [Matsuda et al., 1995; RWMC, 1998; Fujiwara et al., 2001];
- [Mihara et al., 2002];
- [Mihara et al., 2002];
- [Fujisawa et al., 1999]
- [L'Hostis et al., 2011];
- [Jung et al., 2011];
- [Kaesche, 1965; Grubitsch et al., 1970; Grubitsch et al., 1979];

[l] Tafel slope extrapolation method.

[m] Passive Current Density measurements: the passive current densities were derived graphically from the polarisation curves (recorded either potentiostatically or potentiodynamically).

7. Conclusions

The OPERA reference concept for the disposal of Dutch radioactive waste in the 'Rupel' Clay formation is based on the current Belgian Supercontainer concept. In this concept, The radioactive waste is packed in a carbon steel container (i.e. the overpack), which is entirely surrounded by a concrete buffer. In this high alkaline environment (pH ~ 13.6) and under normal conditions (i.e. without the ingress of aggressive species), carbon steel is protected by a passive oxide film, which is believed to result in very low uniform corrosion rates. Considering the long time scales involved in geological disposal, an accurate estimation of the uniform corrosion rate is a crucial part in the safety study.
This report discusses the corrosion rate data of carbon steel exposed to alkaline media that are representative of the environmental conditions according the the OPERA concept. These data are based on a state-of-the-art database, which was build on an extensive review of the published literature that was performed in the framework of the Belgian disposal programme.

The integrated RD&D methodology, which was developed within the framework of the Belgian disposal programme and which aims to provide confidence that the integrity of the carbon steel overpack will not be jeopordized at least for the duration of the thermal phase, was presented. It consisted of three consecutive steps: (1) developing the Corrosion Evolutionary Path (CEP), (2) determining scientifically well-founded estimates of uniform corrosion rates for the different phases established during the CEP, and (3) proving the validity of the 'exclusion principle'.

During the initial period after fabrication of the Supercontainer, the entrapped air will lead to aerobic corrosion of the carbon steel overpack, with the formation of ferric(III) corrosion products, according to the following reaction:

$$4Fe + 6H_2O + 3O_2 \rightarrow 4Fe(OH)_3 \quad \text{(or a ferric salt)} \qquad \text{(eq. 7-1)}$$

Because any residual oxygen or oxidizing radiolysis products will be consumed, the environment surrounding the overpack surface will become anoxic, and the main corrosion reaction can be described by the following reaction:

$$Fe + 2H_2O \rightarrow Fe(OH)_2 + H_2\uparrow \quad \text{(or a ferrous salt)} \qquad \text{(eq. 7-2)}$$

Under anoxic conditions, and depending on temperature (>60°C) and pH, the ferrous hydroxide ($Fe[OH]_2$) may not be the stable corrosion product and may be transformed into magnetite, Fe_3O_4, according to the Schikorr reaction:

$$3Fe(OH)_2 \rightarrow Fe_3O_4 + 2H_2O + H_2\uparrow \qquad \text{(eq. 7-3)}$$

Preliminary geochemical simulations were conducted to gain a first level of understanding of the long-term evolution of the environmental conditions surrounding the carbon steel overpack:

- temperature evolution calculations (2D axisymmetric COMSOL model) predicted a maximum temperature increment at the outer surface of the carbon steel overpack of ~50°C;
- 1D thermo hydraulic analysis of the resaturation time of the concrete materials pointed out that the concrete will resaturate almost completely (up to 95 – 98%) after already one to five years;

- 1D radial chemical diffusive simulations showed that the pH at the outer surface of the carbon steel overpack will remain as high as 12.5 for at least 80,000 years;
- 1D axisymmetric transport calculations of the aggressive species (Cl^-, SO_4^{2-}, $S_2O_3^{2-}$, S^{2-}) estimated a maximum Cl^- concentration, approaching the Rupelian Clay background level (i.e. ~19,000 mg/L), reaching the outer surface of the carbon steel overpack after about 2,000 years;

The various methods, reported in the literature, to measure or calculate the corrosion rate of carbon steel in alkaline media were described. These methods are based on either one of the following three principles:

- weight loss measurements;
- electrochemical measurement techniques (Tafel extrapolation method, linear polarisation resistance technique, galvanostatic pulse technique, electrochemical impedance spectroscopy, electrochemical noise technique, passive current density measurement); or
- quantification of hydrogen gas evolving from the corrosion of steel;

Electrochemical techniques usually give an over-estimation of the long-term corrosion rate, mainly because (1) they do not take properly account for the effects of time-dependent film formation (the corrosion rate decreases in time due to film formation) and (2) all reactions occurring at the overpack's surface are taken into account in the calculations (including the reactions not related to corrosion). Corrosion rates calculated from weight loss are also kown to give higher values than the actual rate at the end of the experiment, because weight loss corrosion rates are averaged over the entire duration of the exposure period. Methods to accurately quantify the amount of hydrogen gas produced during the anaerobic corrosion of carbon steel (eq. 8-2 and eq. 8-3) are considered to provide the most reliable values for the long-term anaerobic corrosion rate.

The corrosion rate data of carbon steel exposed to alkaline media that are representative of the environmental conditions according the the OPERA concept were discussed. These data originated from an extensive review of the published literature (national nuclear waste management programmes and studies for industrial applications) that was performed in the framework of the Belgian disposal programme. The corrosion rate data were classified into aerobic and anaerobic media because the aerobic and anaerobic period have been identified as the two major periods in the course of the Corrosion Evolutionary Path (CEP).

The reported corrosion rate data were critically reviewed based on eight criteria, which have been developed in the framework of the Belgian disposal programme. The corrosion rate data were divided into two ranges, *viz.* a source (SR) and an expert range (ER). The SR and ER of corrosion rates for carbon steel in high alkaline environments (pH ~ 13.6) and under normal conditions (i.e. without the ingress of aggressive species) are summarized in the table below.

Condition	SR	ER
oxic, alkaline media	0.005 – 2.2	0.005 – 2.2
anoxic, alkaline media	0.0015 – 2.4	0.0015 – 0.2

Because of the high chloride content of the Boom Clay host rock formation, located in the Netherlands, and the consequential high chloride concentration expected at the surface of the carbon steel overpack, the effect of chloride on the corrosion rate was evaluated.
A huge amount of information was available in the literature on the effect of chloride on the aerobic corrosion rate of carbon steel, coming from experimental programmes studying

the effect of de-icing salts on the corrosion behaviour of steel reinforcements (for industrial applications). Although a general trend of increasing corrosion rate with increasing chloride concentration was observed from literature, it was very difficult to assign an absolute value (in terms of corrosion rate expressed in µm/year) to the effect of chloride concentration, because from the data reported in the literature it was impossible to discriminate between the effect of increasing exposure time and the effect of increasing chloride concentration (tests, in which the chloride concentration was gradually increased in time, were usually performed).
The anaerobic corrosion rate data of carbon steel in chloride containing media mainly originated from the nuclear waste management literature. It was found that the anaerobic long-term corrosion rate was not affected by the addition of chlorides up to 20,000 mg/L.

Although not subject to this study, the high amounts of chlorides present at the surface of the carbon steel overpack could pose a serious threat to its integrity, in terms of localised corrosion susceptibility. This should be further investigated.

8. Recommendations

Considering the high chloride concentrations (~19,000 mg/L) expected at the surface of the carbon steel overpack in the course of the disposal period (see transport calculations of aggressive species, section 4.4.), combined with the potential risk of the passive film being destroyed locally, may result in a significant increased susceptibility to localised corrosion phenomena (such as pitting corrosion, crevice corrosion and stress corrosion cracking).
The effect of this high chloride concentrations of the stability of the protective oxide film should be studied experimentally. Experiments should be performed to evaluate the effect of chloride (19,000 mg/L) on (1) the corrosion rate of carbon steel under oxic conditions and on (2) the occurrence of localised corrosion phenomena.

9. Acknowledgements

The authors gratefully acknowledge contributions from Yu Li, Eef Weetjens, Lian Wang and Joan Govaerts to this report (geochemical simulations of the major corrosion-related parameters — T, water saturation of the concrete buffer, pH and transport of aggressive species).

10. References

Agg PJ, *Modelling gas generation in radioactive waste repositories*, Nuclear Energy **32**(2) (1993) 81-87.

Ahmad Z, Principles of corrosion engineering and corrosion control (2006), Elsevier Ltd., Amsterdam, The Netherlands.

Akolzin AP, Ghosh P, Kharitonov YY, *Use of calcium hydroxide to prevent corrosion of carbon steels*, Zashchita Metallov **19**(2) (1983) 302-304 (translation).

Akolzin AP, Ghosh P, Kharitonov YY, *Application and peculiarity of $Ca(OH)_2$ as inhibitor in presence of corrosion activators*, British Corrosion Journal **20**(1) (1985a) 32.

Akolzin AP, Ghosh P, Kharitonov YY, *Application of calcium hydroxide preventing corrosion of carbon steel*, Indian Journal of Technology **23** (1985b) 136-140.

Alonso C, Andrade C, *Corrosion of steel reinforcement in carbonated mortar containing chloride*, Advances in Cement Research **1** (1988) 155-163.

Alonso C, Andrade C, González JA, *Relation between resistivity and corrosion rate of reinforcements in carbonated mortar made with several cement types*, Cement and Concrete Research **8**(5) (1988) 687-698.

Alonso C, Andrade C, Castellote M, Castro P, *Chloride threshold value to depassivate reinforcing bars embedded in a standardized OPC mortar*, Cement and Concrete Research **30**(7) (2000) 1047-1055.

Andrade C, González JA, *Quantitative measurements of corrosion rate of reinforcing steels embedded in concrete using polarisation resistance measurements*, Werkstoffe und Korrosion **29** (1978) 515-519.

Andrade C, Jáuregui G, González JA, Influence of mortar mix proportions on corrosion of bare and galvanized reinforcements caused by penetration of chlorides, *In*: proceedings of the 8th International Congress on Metallic Corrosion (8th ICMC), volume II (1981), 6-11 September 1981, Mainz, Germany, DECHEMA, Frankfurt am Main, Germany 1372-1377.

Andrade C, Page CL, *Pore solution chemistry in hydrated cement systems containing chloride salts: A study of cation specific effects*, British Corrosion Journal **21** (1986) 49.

Andrade C, Alonso MC, González JA, An initial effort to use the corrosion rate measurements for estimating rebar durability, *In*: Berke NS, Chaker V, Whiting D, *eds.*, Corrosion Rates of Steel in Concrete, *ASTM STP 1065* (1990), American Society for Testing and Materials (ASTM), Philadelphia, PA, USA 29-37.

Andrade C, Alonso MC, Values of corrosion rate of steel in concrete to predict service life of concrete structures, *In*: Cragnolino G, Sridhar N, *eds.*, Application of Accelerated Corrosion Tests to Service Life Prediction of Materials, *ASTM STP 1194* (1994) 282-295.

Andrade C, Merino P, Nóvoa XR, Pérez MC, Soler L, *Passivation of reinforcing steel in concrete*, Materials Science Forum **192-194** (1995) 891-898.

Andrade C, Alonso C, Gulikers J, Polder R, Cigna R, Venesland Ø, Salta M, Raharinaivo R, Elsener B, *Test methods for on-site corrosion rate measurement of steel reinforcement in concrete by means of the polarization resistance method*, RILEM TC 154-EMC recommendation 'Electrochemical techniques for measuring metallic corrosion', Materials and structures **37**(9) (2004) 623-643.

Angst U, Elsener B, Larsen CK, Vennesland Ø, *Critical chloride content in reinforced concrete: A review*, Cement and Concrete Research **39** (2009) 1122-1138.

Aperador W, Mejía de Gutiérrez R, Bastidas DM, *Steel corrosion behaviour in carbonated alkali-activated slag concrete*, Corrosion Science **51**(9) (2009) 2027-2033.

Arup H, The mechanisms of the protection of steel by concrete, *In*: Crane AP, *ed.*, Corrosion of reinforcement in concrete construction (1983), Ellis Horwood Ltd, Chichester, West Essex, United Kingdom, 151-157.

Arya C, Xu Y, *Effect of cement type on chloride binding and corrosion of steel in concrete*, Cement and Concrete Research **25** (1995) 893-902.

Autolab, 2010, Autolab Application Note 17 – Corrosion: 2. Measurement of corrosion rates, http://www.ecochemie.nl/export/Homepages/Autolab/download/Applicationnotes/Appl017.pdf.

Azizi O, Chen Y, Macdonald DD, Characterization of the passive film on carbon steel in saturated $Ca(OH)_2$+NaOH solution, report submitted to NIRAS/ONDRAF (2008b), Pennsylvania State University, USA.

Baboian R, *ed.*, Corrosion tests and standards (1995), American Society for Testing and Materials (ASTM), Philadelphia, USA.

Badea GE, Cărăban A, Sebesan M, Dzitac S, Cret P, *Polarisation measurements used for corrosion rates determination*, Journal of sustainable Energy **1**(1) (2010).

Behrends T, van der Veen I, Hoving A, Griffoen J, Geochemical characterization of Rupel (Boom) Clay material: pore water composition, reactive minerals and cation exchange capacity, OPERA-PU-UTR521 (2015), Utrecht University, The Netherlands 1-43.

Behrens D, Dechema Corrosion Handbook: Corrosion agents and their interaction with materials, volume 1 – Acetates, aluminium chloride, chlorine and chlorinated water, fluorides, potassiuim hydroxide, steam, sulfonic acids (1987), Wiley-VCH Verlag Gmbh, Weinheim, Germany 172.

Bentur A, Diamond S, Berke NS, Steel corrosion in concrete: fundamentals and civil engineering practice (1997), E & FN Spon, London, United kingdom.

Bertocci U, Mullen JL, Ye YX, Electrochemical noise measurements for the study of localized corrosion and passivity breakdown, *In*: Froment M, *ed.*, Passivity of metals and semiconductors (1983), Elsevier Science Publishers, Amsterdam, The Netherlands 229-234.

Bertocci U, Huet F, *Noise analysis applied to electrochemical systems*, Corrosion **51**(2) (1995) 131-144.

Bertocci U, A comparison of electrochemical noise and impedance spectroscopy for the detection of corrosion in reinforced concrete, *In*: Kearns JR, Scully JR, Roberge PR, Reichert DL, Dawson JL, *eds.*, Electrochemical noise measurement for corrosion applications, *ASTM STP 1277* (1996), American Society for Testing and Materials (ASTM), Philadelphia, PA, USA 39-58.

Bertocci U, Impedance spectroscopy for the evaluation of corrosion inhibitors in highway deicers, report FHWA-RD-96-178 (1997), Federal Highway Administration, Georgetown Pike, McLean, Virginia, USA.

Bertocci U, Gabrielli C, Huet F, Keddam M, *Noise resistance applied to corrosion measurements - I. Theoretical analysis*, Journal of the Electrochemical Society **144**(1) (1997a) 31-37.

Bertoci U, Gabrielli C, Huet F, Keddam M, Rousseau P, *Noise resistance applied to corrosion measurements - II. Experimental tests*, Journal of the Electrochemical Society **144**(1) (1997b) 37-43.

Bertolini L, Elsener B, Pedeferri P, Polder R, Corrosion of steel in concrete: prevention, diagnosis, repair (2004), Wiley-VCH Verlag GmbH & Co., Weinheim, Germany.

Bierwagen GP, Tallman DE, Li J, Balbyshev S, Zidoune M, Electrochemical noise studies of aircraft coatings over Al2024-T3 in accelerated exposure testing, CORROSION/2000 (2000), 26-31 March 2000, Orlando, Florida, USA.

Blackwood DJ, Naish CC, Platts N, Taylor KJ, Thomas MI, The anaerobic corrosion of carbon steel in granitic groundwaters, report AEA-InTec-1414 (1995), AEA Technology, Harwell, Oxfordshire, UK.

Blackwood DJ, Naish CC, Sharland SM, Thompson AM, Experimental and modelling study to assess the initiation of crevice corrosion in stainless steel containers for radioactive waste, report AEAT/ERRA-0300 (2002), AEA Technology, Harwell, Oxfordshire, UK.

Blackwood DJ, Gould LJ, Naish CC, Porter FM, Rance AP, Sharland SM, Smart NR, Thomas MI, Yates T, The localised corrosion of carbon steel and stainless steel in simulated repository environments, report AEAT/ERRA-0318 (2002a), AEA Technology, Harwell, Oxfordshire, UK.

Broomfield JP, Corrosion of steel in concrete: understanding, investigation and repair (second edition) (2007), Taylor & Francis, London, United Kingdom.

Bullard SJ, Covino BS Jr, Russell JH, Holcomb GR, Cramer SD, Ziomek-Moroz M, Electrochemical noise sensors for detection of localized and general corrosion of natural gas transmission pipelines, report DOE/ARC-TR-03-0002 (2002), Albany Research Center (ARC), Albany, OR, USA.

Bürchler D, Elsener B, Böhni H, Electrical resistivity and dielectrical properties of hardened cement paste and mortar, *In*: Page CL, Bamforth PB, Figg J, *eds.*, Corrosion of Reinforcement in Concrete Structures (1996), Society of Chemical Industry, United Kingdom 283-293.

Byakova SA, Loskutov VF, Pogrebova IS, *Influence of vanadising on the corrosion rate of steels*, Zashchita Metallov **12** (1976) 552-553.

Carino NJ, *Nondestructive techniques to investigate corrosion status in concrete structures*, Journal of Performance of Constructed Facilities **13**(3) (1999) 96-106.

Chambers AV, Williams SJ, Wisbey SJ, Science Report - Nirex Safety Assessment Research Programme. Nirex Near Field Research: Report on the Current Status in 1994, report S/95/011 (1995), NIREX, UK.

Chen CT, *Skerry BS, Assessing the corrosion resistance of painted steel by AC impedance and electrochemical noise techniques*, Corrosion **47**(8) (1991) 598-611.

Chitty WJ, Dillmann P, L'Hostis V, Lombard C, *Long-term corrosion resistance of metallic reinforcements in concrete – A study of corrosion mechanisms based on archaeological artefacts*, Corrosion Science **47**(6) (2005) 1555-1581.

Christensen BJ, Mason TO, Jennings HM, *Influence of silica fume on the early hydration of Portland cements using impedance spectroscopy*, Journal of the American Ceramic Society **75**(4) (1992) 939-945.

Christensen BJ, Coverdale T, Olson RA, Ford SJ, Garboczi EJ, Jennings HM, Mason TO, *Impedance spectroscopy of hydrating cement-based materials: Measurement, interpretation and application*, Journal of the American Ceramic Society **77**(11) (1994) 2789-2804.

Clear KC, Measuring the rate of corrosion of steel in field concrete structures, *Transportation Research Record* **1211** (1989), Transportation Research Board, National Research Council, Washington, DC, USA.

COMSOL, COMSOL Multiphysics 3.5a, Earth Science Module (2008), COMSOL AB, Stockholm, Sweden.

Constantiner D, Diamond S, Pore solution analysis: are there pressure effects?, *In*: Scrivener KL, Young JF, *eds.*, Mechanisms of chemical degradation of cement-based systems (1997), E & FN Spon, London, United Kingdom 22-29.

Cottis RA, Loto CA, *Electrochemical noise generation during SCC of a high-strength carbon steel*, Corrosion **46**(1) (1990) 12-19.

Cottis RA, Turgoose S, *Electrochemical noise measurements – A theoretical basis*, Materials Science Forum **192-194** (1995) 663-672.

Cottis RA, Turgoose S, Electrochemical impedance and noise, *In*: Syrett BC, *ed.*, Corrosion Testing Made Easy series of books (1999), NACE International, Houston, Texas, USA.

Cottis RA, 2001, *Interpretation of electrochemical noise data*, Corrosion **57**(3) (2001) 265-285.

Cottis R, Chapter 4. Electrochemical noise for corrosion monitoring, *In*: Yang L, *ed.*, Techniques for corrosion monitoring (2008), Woodhead Publishing Ltd., Cambridge, UK 86-110.

Crossland I, Corrosion of iron-based alloys: evidence from nature and archaeology, report Crossland CCL/2006/02 (2006), Nirex Ltd, United Kingdom.

Cuñado M, Final Report on Waste Composition and Waste Package Description for Each Selected Equilibrium Scenario (2007), Red-Impact Project, Deliverable 3.7.

Davis JR, Corrosion: Understanding the basics (2000), ASM International, Materials Park, Ohio, USA.

Dawson JL, Corrosion monitoring of steel in concrete, *In*: Crane AP, *ed.*, Corrosion of reinforcement in concrete construction (1983), Ellis Horwood Ltd, Chichester, West Essex, United Kingdom 175-191.

Dawson JL, Electrochemical noise measurement: The definitive in-situ technique for corrosion applications, *In*: Kearns JR, Scully JR, Roberge PR, Reichert DL, Dawson JL, *eds.*, Electrochemical noise measurement for corrosion applications, *ASTM STP 1277* (1996), American Society for Testing and Materials (ASTM), Philadelphia, PA, USA, 3-38.

De Craen M, Wang L, Van Geet M, Moors H, Geochemistry of Boom Clay pore water at the Mol site, report SCK•CEN-BLG-990 (2004), SCK•CEN, Mol, Belgium.

Deshpande PG, Seddelmeyer JD, Wheat HG, Fowler DW, Jirsa JO, Corrosion performance of polymer-coated, metal-clad and other rebars as reinforcement in concrete, report FHWA/TX-03/4904-2 (2000), Texas Department of Transportation (TxDOT), Austin, Texas, USA.

Dhoubi L, Triki E, Raharinaivo A, *The application of electrochemical impedance spectroscopy to determine the long-term effectiveness of corrosion inhibition for steel in concrete*, Cement & Concrete Composites **24**(1) (2002) 35-43.

Diamond S, *Effects of two Danish fly ashes on alkali contents of pore solutions of cement-fly ash pastes*, Cement and Concrete Research **11** (1981) 383-394.

Diamond S, *Effects of microsilica (silica fume) on pore-solution chemistry of cement pastes*, Communications of American Ceramic Society (1983) C82-C84.

Dražić DM, Hao CS, *Inhibition of the anodic dissolution of iron in alkaline solution by metal complex ions*, Corrosion Science **23**(7) (1983) 683-686.

Duchesne J, Berube MA, *Evaluation of the validity of the pore solution expression method from hardened cement pastes and mortars*, Cement and Concrete Research **24** (1994) 456-462.

Eden DA, Hoffman M, Skerry BS, Chapter 4. Application of electrochemical noise measurements to coated systems, *In*: Dickiee RA, Floyd FL, *eds.*, Polymeric materials for corrosion control, ACS Symposium Series, vol. 322 (1986), American Chemical Society (ACS), Washington, D.C., USA 36-47.

Eden DA, Rothwell AN, Electrochemical noise data: Analysis, interpretation and presentation, CORROSION/92, paper no. 292 (1992), 27 April – 1 May 1992, Nashville, TN, USA.

Eden DA, Electrochemical noise – The first two octaves, CORROSION/98, paper no. 386 (1998), 22-27 March 1998, San Diego, CA, USA.

Elsener B, Klinghoffer O, Frølund T, Rislund E, Schiegg Y, Böhni H, Assessment of reinforcement corrosion by means of galvanostatic pulse technique, *In*: Blankvoll A, *ed.*, Proceedings of the International Conference on Repair of Concrete Structures—From theory to practice in a marine environment (1997), 28-30 May, 1997, Svolvær, Norway, pp. 391-400.

Elsener B, *Corrosion rate of steel in concrete - Measurements beyond the Tafel law*, Corrosion Science **47** (2005) 3019-3033.

Evans UR, An introduction to metallic corrosion (third edition) (1981), Edward Arnold Publishers Ltd, London, United Kingdom.

Feliu S, González JA, Andrade C, Feliu V, *On-site determination of the polarization resistance in a reinforced concrete beam*, Corrosion **44**(10) (1988) 761-765.

Feliu S, González JA, Miranda JA, Feliu V, *Determining polarization resistance in reinforced concrete slabs*, Corrosion Science **29**(1) (1989) 105-113.

Feliu S, González JA, Miranda JA, Feliu V, *Possibilities and problems of in situ techniques for measuring steel corrosion rates in large reinforced concrete structures*, Corrosion Science **47**(1) (2005) 217- 238.

Frølund T, Jensen FM, Bassler R, Smart structures: Determination of reinforcement corrosion rate by means of the galvanostatic pulse technique, presented at the First International Conference on Bridge Maintenance, Safety and Management (IABMAS 2002), 14-17 July, 2002, Barcelona, Spain.

Fujisawa R, Cho T, Sugahara K, Takizawa Y, Horikawa Y, Shiomi T, Hironaga M, *The corrosion behavior of iron and aluminium under waste disposal conditions*, Mat. Res. Soc. Symp. Proc. **465** (1997) 675-682.

Fujisawa R, Kurashige T, Inagaki Y, Senoo M, *Gas generation behavior of transuranic waste under disposal conditions*, Mat. Soc. Res. Symp. Proc. **556** (1999) 1199-1206.

Fujiwara A, Yasutomi I, Fukudome K, Tateishi T, Fujiwara K, *Influence of oxygen concentration and alkalinity on the hydrogen gas generation by corrosion of carbon steel*, Mat. Res. Soc. Symp. Proc. **663** (2001) 497-505.

Fujiwara A, Gas generation by steel corrosion under reductive conditions – Continuous measurement test, presented at the *GASNET Workshop* (2002), 12-14 November 2002, Cologne, Germany.

Gabrielli C, Huet F, Keddam M, Takenouti H, *Application of electrochemical noise measurements to the study of localized and uniform corrosion*, 8th European Congress on Corrosion, vol. 2, paper no. 37 (1985) 37.1-37.7.

Gabrielli C, Keddam M, *Review of applications of impedance and noise analysis to uniform and localized corrosion*, Corrosion **48**(10) (1992) 794-811.

Gamry, Application note 'DC Corrosion Techniques' (2007), Gamry Instruments, Warminster, PA, USA.

Gamry, Application note 'Basics of Electrochemical Impedance Spectrosopy' (2010a), Gamry Instruments, Warminster, PA, USA.

Gamry, Application note 'Electrochemical Noise' (2010b), Gamry Instruments, Warminster, PA, USA.

Gepraegs OK, Comparison and evaluation of electrochemical techniques and monitoring instruments to determine the corrosion rate of steel in concrete, PhD Thesis (2002), University of Waterloo, Ontario, Canada.

GI, Germann Instruments NDT Systems catalog 2010 (2010) 61-64.

Glass GK, Page CL, Short NR, Zhang JZ, *The analysis of potentiostatic transients applied to the corrosion of steel in concrete*, Corrosion Science **39**(9) (1997) 1657-1663.

Goñi S, Andrade C, *Synthetic concrete pore solution chemistry and rebar corrosion rate in the presence of chlorides*, Cement and Concrete Research **20**(4) (1990) 525-539.

González JA, Algaba S, Andrade C, *Corrosion of reinforcing bars in carbonated concrete*, British Corrosion Journal **15**(3) (1980) 135-139.

González JA, Andrade C, Alonso C, Feliú S, *Comparison of rates of general corrosion and maximum pitting penetration on concrete embedded steel reinforcement*, Cement and Concrete research **25**(2) (1995) 257-264.

González JA, Feliú S, Rodríguez P, Ramírez E, Alonso C, Andrade C, 1996, *Some questions on the corrosion of steel in concrete – Part I: when, how and how much steel corrodes*, Materials and Structures **29** (1996) 40-46.

Govaerts J, Weetjens E, Scoping calculation: when and in which concentration will aggressive species reach the overpack surface?, report SCK•CEN-ER-133 (2010), SCK•CEN, Mol, Belgium.

Gowers KR, Millard SG, *Electrochemical technology for corrosion assessment of reinforced concrete structures*, Proceedings of the Institution of Civil Engineers – Structures and Buildings, **134**(2) (1999) 129-137.

Grauer R, The corrosion behaviour of carbon steel in portland cement, report NAGRA NTB 88-02^{E} (1988), NAGRA, Switzerland.

Grauer R, Knecht B, Kreis P, Simpson JP, *Hydrogen evolution from corrosion of iron and steel in intermediate level waste repositories*, Mat. Res. Soc. Symp. Proc. **212** (1991a) 295-302.

Grauer R, Knecht B, Kreis P, Simpson JP, *The long term corrosion rate of passive iron in anaerobic alkaline solutions*, Werkstoffe und Korrosion **42** (1991b) 637-642.

Grubitsch H, Miklautz H, Hilbert F, *Potentiodynamische und potentiostatische Messungen an gespannten Drahtelektroden in gesättigten $Ca(OH)_2$-Lösungen mit verschiedenen Zusätzen*, Werkstoffe und Korrosion **21**(6) (1970) 485-495.

Grubitsch H, Binder L, Hilbert F, *The influence of various concentrations of chloride ions on the active-passive corrosion susceptibility of steel in saturated calcium hydroxide solution*, Werkstoffe und Korrosion **30**(4) (1979) 241-245.

Gu P, Elliott S, Beaudoin JJ, Arsenault B, *Corrosion resistance of stainless steel in chloride contaminated concrete*, Cement and concrete Research **26**(8) (1996) 1151-1156.

Gu P, Elliott S, Hristova R, Beaudoin JJ, Brousseau RJ, Baldock B, *A study of corrosion inhibitor performance in chloride contaminated concrete by electrochemical impedance spectroscopy*, ACI Materials Journal **94**(5) (1997) 385-395.

Gu P, Beaudoin JJ, *Estimation of steel corrosion rate in reinforced concrete by means of equivalent circuit fittings of impedance spectra*, Advances in Cement Research **10**(2) (1998) 43-56.

Hachani L, Carpio J, Fiaud C, Raharinaivo A, Triki E, *Steel corrosion in concretes deteriorated by chlorides and sulphates: Electrochemical study using impedance spectrometry and "stepping down the current" method*, Cement and Concrete Research **22** (1992) 56-66.

Hachani L, Fiaud C, Triki E, Raharinaivo A, *Characterisation of steel/concrete interface by electrochemical impedance spectroscopy*, British Corrosion Journal **29**(2) (1994) 122-127.

Hansson CM, *Comments on electrochemical measurements of the rate of corrosion of steel in concrete*, Cement and Concrete Research **14**(4) (1984) 574-584.

Hansson CM, The corrosion rate of mild steel in deaerated synthetic cement pore solution, report SKB TR 1984-11-14 (1984c), SKB, Sweden.

Hansson CM, Hydrogen evolution in anaerobic concrete resulting from corrosion of steel reinforcement, report SKB Teknisk PM Nr. 30 (1985), SKB, Sweden.

Hansson CM, *The corrosion of steel and zirconium in anaerobic concrete*, Mat. Res. Soc. Symp. Proc. **50** (1985a) 475-482.

Hansson CM, The corrosion of steel in anaerobic concrete and the associated evolution of hydrogen, report SFR-87-02 (1987), SKB, Sweden.

Hausmann DA, *Steel corrosion in concrete. How does it occur?*, J. Mater. Prot. **6**(11) (1967) 19-23.

Heitz E, Schwenk W, *Theoretische Grundlagen der Ermittlung von Korrosionsstromdichten aus Polarisationswiderständen*, Werkstoffe und Korrosion **27**(4) (1976) 241-245.

Herms E, General criteria for the selection of carbon steels to face hydrogen embrittlement in the context of deep geological disposal, report NT DPC/SCCME 09-474-A (2009), French Atomic Energy Commission (CEA Saclay), Gif-sur-Yvette, France.

Heusler KE, Weil KG, Bonhoeffer KF, *Die Bedeutung des Flade-Potentials für die Passivität des Eisens in alkalischen Lösungen*, Z. Physik. Chem. Neue Folge **15** (1958) 149-161.

Hladky K, Dawson JL, *The measurement of localized corrosion using electrochemical noise*, Corrosion Science **21**(4) (1981) 317-322.

Holcomb GR, Covino BS Jr, Eden D, State-of-the-art review of electrochemical noise sensors, report DOE/ARC-TR-2001-016 (2001), Albany Research Center (ARC), Albany, OR, USA.

Holden WR, Page CL, Short NR, The influence of chlorides and sulfates on durability, *In*: Crane AP, ed., Corrosion of Reinforcement in Concrete Construction, chapter 9 (1983), Ellis Horwood Limited, United Kingdom 143-150.

Honda A, Kato T, Tateishi T, Imakita T, Masuda K, Kato O, Nishimura T, *Chemical transition of nitrate ions accompanied by corrosion of carbon steel under alkaline conditions*, Corrosion Enginering **55**(10) (2006) 635-649.

Honda A, Masuda K, Imakita T, Kato O, Nishimura T, *Modelling of chemical transition of nitrate accompanied by corrosion of carbon steel under alkaline conditions*, Corrosion Enginering **58**(5) (2009) 219-234.

Hope BB, Page JA, Ip AKC, *Corrosion rates of steel in concrete*, Cement and concrete Research **16**(5) (1986) 771-781.

Hubbe MA, *Polarisation resistance corrosivity test with a correction for resistivity*, British Corrosion Journal **15**(4) (1980) 193-197.

Huet B, L'Hostis V, Idrissi H, Tovena I, A review on corrosion mechanisms of reinforced concrete degradation, proceedings of the International Conference on Environmental Degradation of Engineering Materials (EDEM2003) (2003), 29 June – 2 July 2003, Bordeaux, France.

Huet B, Comportement à la corrosion des armatures dans un béton carbonaté. Influence de la chimie de la solution interstitielle et d'une barrière de transport, PhD Thesis, report 05 ISAL 0075 (2005a), Institut National des Sciences Appliqués de Lyon (INSA), Lyon, France.

Huet B, L'Hostis V, Miserque F, Idrissi H, *Electrochemical behavior of mild steel in concrete: Influence of pH and carbonate content of concrete pore solution,* Electrochimica Acta **51** (2005b) 172-180.

Huet B, Peycelon H, Le Bescop P, L'Hostis V, Idrissi H, Dissolution of iron oxides in carbonated concrete, proceedings of EUROCORR2005 (2005c), 4-8 September 2005, Lisbon, Portugal.

Huet B, Chapter 14. Electrochemical noise technique, *In*: Marcus Ph, Mansfeld F, *eds.*, Analytical methods in corrosion science and engineering (2006), CRC Press 507-564.

Hurley MF, Scully JR, Clemeña GG, Selected issues in corrosion resistance of stainless steel clad rebar, CORROSION2001, paper no. 01646 (2001), 11-16 March 2001, Houston, Texas, USA.

Hurley MF, Scully JR, Chloride threshold levels in clad 316L and solid 316LN stainless steel rebar, CORROSION2002, paper no. 02224 (2002), 7-11 April 2002, Denver, Colorado, USA.

Ismail MA, Ohtsu M, Monitoring corrosion rate of concrete by AC impedance spectroscopy, 11th International Conference on Fracture (ICF XI) (2005), 20-25 March, 2005, Turin, Italy.

Ismail MA, Ohtsu M, *Corrosion rate of ordinary and high-performance concrete subjected to chloride attack by AC impedance spectroscopy*, Construction and Building Materials **20**(7) (2006) 458-469.

Jelinek J, Neufeld P, *Kinetics of hydrogen formation from mild steel in water under anaerobic conditions*, Corrosion **38**(2) (1982) 98-104.

John DG, Searson PC, Dawson JL, *Uses of ac impedance technique in studies on steel in concrete in immersed conditions*, British Corrosion Journal **16**(2) (1981) 102-106.

Jung H, Kwon KJ, Lee E, Kim DG, Kim GY, *Effect of dissolved oxygen on corrosion properties of reinforcing steel*, Corrosion Engineering, Science and Technology **46**(2) (2011) 195-198.

Kaesche H, *Untersuchungen über die Korrosion ungelegierter Stähle in Kalziumhydroxydlösung und in feuchtem Beton*, Arch. Eisenhüttenwesen **36**(12) (1965) 911-922.

Kaneko M, Miura N, Fujiwara A, Yamamoto M, Evaluation of gas generation rate by metal corrosion in the reducing environment, report RWMC-TRE-03003 (2004), Radioactive Waste Management Funding and Research Center (RWMC), Japan.

Kawamura M, Kayyali OA, Haque MN, *Effects of a fly ash on pore solution composition in calcium and sodium chloride-bearing mortars*, Cement and Concrete Research **18** (1988) 763-773.

Kayyali OA, Haque MN, *Environmental factor and concentration of Cl^- and OH^- in mortars*, Journal of Materials in Civil Engineering **2** (1990) 24-34.

Kelly RG, Scully JR, Shoesmith DW, Buchheit RG, Electrochemical techniques in corrosion science and engineering (2003), Marcel Dekker, Inc., New York, USA.

King F, Overview of a carbon steel container corrosion model for a deep geological repository in sedimentary rock, report NWMO TR-2007-01 (2007), Nuclear Waste Management Organization, Canada.

King F, Corrosion of carbon steel under anaerobic conditions in a repository for SF and HLW in Opalinus Clay, report NAGRA NTB 08-12 (2008), NAGRA, Switzerland.

Kreis P, Hydrogen evolution from corrosion of iron and steel in low/intermediate level waste repositories, report NAGRA NTB 91-21 (1991), NAGRA, Switzerland.

Kreis P, Simpson JP, Hydrogen gas generation from the corrosion of iron in cementitious environments, *In*: Corrosion problems related to nuclear waste disposal, European Federation of Corrosion Publication number 7 (1992), Institute of Materials, London, UK 57-72.

Kreis P, Wasserstoffentwicklung durch Korrosion von Eisen und Stahl in Anaeroben, Alkalischen Medien im Hinblick auf ein SMA-Endlager, report NAGRA NTB 93-27 (1993), NAGRA, Switzerland.

Kursten B, Druyts F, *Methodology to make a robust estimation of the carbon steel overpack lifetime with respect to the Belgian Supercontainer design*, J. Nucl. Mater. **379** (1-3) (2008) 91-96.

Kursten B, Druyts F, Macdonald DD, Smart NR, Gens R, Wang L, Weetjens E, Govaerts J, *Review of corrosion studies of metallic barrier in geological disposal conditions with respect to Belgian Supercontainer concept*, Corrosion Engineering, Science and Technology **46** (2) 91-97.

Kursten B, Druyts F, Smart NR, Macdonald DD, Gens R, Wang L, Weetjens E, Govaerts J, *Review of passive corrosion studies of carbon steel in concrete in the context of disposal of HLW and spent fuel in Belgium*, ASME proceedings of the 15th International Conference on Environmental Remediation and Radioactive Waste Management (ICEM2013), paper no. ICEM2013-96275 (2013), 8-12 September 2013, Brussels, Belgium.

Kursten, B, Uniform corrosion rate data of carbon steel in cementitious environments relevant to the Supercontainer design – 'best estimate' from available literature data. First full draft report, report SCK•CEN-ER-94 (to be published), SCK•CEN, Mol, Belgium.

Larbi JA, Fraay ALA, Bijen JL, *The chemistry of the pore fluid of silica fume-blended cement systems*, Cement and Concrete Research **20**(4) (1990) 506-516.

Lay P, Lawrence PF, Wilkins NJM, Williams DE, *An a.c. impedance study of steel in concrete*, Journal of Applied electrochemistry **15**(5) (1985) 755-766.

Leban M, Doleček V, Legat A, *Comparitive analysis of electrochemical noise generated during stress corrosion cracking of AISI 304 stainless steel*, Corrosion **56**(9) (2000) 921-927.

Lee CC, Mansfeld F, *Analysis of electrochemical noise data for a passive system in the frequency domain*, Corrosion Science **40**(6) (1998) 959-962.

Legat A, Govekar E, *Detection of corrosion by analysis of electrochemical noise*, Fractals **2**(2) (1994) 241-244.

Legat A, Doleček V, *Corrosion monitoring system based on measurement and analysis of electrochemical noise*, Corrosion **51**(4) (1995) 295-300.

Legat A, Leban M, Bajt Ž, *Corrosion processes of steel in concrete characterized by means of electrochemical noise*, Electrochimica Acta **49** (2004) 2741-2751.

Lemoine L, Wenger F, Galland J, Study of the corrosion of concrete reinforcement by electrochemical impedance measurement, *In:* Berke NS, Chaker V, Whiting D, *eds.*, Corrosion Rates of Steel in Concrete, *ASTM STP 1065* (1990), American Society for Testing and Materials (ASTM), Philadelphia, PA, USA, 118-133.

Lesnikova PK, Frejd MK, *The effect of boriding on the corrosion resistance of carbon steels*, Zashchita Metallov **16**(2) (1980) 163-164 (translated from Russian).

L'Hostis V, Amblard E, Blanc C, Miserque F, Paris C, Bellot-Gurlet L, *Passive corrosion of steel in concrete in context of nuclear waste disposal*, Corrosion Engineering, Science and Technology **46**(2) (2011) 177-181.

Li L, Pitting corrosion and chloride corrosion threshold of reinforcing steel in alkaline solutions, PhD Thesis (2000), University of South Florida, Tampa, Florida, USA.

Li L, Sagüés AA, Metallurgical effects on chloride ion corrosion threshold of steel in concrete, report WPI 0510806 (2001), University of South Florida, USA.

Linke WF, Seidell A, Solubilities of inorganic and metal organic compounfds: a compilation of solubility data from the periodical literature (fourth edition) (1958), Van Vostrand, Inc., New York, USA.

Linnenbom VJ, *The reaction between iron and water in the absence of oxygen*, J. Electrochem. Soc. **105** (1958) 321.

Macdonald DD, McKubre MCH, Urquidi-Macdonald M, *Theoretical assessment of AC impedance spectroscopy for detecting corrosion of rebar in reinforced concrete*, Corrosion **44**(1) (1988) 2-7.

Macdonald DD, Urquidi-Macdonald M, Rocha-Filho RC, El-Tantawy Y, *Determination of the polarization resistance of rebar in reinforced concrete*, Corrosion **47**(5) (1991) 330-334.

Macdonald DD, Azizi O, Saleh A, The passivity and corrosion resistance of carbon steel in simulated Boom Clay HLNW environments, *In*: L'Hostis V, Gens R, Gallé C, *eds.*, NUCPERF 2009, Long-Term Performance of Cementitious Barriers and Reinforced Concrete in Nuclear Power Plants and Waste Management, RILEM proceedings PRO 64 (2009c) 35-44.

Macdonald M, El-Tantawy YA, Rocha-Filho RC, Urquidi-Macdonald M, Evaluation of electrochemical impedance techniques for detecting corrosion on rebar in reinforced concrete, report SHRP-ID/UFR-91-524 (1994), Strategic Highway Research Program (SHRP), National Research Council, Washington, D.C., USA.

Mansfeld F, Evaluation of polarisation resistance round robin testing conducted by ASTM G01.11, CORROSION/76, paper no. 106 (1976), March 22-26, 1976, Houston, Texas, USA.

Mansfeld F, Han LT, Lee CC, Zhang G, *Evaluation of corrosion protection by polymer coatings using electrochemical impedance spectroscopy and noise analysis*, Electrochimica Acta **43**(19-20) (1998) 2933-2945.

Mansfeld F, Sun Z, Speckert E, Hsu CH, Electrochemical noise analysis (ENA) for active and passive systems, CORROSION/2000, paper no. 00418 (2000), 26-31 March, 2000, Orlando, Florida, USA.

Mansfeld F, Sun Z, Hsu CH, *Electrochemical noise analysis (ENA) for active and passive systems in chloride media*, Electrochimica Acta **46** (2001) 3651-3664.

Mansfeld F, Electrochemical methods of corrosion testing, *In*: Cramer SD, Covino S Jr, *eds.*, ASM Handbook, Volume 13A – Corrosion: fundamentals, testing and protection (2003), ASM International, Materials Park, Ohio, USA 446-462.

Matsuda F, Wada R, Fujiwara K, Fujiwara A, *An evaluation of hydrogen evolution from corrosion of carbon steel in low/intermediate level waste repositories*, Mat. Res. Soc. Symp. Proc. **353** (1995) 719-726.

McCafferty E, Introduction to corrosion science (2010), Springer, New York, USA.

McCarter WJ, Brousseau B, *The A.C. response of hardened cement paste*, Cement and Concrete Research **20**(6) (1990) 891-900.

Mendoza AR, Corrosion of reinforcing steel in loaded cracked concretes exposed to de-icing salts, PhD Thesis (2003), University of Waterloo, Waterloo, Ontario, Canada.

Mihara M, Nishimura T, Wada R, Honda A, *Estimation on gas generation and corrosion rates of carbon steel, stainless steel and zircaloy in alkaline solutions under low oxygen condition*, JNC Technical Review **15** (2002) 91-101 (in Japanese).

Mohamed N, Comparative study of the corrosion behaviour of conventional carbon steel and corrosion resistant reinforcing bars, PhD Thesis (2009), University of Saskatchesan, Saskatoon, Canada.

Mojica J, Rodriguez FJ, Garcia-Ochoa E, Genesca J, *Evaluation of thick industrial coating films by EIS and EN*, Corrosion Engineering, Science and Technology **39**(2) (2004) 131-136.

Montemor MF, Simões AMP, Salta MM, *Effect of fly ash on concrete reinforcement corrosion studied by EIS*, Cement & Concrete composites **22** (2000) 175-185.

Moreland PJ, Rowlands JC, *Technique and instrumentation for polarisation reisistance measurements: report prepared for the European Federation of Corrosion Working Party on 'Physicochemical Testing Methods of Corrosion – Fundamentals and applications'*, British corrosion Journal **12**(2) (1977) 72-79.

Morgan DR, Comparative performance of MMFX microcomposite reinforcing steel and other types of steel with respect to corrosion resistance and service life prediction in reinforced concrete structures, report VA06451 (2006), AMEC Earth & Environmental, Burnaby, Canada.

Mortimer CE, Chemistry (sixth edition) (1986), Wadsworth, Inc., Belmont, California, USA.

Naish CC, Balkwill PH, O'Brien TM, Taylor KJ, Marsh GP, The anaerobic corrosion of carbon steel in concrete, report NSS/R273 (1990), AEAT Technology, UK.

Naish CC, Balkwill PH, O'Brien TM, Taylor KJ, Marsh GP, The anaerobic corrosion of carbon steel in concrete, report EUR-13663 EN (1991), European Commission, Belgium.

Naish CC, Corrosion Aspects of the Proposed Sellafield Waste Repository, UK Corrosion '93 (1993).

Naish CC, Blackwood DJ, Taylor KJ, Thomas MI, The Anaerobic Corrosion of Stainless Steels in Simulated Repository Backfill Environments, report NSS/R307 (1995), AEA Technology, U.K.

Naish CC, Blackwood DJ, Thomas MI, Rance AP, The anaerobic corrosion of carbon steel and stainless steel, report AEAT/R/ENV/0224 (2001), AEA Technology, U.K.

Nam J, Effects of cement alkalinity, exposure conditions and steel-concrete interface on the time-to-corrosion and chloride threshold for reinforcing steel in concrete, PhD Thesis (2004), Florida Atlantic University, Boca Raton, Florida, USA.

Neff D, Dillmann P, Descotes M, Béranger G, *Corrosion of iron archaeological artefacts in soil: Estimation of the average corrosion rates involving analytical techniques and thermodynamic calculations*, Corrosion Science **48**(10) (2006) 2947-2970.

Neff D, Vega E, Dillmann P, Descotes M, Bellot-Gurlet L, Béranger G, Contribution of iron archaeological artefacts to the estimation of average corrosion rates and the long-term corrosion mechanisms of low-carbon steel buried in soil, *In:* Dillmann P, Béranger G, Picardo P, Matthiesen H, *eds.*, Corrosion of metallic heritage artefacts – Investigation, conservation and prediction for long-term behaviour, European Federation of Corrosion Publication no. 48 (2007), Woodhead Publishing Limited, Cambridge, UK 41-76.

Newton CJ, Sykes JM, *A galvanostatic pulse technique for investigation of steel corrosion in concrete*, Corrosion Science **28**(11) (1988) 1051-1074.

Nishimura T, Wada R, Fujiwara K, *Evaluation of gas generation rates caused by metal corrosion under the geological repository conditions*, R&D Kobe Steel Engineering Reports **53**(3) (2003) 78-83 (in Japanese).

Olivella S, Gens A, Carrera J, Alonso EE, *Numerical formulation for a simulator (CODE_BRIGHT) for the coupled analysis of saline media*, Engineering computations **13**(7) (1996), 87-112.

ONDRAF/NIRAS, Research, Development and Demonstration (RD&D) Plan, report NIROND-TR-2013-12 E (2013), ONDRAF/NIRAS, Brussels, Belgium, 1-411.

Page CL, Treadaway KWJ, *Aspects of the electrochemistry of steel in concrete: review article*, Nature **297** (1982) 109-115.

Page CL, Vennesland Ø, *Pore solution composition and chloride binding capacity of silica fume cement pastes*, Materials and Structures **16**(91) (1983) 19-25.

PAR, Application note CORR1 'Basics of corrosion measurements' (2010), Princeton Applied Research, Oak Ridge, TN, USA.

PAR, Application note AC-1 'Basics of electrochemical impedance spectroscopy' (2010a), Princeton Applied Research, Oak ridge, TN, USA.

Perdomo J, Singh P, A review and application of electrochemical noise (ECN) measurements as a corrosion monitoring tool, IPST technical paper series number 950 (2002), Institute of Paper Science and Technology (IPST), Atlanta, Georgia, USA.

Plouzennec MH, Féron D, Tachon M, Atabek R, Corcos J, Qualification protocol of cast iron container for subsurface disposal, proceedings of the International Conference on Waste Management '97 (WM97) (1997), 2-6 March 1997, Tucson, Arizona, USA.

Polder RB, Chloride in cement-sand mortar – A. Expression experiments, report BI-86-21 (1986), TNO, The Netherlands.

Pourbaix M, Atlas of electrochemical equilibria in aqueous solutions (second edition) (1974), National Association of Corrosion Engineers (NACE), Houston, Texas, USA.

Poursaee A, An analysis of the factors influencing electrochemical measurements of the condition of reinforcing steel in concrete structures, PhD Thesis (2007), University of Waterloo, Waterloo, Ontario, Canada.

Poursaee A, *Numerical analysis of the function of galvanostatic pulse technique with the current confinement guard ring in cracked concrete*, Concrete Research Letters **1**(2) (2010) 67-72.

Preece CM, Corrosion of steel in concrete, report SKBF-TR-82-19 (1982), SKB, Sweden.

Preece CM, Grønvold FO, Frølund T, The influence of cement type on the electrochemical behaviour of steel in concrete, *In*: Crane AP, *ed.*, Corrosion of reinforcement in concrete construction (1983), Ellis Horwood Ltd, Chichester, West Essex, UK, 393-405.

Pujar MG, Anita T, Shaikh H, Dayal RK, Khatak, HS, *Analysis of electrochemical noise (EN) data using MEM for pitting corrosion of 316 SS in chloride solution*, Int. J. Electrochem. Sci. **2** (2007) 301-310.

Put M, Henrion P, Modelling of radionuclide migration and heat transport from an HLW-repository in Boom Clay, report EUR-14156 (1992), E.C. Nuclear Science and Technology, Luxembourg, 153.

Reardon EJ, *Problems and approaches to the prediction of the chemical composition in cement/water systems*, Waste Management **12** (1992) 221-239.

Roberge PR, Handbook of corrosion engineering (2000), McGraw-Hill, Inc., New York, USA.

Roberge PR, Klassen RD, Tullmin M, Electrochemical noise analysis for corrosivity assessment, CORROSION/2000, paper no. 00281 (2000), 26-31 March 2000, Orlando, Florida, USA.

RWMC, Verification test on advanced radioactive waste disposal systems, volume 1 and 2 – 1998 report (1998), Radioactive Waste Management Funding and Research Center (RWMC), Japan.

Sagoe-Crentsil KK, Glasser FP, Irvine JTS, *Electrochemical characteristics of reinforced concrete corrosion as determined by impedance spectroscopy*, British Corrosion Journal **27**(2) (1992a) 113-118.

Sagoe-Crentsil KK, Yilmaz VT, Glasser FP, *Impedance spectroscopy analysis of the influence of superplasticizers on steel corrosion in OPC mortar*, Journal of Materials Science **27** (1992b) 3400-3404.

Sagüés AA, Kranc SC, Moreno EI, *The time-domain response of a corroding system with constant phase angle interfacial component: Application to steel in concrete*, Corrosion Science **37**(7) (1995) 1097-1113.

Samson E, Lemaire G, Marchand J, Beaudoin JJ, *Modelling chemical activity effects in strong ionic solutions*, Computational Materials Science **15** (1999) 285-294.

Schenk R, Untersuchungen über die Wasserstoffbildung durch Eisenkorrosion unter Endlagerbedingungen, report NAGRA NTB 86-24 (1988), NAGRA, Switzerland.

Schenk R, Noack W, *Wasserstoffbildung durch Eisenkorrosion unter den Bedingungen des geplanten Endlagers Konrad*, *In:* Bauer KG, ed., Proceedings of the Annual Meeting on Nuclear Technology '95, 16-18 May 1995, Jahrestagung Kerntechnik '95 (1995) 266-269.

Schwenk W, *Some aspects of the corrosion of iron ion alkaline solutions and associated fundamental questions*, Werkstoffe und Korrosion **34** (1983) 287.

Scully JR, Electrochemical, *In*: Baboian R, *ed.*, Corrosion tests and standards: Application and interpretation (1995), American Society for Testing and Materials (ASTM), Philadelphia, PA, USA.

Scully JR, Marks CA, Hurley MF, Testing of selected metallic reinforcing bars for extending the service life of concrete bridges: Testing in solutions, report FHWA/VTRC 03-CR11 (2003), Virginia Transportation Research Council, Charlottesville, Virginia, USA.

Sedriks AJ, Corrosion of stainless steels (second edition) (1996), John Wiley & Sons, Inc., New york, USA.

Seetharam S, Mallants D, Wang L, Jacques D, Perko J, Schneider S, Leterme B, Additional parameters for the cementitious near field and multi-layer cover of the Dessel near surface repository. Project near surface disposal of category A waste at Dessel, report NIROND-TR 2010-07E (2011), Ondraf/Niras, Brussels, Belgium.

Sergi G, Corrosion of steel in concrete: cement matrix variables, PhD Thesis (1986), University of Aston, Birmingham, United Kingdom.

Shreir LL, Jarman RA, Burstein GT, Corrosion (third edition) (1994), Butterworth-Heinemann, Oxford, United Kingdom.

Sillen X, Marivoet J, Thermal impact of a HLW repository in clay. Deep disposal of vitrified high-level waste and spent fuel, report SCK•CEN-ER-38 (2007), SCK•CEN, Mol, Belgium, ISSN 1782-2335.

Simpson JP, Schenk R, *Corrosion induced hydrogen evolution on high level waste overpack materials in synthetic groundwaters and chloride solutions*, Mat. Res. Soc. Symp. Proc. **127** (1989) 389-396.

Skoog DA, West DM, Holler FJ, Fundamentals of analytical chemistry (sixth edition) (1992), Saunders College Publishing, USA.

Slater JE, Corrosion of structures, *In*: Cramer SD, Covino BS, Jr., *eds.*, ASM Handbook. Volume 13C – Corrosion: environments and industries (2006), ASM International, Materials Park, Ohio, USA, 1056.

Smart NR, Blackwood DJ, Werme L, *Anaerobic corrosion of carbon steel and cast iron in artificial groundwaters: part 1 - electrochemical aspects*, Corrosion **58**(7) (2002) 547-559.

Smart NR, Blackwood DJ, Marsh GP, Naish CC, O'Brien TM, Rance AP, Thomas MI, The anaerobic corrosion of carbon and stainless steels in simulated cementitious repository environments: a summary review of Nirex research, report AEAT/ERRA-0313 (2004), AEA Technology, United Kingdom.

Smart NR, The corrosion behaviour of carbon steel radioactive waste packages: A summary review of Swedish and U.K. research, CORROSION/2008, paper no. P3013 (2008), 16-20 March 2008, New Orleans, LA, USA.

Smart NR, *The corrosion behaviour of carbon steel radioactive waste packages: A summary review of Swedish and U.K. research*, Corrosion **65**(3) (2009) 195-212.

Song G, *Theoretical analysis of the measurement of polarisation resistance in reinforced concrete*, Cement and Concrete Composites **22** (2000) 407-415.

Song G, Shayan A, Monitoring of steel corrosion in concrete, report AP-T06/00 (2000), Austroads, Inc., Sydney, Australia.

Song HW, Saraswathy V, *Corrosion monitoring of reinforced concrete structures - A review*, Int. J. Electrochem. Sci. **2** (2007) 1-28.

Stansbury EE, Buchanan RA, Fundamentals of electrochemical corrosion (2000), ASM International, Materials Park, Ohio, USA.

Stern M, Weisert ED, *Experimental observations on the relation between polarization resistance and corrosion rate*, Proc. Am. Soc. Testing Materials **59** (1959) 1280-1291.

Stumm W, Morgan JJ, Aquatic chemistry: chemical equilibria and rates in natural waters (third edition) (1996), John Wiley & Sons, Inc., New York, USA.

Tallman DE, Bierwagen GP, Touzain S, Smith A, Twite R, Balbyshev V, Pae Y, Electrochemical noise methods applied to the study of organic coating and pretreatments, CORROSION/98, paper no. 98-380 (1998), 22-27 March, 1998, San Diego, California, USA.

Tang L, Calibration of the electrochemical methods for the corrosion rate measurement of steel in concrete. Nordtest project No. 1531-01, SP report 2002:25 (2002), Swedish National Testing and Research Institute, Sweden.

Thompson NG, Lawson KM, Beavers JA, *Monitoring cathodically protected steel in concrete structures with electrochemical impedance techniques*, Corrosion **44**(8) (1988) 581-588.

Thompson NG, Lawson KM, An electrochemical method for detecting ongoing corrosion of steel in a concrete structure with CP applied, report SHRP-ID/UFR-91-512 (1991), Strategic Highway Research Program (SHRP), National Research Council, Washington, D.C., USA.

Tritthart J, *Chloride binding in concrete: II. The influence of the hydroxide concentration in the pore solution of hardened cement paste on chloride binding*, Cement and Concrete Research **19** (1989) 683-691.

Tuuti K, Corrosion of steel in concrete, report no. 4-82 (1982), Swedish Cement and Concrete Research Institute, Sweden.

Uhlig HH, Corrosion and corrosion control (1971), John Wiley & Sons, Ltd, New York, USA.

Uhlig HH, Revie RW, Corrosion and corrosion control: An introduction to corrosion science and engineering (third edition) (1985), John Wiley & Sons, Inc., New York, USA.

Vagn Nygaard P, Non-destructive electrochemical monitoring of reinforcement corrosion, DTU Civil Engineering Report R-202, PhD Thesis (2008), Technical University of Denmark, Lyngby, Denmark.

Van Geet M, De Craen M, Weetjens E, Sillen X, Extent of oxidising conditions in the host formation, report SCK•CEN-ER-05 (2006a), SCK•CEN, Mol, Belgium.

Van Geet M, Wang L, De Boever P, De Craen M, Geochemical boundary conditions relevant for assessing corrosion processes for the supercontainer design, report SCK•CEN-ER-14 (2006b), SCK•CEN, Mol, Belgium.

Van Geet M, Wang L, De Boever P, De Craen M, Geochemical boundary conditions for *in situ* corrosion experiments, report SCK•CEN-R-4308 (2006c), SCK•CEN, Mol, Belgium.

Verhoef E, Schröder T, OPERA Research plan, OPERA-PG-COV004 (2011), COVRA N.V., The Netherlands.

Verhoef EV, Neeft EAC, Poley AD, Grupa JB, Outline of a disposal concept in clay, OPERA-PG-COV008 (2014) first revision 1-18.

Wang L, Near-field chemistry of a HLW/SF repository in Boom Clay – Scoping calculations relevant to the Supercontainer design, First full draft, report SCK•CEN-ER-17 (2006), SCK•CEN, Mol, Belgium.

Weetjens E, Sillen X, Thermal analysis of the supercontainer concept, report SCK•CEN-R-4277 (2005), SCK•CEN, Mol, Belgium.

Wenger F, Galland J, Azou P, *Étude de la corrosion des armatures de béton par la mesure de l'impédance électrochimique*, C. R. Acad. Sc. Paris, Série C **291**(5) (1980) 149-152.

Wenger F, Galland J, Lemoine L, *Étude des diagrammes d'impédance électrochimique dans le cas d'une distribution des constantes de temps de relaxation - Application au cas d'armatures de béton*, C. R. Acad. Sc. Paris, Série II **301**(18) (1985) 1281-1284.

Wenger F, Galland J, *Analysis of local corrosion of large metallic structures or reinforced concrete structures by electrochemical impedance spectroscopy*, Electrochimica Acta **35**(10) (1990) 1573-1578.

WIKI1, http://en.wikipedia.org/wiki/Lime_water, Wikipedia.

Yasuda M, Fukumoto F, Koizumi H, Ogata Y, Hine F, *On the Active Dissolution of Metals and Alloys in Hot Concentrated Caustic Soda*, Corrosion **43**(8) (1987) 492.

Yoshikawa H, Ueno K, Honda T, Yamaguchi S, Yui M, Analysis of the excavated archaeological iron using XRAY-CT, proceedings of the 9th International Conference on Radioactive Waste Management and Environmental Remediation (ICEM'03), paper no. icem03-4776 (2003), 21-25 September 2003, Oxford, UK.

Yoshikawa H, Gunji E, Tokuda M, *Long term stability of iron for more than 1500 years indicated by archaeological samples from the Yamato 6th tumulus*, Journal of Nuclear Materials **379** (2008) 112-117.

Zhang JY, Qian SY, Baldock B, Laboratory study of corrosion performance of different reinforcing steels for use in concrete structures, report IRC-RR-284 (2009), National Research Council Canada (NRCC), Ottowa, Ontario, Canada.

Zhou XY, Lvov SN, Wei XJ, Benning LG, Macdonald DD, *Quantitative evaluation of general corrosion of type 304 stainless steel in subcritical and supercritical aqueous solutions via electrochemical noise analysis*, Corrosion Science **44** (2002) 841-860.

Appendix 1 - Faraday's laws of electrolysis and its application in determining the corrosion rate of metals

The First Law of Electrolysis states that the amount of a substance deposited or liberated at any electrode surface during an electrochemical process is directly proportional to the quantity of electrical charge (q) passed through the aqueous electrolyte:

$$w \propto q$$

with $q = I \cdot t$

giving $$w = Z \cdot I \cdot t \qquad \text{(eq. B-1)}$$

where w = mass of the primary product (g)
q = electric charge (C = A.s)
I = current (A)
t = time (s)
Z = constant of proportionality (electrochemical equivalent) (g/A)

The Second Law of Electrolysis states that for a given quantity of electrical charge, the amount of a substance altered at an electrode is directly proportional to the ratio of molar mass to the number of electrons involved with a particular reaction:

$$w \propto \frac{M}{n} \propto Z \qquad \text{(eq. B-2)}$$

w is also directly proportional to Z, which is, by definition, the mass of a substance liberated by 1 Coulomb of an electrical charge.

Therefore, Z is defined by:

$$Z = \frac{1}{F} \cdot \frac{M}{n} \qquad \text{(eq. B-3)}$$

where M is the atomic weight (g/mol), n is the charge number (which indicates the number of electrons exchanged in the dissolution reaction), and F is Faraday's constant (96485 $C.mol^{-1}$).

Substituting equation (B-3) into equation (B-1) gives:

$$w = \frac{1}{F} \cdot \frac{M}{n} \cdot I \cdot t \qquad \text{(eq. B-4)}$$

where w is the mass of a substance liberated, deposited or dissolved in the electrochemical reaction; in terms of corrosion, *i.e.* the mass of the corroded metal (in grams, g),
M is the atomic weight ($g.mol^{-1}$),
I is the current passed (in amperes, A),
nF is the number of Coulombs (C) required to convert one mole of metal to corrosion product, where n is the number of electrons involved in the metal dissolution reaction, and F is the Faraday constant (96485 $C.mol^{-1}$), and

t is the time (in seconds, s) for which the current has flowed.

Because the corrosion rate is expressed as mass × reciprocal of time (*e.g.* g.y^{-1}), equation (B-4) can be written as follows:

$$\frac{w}{t} = \frac{MI}{nF} \qquad \text{(eq.-5)}$$

Dividing equation (B-5) by the exposed area of the metal and substituting $\frac{I}{A} = i\ (current\ density)$

gives:

$$\frac{w}{At} = \frac{Mi}{nF} \qquad \text{(eq. B-6)}$$

The corrosion rate, expressed as a penetration unit time, can be obtained by dividing equation (B-6) by the density of the metal:

$$v_{CORR} = C \cdot \frac{Mi}{n\rho} \qquad \text{(eq. B-7)}$$

where ρ = density of the metal (g.cm^{-3})
i = current density (A.cm^{-2})
M = atomic weight (g.mol^{-1})
n = number of electrons involved in the metal dissolution reaction
C = constant, which includes the reciprocal of F (Faraday's constant) and any other conversion factor for units (mol.C^{-1})

The unit of v_{CORR} is $\frac{1}{C/mol} \cdot \frac{g}{mol} \cdot \frac{A}{cm^2} \cdot \frac{1}{g/cm^3} = \frac{mol}{A \cdot s} \cdot \frac{g}{mol} \cdot \frac{A}{cm^2} \cdot \frac{cm^3}{g} = \frac{cm}{s}$

If one wants to express the corrosion rate in µm.y^{-1}, the conversion factor, C, becomes:

$$C = \frac{1}{96485} \cdot \frac{10^4\ (cm \rightarrow \mu m)}{\frac{1}{60 \times 60 \times 24 \times 365\ (s \rightarrow year)}} = 3.27 \times 10^6$$

The corrosion rate is then given by the following expression:

$$v_{CORR}\ (in\ \mu m / year) = 3.27 \times 10^6 \cdot \frac{Mi}{n\rho} \qquad \text{(eq. B-8)}$$

Appendix 2 - Measurement techniques of uniform corrosion rates reported in the literature

In the literature, uniform corrosion rate data for mild steel in alkaline environments are derived from investigations using various techniques, most of which are based on either one of the following three principles

- gravimetric-based weight loss measurements;
- electrochemical measurement techniques; or
- quantification of hydrogen gas evolving from the corrosion of steel;

Additionally, some novel methods were reported in the literature that use archaeological artefacts to estimate uniform corrosion rates.

A2.1. Corrosion rate calculated from weight loss measurements

Uniform corrosion rates derived from weight loss measurements consist in exposing coupons to a test medium and subsequently measuring the loss of weight of the material at the end of the predetermined testing period. Weight loss is a measure of the difference between the original mass of the specimen and its mass when sampled after exposure and after removing any corrosion product adhering to the specimen. Uniform corrosion rates can be calculated from weight loss coupons using the following equation:

$$v_{CORR} = \frac{3{,}650 \times \Delta M}{\rho \times A \times t} \qquad \text{(eq. A2-1)}$$

with v_{CORR} : corrosion rate (in mm/year)
ΔM : weight loss (in grams)
ρ : metal density (in g/cm^3)
A : coupon area (in cm^2)
t : exposure time (in days)

A2.2. Electrochemical measurement techniques

Since corrosion is an electrochemical process that involves charge transfer (electrons) through an electrolyte (concrete pore solution), different electrochemical test methods can be used to evaluate the state of a specimen from a corrosion point of view and to predict corrosion rates [Mohamed, 2009; Autolab, 2010]. All electrochemical techniques for corrosion rate determination are based on the measurement of the corrosion current, I_{CORR}, from which the corrosion current density, i_{CORR} (= I_{CORR}/A), and ultimately the corrosion rate are calculated, providing the surface of the exposed area[n] of the specimen is known (Stansbury and Buchanan, 2000).

If the corrosion current density, i_{CORR}, is known, the uniform corrosion rate (as a penetration rate) can be calculated by the following equation:

[n] in the limit, only the area of the anodic sites is taken into account. In the case of uniform corrosion, however, the anodic sites are assumed to be uniformly distributed on a scale approaching atom dimensions and can not be distinguished from sites of the cathodic reaction supporting corrosion. Therefore, the total specimen area can be taken equal to the area of the anodic sites (Stansbury and Buchanan, 2000).

$$v_{CORR} = 3.27 \times \frac{i_{CORR}}{\rho} \times EW \qquad \text{(eq. A2-2)}$$

with v_{CORR} : corrosion rate (in µm/year)
i_{CORR} : corrosion current density (µA/cm²)
ρ : metal density (in g/cm³) → ρ_{Fe} = 7.8
EW : equivalent weight (in gram/equivalent) → EW_{Fe} = 28

where the equivalent weight, EW, for a pure element is given by

$$EW = \frac{M}{n} \qquad \text{(eq. A2-3)}$$

with M : atomic weight (in g/mol) → M_{Fe} = 56
n : valence of the metal (in equivalent/mol) → n_{Fe} = 2

(the conversion calculation from corrosion current density to a penetration rate is given in Appendix 1)

Substituting the value for ρ_{Fe} (=7.8) and EW_{Fe} (=28) in equation (A2-2) gives the following straightforward correlation between the corrosion current density and the corrosion rate for steel:

$$v_{CORR}\ (in\ \mu m/year) = 11.7 \times i_{CORR}\ (in\ \mu A/cm^2) \qquad \text{(eq. A2-4)}$$

However, direct measurement of the corrosion current is not feasible (the corrosion current density is equivalent to the corrosion current divided by the electrode surface area). The corrosion current is the current that flows between the anodic and cathodic sites and because the charge balance criterion requires that the rates of production and consumption of electrons by the anodic and cathodic half-cell reactions must be equal, no net current can be measured. The estimation of the corrosion current in many of the electrochemical techniques, therefore, is based on displacing the system away from equilibrium by applying an external potential, measuring the resultant net current and then extrapolating it back to the equilibrium potential (Preece, et al, 1983).

Thus, the application of an appropriate electrochemical technique can ultimately result in the estimation of a corrosion current density (*i.e.* the corrosion current per unit of area). The electrochemical methods, found in literature, that are used to derive corrosion rates include:

- graphical extrapolation of polarisation curves (PC);
- Tafel extrapolation method (TP);
- linear polarisation resistance technique (LPR);
- galvanostatic pulse technique (GP);
- electrochemical impedance spectroscopy (EIS);
- electrochemical noise technique (EN); and
- passive current density measurements (PCD);

A2.2.1. Corrosion rate calculated from the graphical extrapolation of i_{CORR} from a polarisation curve (PC)

To obtain a potentiodynamic scan, the electrode potential is ramped continuously with time over a predetermined range, and the resulting current is simultaneously recorded along with the applied potential. The graphical output of a potentiodynamic scan is referred to as a polarisation curve, which plots the electrode potential (E) versus the logarithm of the

current density (log i) (Mohamed, 2009; McCafferty, 2010). A typical polarisation curve for a passivating metal (e.g. carbon steel in concrete) is shown in Figure A2-1.

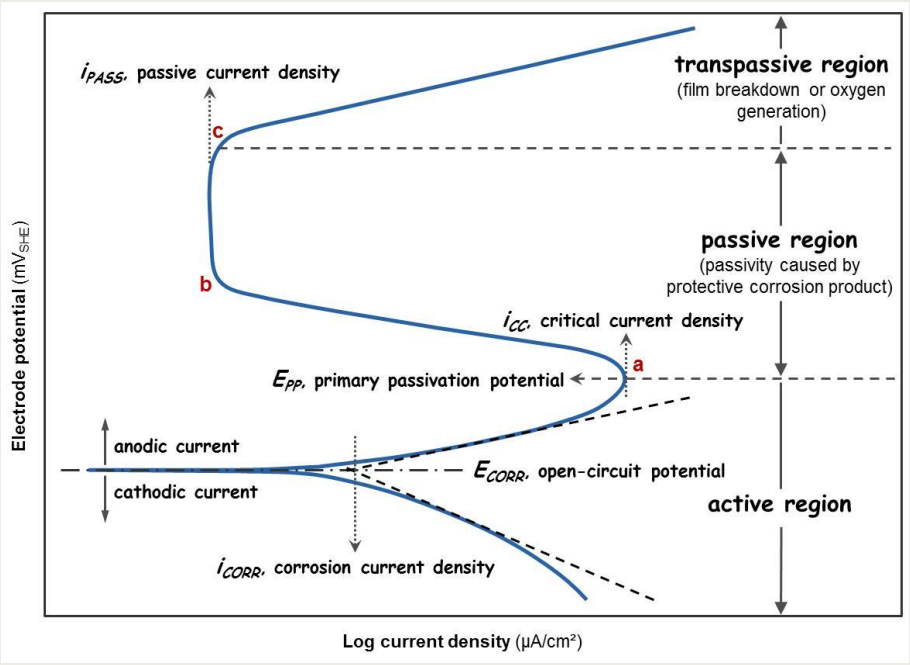

Figure A2-1. Schematic representation of a polarisation curve for a passive metal.

When the electrode potential is progressively scanned from the *open-circuit potential* (E_{CORR}), in the noble direction, the corrosion current density initially increases, corresponding to a region of *active corrosion*. As the potential continues to become more oxidising, a critical potential (point 'a' in Figure A2-1), called the *primary passivation potential* (E_{PP}), may be reached at which the corrosion current density rapidly decreases over several orders of magnitude to a small value (point 'b' in Figure A2-1).
The sharp decrease in current density from a to b is associated with the formation of an insoluble corrosion product (usually an oxide), which is called the *passive film*. The presence of this film can significantly lower the rate at which the underlying metal corrodes. The more adherent and nonporous the oxide film, the greater the decrease in current density will be. From b to c, the passive film thickens and its protective character increases, holding the current density to small values, called the *passive current density*. Within this passive range (region b-c in Figure A2-1), the small current density is virtually independent of potential, as indicated by the vertical line in the plot.
This low current density will persist until the potential becomes sufficiently positive (point 'c' in Figure A2-1) to break down the protective film or to produce oxygen directly from water by electrolysis. In either event, the current density (and hence the corrosion rate) will rise sharply. This latter region is the *transpassive region* (Baboian, 1995; Davis, 2000; Stansbury and Buchanan, 2000; Blackwood, et al, 2002).

Theory tells us that within a limited voltage range (10-20 mV) either side of the open-circuit potential, E_{CORR}, the cathodic and anodic branches of a polarisation curve exhibit linear behaviour. Thus, the corrosion current, i_{CORR}, can be estimated graphically by extrapolating the linear regions of the anodic and cathodic curves to their common value at the open-circuit potential, as illustrated in Figure A2-1. In some cases, where no numerical data could be found in the literature, such a graphical approximation of i_{CORR} was made.

A2.2.2. Tafel extrapolation method (TP)

The potential of a corroding electrode is related to the applied current density by the following relationship (known as the Butler-Volmer equation) (Kelly, et al, 2003):

$$i_{APP} = i_{CORR}\left(e^{\left[\frac{2.303\,(E-E_{CORR})}{\beta a}\right]} - e^{\left[\frac{-2.303\,(E-E_{CORR})}{\beta c}\right]}\right) \qquad \text{(eq. A2-5)}$$

where i_{CORR} is the corrosion current density, E_{CORR} is the open-circuit potential and $ß_a$ and $ß_c$ are the anodic and cathodic Tafel parameters, which are given by the slopes of the anodic and cathodic branches of the polarisation curves (Kelly, et al, 2003).

In the Tafel extrapolation method (TP), the test electrode is polarised about 250-300 mV either side of the open-circuit potential. This can be accomplished either potentiostatically by changing the potential of the reinforcing steel by a fixed amount and monitoring the current or galvanostatically by applying a small fixed current to the reinforcing steel and measuring the resulting potential. The obtained polarisation curve is called a *Tafel plot* (Ahmad, 2006; Song and Saraswathy, 2007; PAR, 2010).

The corrosion current density, i_{CORR}, can be obtained directly from a Tafel plot by extrapolating the tangent line of the linear portion of the anodic or cathodic branch of the polarisation curve back to the intersection with the open-circuit potential, as illustrated in Figure A2-2 (Davis, 2000). The more recent corrosion test softwares make use of sophisticated numerical fitting procedures of the Butler-Volmer equation to yield values for i_{CORR}, $ß_a$ and $ß_c$ (GAMRY, 2007).

The corrosion rate can then be calculated from i_{CORR} using equation (A2-2) (or the simplified equation (A2-4) for the corrosion of steel).

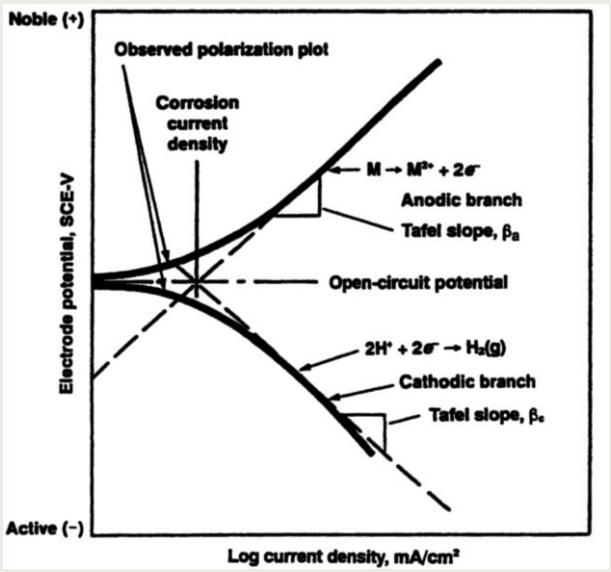

Figure A2-2. Schematic illustration of a hypothetical Tafel plot, with indication of the corrosion current and the Tafel slopes $ß_a$ and $ß_c$ (source: adapted from [Davis, 2000]).

A2.2.3. Corrosion rate calculated from polarisation resistance (R_P) measurements

As already mentioned earlier in this report, a linear relationship exists between the current and potential in a narrow voltage region around the free corrosion potential, E_{CORR} (see Figure A2-3). Many of the electrochemical techniques for determining the corrosion rate rely on the empirical relationship between the corrosion current, I_{CORR}, and the slope of the polarisation curve around the free corrosion potential, dE/dI, where dE is the potential shift

from the free corrosion potential, E_{CORR}, and dI is the applied current. The slope of the polarisation curve is referred to as the polarisation resistance, R_P.

R_P measurements give as result an instantaneous corrosion rate (Elsener, 2005).

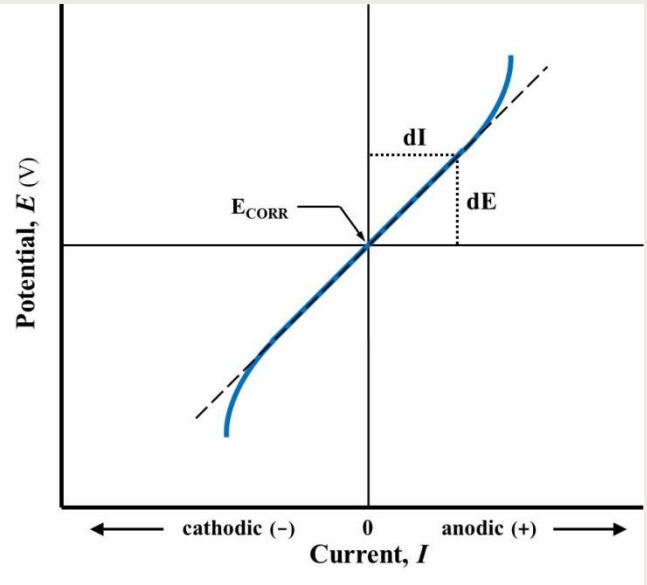

Figure A2-3. Linear correlation between polarising potential and current around the free corrosion potential (source: adapted from [Mohamed, 2009]).

A2.2.3.1. Linear polarisation resistance technique (LPR)

The linear polarisation technique (LPR) is based on the same principle as the Tafel extrapolation method. In the LPR technique, however, the reinforcing steel is perturbed from its equilibrium by only a very small amount (±10-20 mV) (Mendoza, 2003; Song and Saraswathy, 2007; Mohamed, 2009).

At these low overpotentials, the Butler-Volmer equation (A2-5) can be further simplified[o] and becomes approximately linear (Kelly, et al, 2003; GAMRY, 2007; Badea, et al, 2010). The corrosion density is then inversely proportional to the polarisation resistance and is given by the following relationship, often referred to as the Stern-Geary equation (Stern and Weisert, 1959; Carino, 1999; Stansbury and Buchanan, 2000; Davis, 2000; Mendoza, 2003; Kelly,et al, 2003; Elsener, 2005; Poursaee, 2007; Vagn Nygaard, 2008; Mohamed, 2009; Badea, et al, 2010; PAR, 2010):

$$i_{CORR} = \frac{1}{(2.303 \cdot R_P)} \cdot \left(\frac{\beta_a \beta_c}{\beta_a + \beta_c}\right) = \frac{B}{R_P} \qquad \text{(eq. A2-6)}$$

with $\frac{\beta_a \cdot \beta_c}{2.303 \cdot (\beta_a + \beta_c)} = B$, a proportionality constant (the Stern-Geary constant, in V).

where i_{CORR} is the corrosion current density (in μA·cm^{-2}), and B_a and B_c are the anodic and cathodic Tafel constants (in kΩ·cm^2), respectively.

Knowledge of R_P, B_a and B_c enables direct determination of the corrosion current density at any instant in time using equation (A2-6). The polarisation resistance, R_P, is determined from the slope of the polarisation curve (the more recent corrosion test softwares use a numerical

[o] the Butler-Volmer equation (A2-5) can be mathematically linearised by approximating the exponential terms with the first two terms of a power series expansion (e.g., $e^x = 1 + x + {}^{x^2}/_{2!} + {}^{x^3}/_{3!} + \cdots + {}^{x^n}/_{n!}$) (Stansbury and Buchanan, 2000; Kelly, et al, 2003; GAMRY, 2007).

fitting procedure to yield a value for R_P). The anodic and cathodic Tafel constants, β_a and β_c, are obtained from a Tafel plot (Kelly, et al, 2003; GAMRY, 2007).

The corrosion rate can then be calculated from i_{CORR} using equation (A2-2) (or the simplified equation (A2-4) for the corrosion of steel).

The Stern-Geary constant, B, can be calculated from the values of β_a and β_c. In practice, however, an empirical value is often used for B. Vagn Nygaard [Vagn Nygaard, 2008) provides a good overview of B values that have been used in the literature. Andrade and González [Andrade and González, 1978) proposed B values of 26 mV and 52 mV for steel in the active and passive corrosion state, respectively. These values were based on results of electrochemical and gravimetric measurements of steel immersed in calcium hydroxide ($Ca[OH]_2$) solutions and embedded in mortar specimens. A very good correlation was found for the results between the electrochemical and gravimetric measurements in solution. However, for the reinforced mortar specimens, deviations of up to two and three orders of magnitude were observed. Nevertheless, these proposed values have, since their publication, been used in a vast amount of studies on corrosion in concrete (González, et al, 1980; Hansson, 1985; Andrade and Page, 1986; Alonso, et al, 1988; Glass, et al, 1997; Andrade, et al, 2004).
In a more recent study, Song (Song, 2000) and Tang (Tang, 2002) analysed B values from four different corrosion scenarios and concluded that B can range from 8 mV to infinite. However, in this respect it needs to be mentioned that an infinite value of B is unrealistic since it would result in infinite corrosion rates (see equation (A2-5)) which can not be true.
Naish and co-workers (Naish, et al, 1990; Naish, et al, 1991) used a B value of 10 mV.
Hubbe (Hubbe, 1980) used linear regression of the calculated values of the corrosion rate (obtained from polarisation resistance measurements) *vs.* weight loss data to yield an empirical value of B of 27.1 mV for mild steel in a NaOH solution with a pH of 9.8.
Pourbaix (Pourbaix, 1974) suggested that an average value of 100 mV per logarithmic decade of current may be taken as an estimate of the anodic and cathodic Tafel constants. This value substituted into $\frac{\beta_a \cdot \beta_c}{2.303 \cdot (\beta_a + \beta_c)}$ gives a B value of 21.7 mV.
Moreland and Rowlands (Moreland and Rowlands, 1977) concluded from many measurements on different corroding systems that B equal to 20 mV can be considered as a good average value.
Stern and Weisert (Stern and Weisert, 1959; Uhlig and Revie, 1985) showed that B can vary from about 13 mV (for systems under activation control) to 52 mV (for systems under diffusion control).
Mansfeld (Mansfeld, 1976) reported values of B in the range of 12 mV to 27 mV for the system 1008 steel/1N Na_2SO_4. This range of B values was the result of a series of 'round robin' tests performed at various laboratories that employed the polarisation resistance test.
Yasuda et al. (Yasuda, et al, 1987) used 45 and 165 mV/decade as an estimate of β_a and β_c, respectively, in 30% and 50% NaOH solutions. This gives a B value of 15.4 mV.

A2.2.3.2. Galvanostatic pulse technique (GP)

The galvanostatic pulse technique has been studied by many researchers as a technique to measure the corrosion rate of steel reinforcements in concrete structures (Clear, 1989; Elsener, et al, 1997; Frølund, et al, 2002; Elsener, 2005; Feliu, et al, 2005; Song and Saraswathy, 2007; Poursaee, 2007; Vagn Nygaard, 2008; Poursaee, 2010). And, over the past years, portable instruments based on the galvanostatic pulse technique have been developed commercially (e.g. the GalvaPulse system) to perform on-site corrosion rate measurements (Poursaee, 2007; GI, 2010).

In the galvanostatic pulse technique, a short time anodic current pulse is imposed galvanostatically on the reinforcement form a counter electrode placed on the concrete

surface. The applied current is usually in the range of 5 to 400 µA and the typical pulse duration is between 5 to 10 seconds. The reinforcement is anodically polarised compared to its free corrosion potential. The resulting potential change of the reinforcement is recorded as a function of polarisation time using a reference electrode, which is also located on the surface of the concrete. A typical potential response for a corroding reinforcement is shown in Figure A2-4.

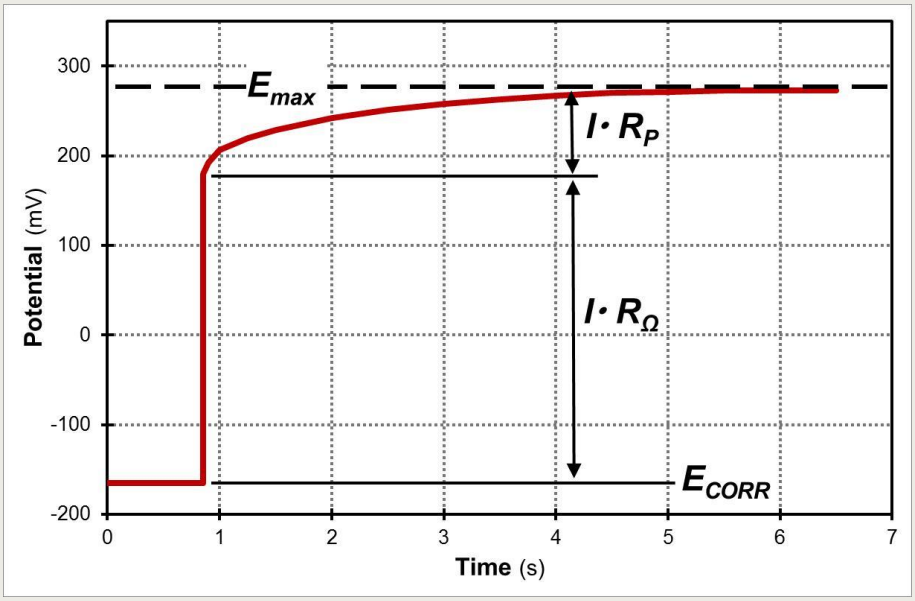

Figure A2-4. Schematic illustration of galvanostatic pulse measurement results (source: adapted from [GI, 2010]).

When a current is applied to the system, there is an ohmic potential drop, $I \cdot R_\Omega$, as well as a change in potential due to polarisation of the reinforcement, $I \cdot R_p$. The potential response of the reinforcement, $V_t(t)$, at a given time t can be expressed as (Frølund, et al, 2002; Elsener, 2005; Song and Saraswathy, 2007; Poursaee, 2007; GI, 2010):

$$V_t(t) = I_{app} \times \left[R_p \times \left(1 - e^{\left(\frac{-t}{R_p \cdot C_{dl}} \right)} \right) + R_\Omega \right] \qquad \text{(eq. A2-7)}$$

where R_p is the polarisation resistance, C_{dl} is the double layer capacitance and R_Ω is the ohmic resistance.

The values of R_p, C_{dl} and R_Ω can be determined by applying an appropriate fitting procedure (linear or exponential) of the resulting potential-time curve (Figure A2-4) and extrapolation of the fitted potential response $V_t(t)$ either to time zero or infinity.

After the polarisation resistance, R_p, has been calculated by means of this analysis, the corrosion current density can be calculated from the Stern-Geary equation (A2-6).

The corrosion rate can then be calculated from i_{CORR} using equation (A2-2) (or the simplified equation (A2-4) for the corrosion of steel).

A2.2.3.3. Electrochemical impedance spectroscopy (EIS)

Electrochemical impedance spectroscopy (EIS) is a non-destructive technique that has gained an increasing interest over the last two decades in the investigation of the corrosion behaviour of reinforced steel in concrete (Alonso and Andrade, 1988; Lemoine, et al, 1990; Wenger and Galland, 1990; Sagoe-Crentsil, et al, 1992a; Sagoe and Crentsil, et al, 1992b;

Hachani, et al, 1992; Hachani, et al, 1994; Macdonald, et al, 1994; Gu, et al, 1997; Gu and Beaudoin, 1998; Montemor, et al, 2000; Dhoubi, et al 2002; Ismail and Ohtsu, 2005; Ismail and Ohtsu, 2006). EIS can provide information related to corrosion rate estimation, but it may also give complementary information on the corrosion process, the chemical-physical and dielectric properties of the concrete, the characteristics of the passivating film, detection of localised corrosion, the degree of protection provided by coatings, … (Song and Shayan, 2000; Song and Saraswathy, 2007; Poursaee, 2007).

Basic principle

In the techniques described in previous sections (TP, LPR, GP), a DC (Direct current) potential is applied to the corrosion cell, the resulting current is measured and the resistance (R_p), from which the corrosion rate can finally be calculated, is computed.
In the EIS technique, an AC (Alternation Current)[p] potential with varying frequencies is applied to the corrosion cell and the induced current response is measured. The AC equivalent of resistance is called the impedance (Mohamed, 2009; PAR, 2010a).
The impedance, which is a complex quantity, is measured over a wide range of frequencies[q]. An AC potential perturbation is applied to the working electrode over a range of frequencies and the resulting current response of the electrochemical system is measured. The system's impedance is calculated by analysing the response signal at each frequency (PAR, 2010a). The impedance data can be graphically represented (Nyquist plot; Bode plots). The plot has to be modelled and fitted with an appropriate equivalent electrical circuit that is representative of the ongoing electrochemical processes at the interface (Mohamed, 2009). The value of various parameters (e.g. solution resistance, double layer capacitance, polarisation resistance) can then be determined by applying a fitting procedure (a non-linear least squares fitting, NLLS, algorithm is often used) that provides the best agreement between the measured spectrum (i.e. the plot) and the model's impedance spectrum (i.e. the equivalent electrical circuit) (Gamry, 2010a).

After the polarisation resistance, R_p, has been calculated by means of this analysis, the corrosion current density can be calculated from the Stern-Geary equation (A2-6). Note that i_{CORR} determination in equation (A2-6) requires the knowledge of B_a and B_c, which are not obtained from an impedance experiment.

The corrosion rate can then be calculated from i_{CORR} using equation (A2-2) (or the simplified equation (A2-4) for the corrosion of steel).

The main advantage of the EIS technique is that the amplitude of the excitation signal is very small, generally in the range of 5 to 10 mV peak-to-peak, so that the corrosion system under study (the steel, attached corrosion products or absorbed species) is minimally perturbed (Mendoza, 2003; Song and Saraswathy, 2007).

---

[p] Alternation Current that changes its magnitude and direction with time according to a certain function, *i.e.* sinusoidal function.

[q] The general principle of EIS is based on the fact that corrosion of steel in concrete usually consists of several different individual processes. These processes have different rates at a given potential, and their responses to a changing potential are also different. These responses are generated by the electrochemical reactions at the surface of the steel, as well as other relevant processes within the concrete. A process can generate a significant current fluctuation in response to a changing potential, only if the rate of the process matches the changing rate of the applied potential. Therefore, if a series of small AC potentials with different frequencies, from 0 to ∞, are applied to the reinforced concrete, then the current responses of the individual processes involved in the corrosion of the reinforcement would be strongly displayed in different frequency ranges. By analysing these responses in the frequency domain, the individual processes involved may be deduced and studied (Song and Shayan, 2000).

AC circuit theory

In DC theory, the electrical resistance, *R*, is defined by Ohm's Law as the ratio between voltage, *E*, and current, *I* (Ahmad, 2006; Gamry, 2010a):

$$R = \frac{E}{I} \qquad \text{(eq. A2-8)}$$

Unfortunately, this relationship (equation (A2-8)) is only applicable for the *ideal resistor*. In reality, however, the circuit elements exhibit a much more complex behaviour. Therefore, a more general circuit parameter, *the impedance* (*Z*), is used (Gamry, 2010a).

DC theory can, in fact, be viewed as a special case of the AC theory where the frequency equals 0 Hz (Poursaee, 2007; PAR, 2010a)

The electrochemical impedance is usually measured by applying an AC potential to an electrochemical cell at a number of discrete frequencies (ω) and then measuring the current through the cell. Assuming that a sinusoidal potential excitation is applied, the resulting current response will exhibit a sinusoidal response at the same frequency but shifted in phase (φ) (see Figure A2-5) (GAMRY, 2010a).

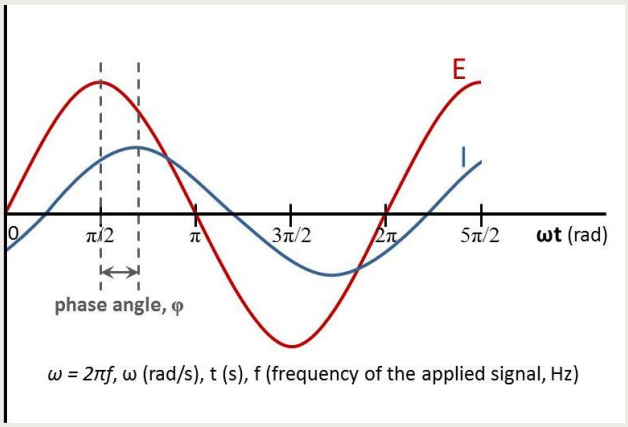

Figure A2-5. Applied potential and resultant external current relative to the electrochemical impedance spectroscopy method (source: adapted from [Stansbury and Buchanan, 2000]).

The excitation signal, expressed as a function of time, has the form (Gamry, 2010a):

$$E_t = E_0 \sin(\omega t) \qquad \text{(eq. A2-9)}$$

where E_t is the potential at time t, E_0 is the amplitude of the signal and ω is the radial frequency.

The relationship between radial frequency, ω (expressed in radians/second), and frequency, *f* (expressed in hertz) is (Gamry, 2010a):

$$\omega = 2\pi f \qquad \text{(eq. A2-10)}$$

In a linear system, the response signal, I_t, is shifted in phase (φ) and has a different amplitude, I_0 (Gamry, 2010a):

$$I_t = I_0 \sin(\omega t + \varphi) \qquad \text{(eq. A2-11)}$$

An expression analogous to Ohm's Law allows us to calculate the impedance of the system as (Gamry, 2010a):

$$Z = \frac{E_t}{I_t} = \frac{E_0 \sin(\omega t)}{I_0 \sin(\omega t + \varphi)} = Z_0 \frac{\sin(\omega t)}{\sin(\omega t + \varphi)} \qquad \text{(eq. A2-12)}$$

The impedance is therefore expressed in terms of a magnitude, Z_0, and a phase shift, φ.

AC currents and potentials are vector quantities (Gamry, 2010a):

$$E_t = E_0 \cdot e^{j\omega t} \quad \text{(eq. A2-13)}$$

$$I_t = I_0 \cdot e^{(j\omega t - \varphi)} \quad \text{(eq. A2-14)}$$

The impedance can then be represented as a complex number with real and imaginary components whose values are frequency dependent (Kelly, et al, 2003; Mohamed, 2009; Gamry, 2010a):

$$Z(\omega) = Z'(\omega) + jZ''(\omega) = \frac{E_t(\omega)}{I_t(\omega)} = Z_0 \cdot e^{j\varphi} = Z_0(\cos\varphi + j\sin\varphi) \quad \text{(eq. A2-15)}$$

where *j* is the imaginary number, given by the square root of (-1)[r].

The magnitude and phase shift of the impedance are then defined by (Kelly, et al, 2003; Poursaee, 2007):

$$|Z_0| = \sqrt{Z'(\omega)^2 + Z''(\omega)^2} \quad \text{(eq. A2-16)}$$

$$\varphi = \tan^{-1}\left(\frac{Z''(\omega)}{Z'(\omega)}\right) \quad \text{(eq. A2-17)}$$

Data presentation

EIS data can be presented in different formats. The most common plots to illustrate the response of an electrochemical system to an applied AC signal are the *Nyquist plot* and the *Bode plots* (Mendoza, 2003; Poursaee, 2007; Mohamed, 2009; Gamry, 2010a):

- the expression for the impedance, Z, is composed of a real and an imaginary part. If the real part (ReZ) is plotted on the X-axis and the imaginary part (ImZ) is plotted on the Y-axis of a chart, we get a *Nyquist plot* (see Figure A2-6**(a)**). The impedance is represented as a vector (arrow) of length |Z| and the angle between this vector and the X-axis, commonly called the phase shift, φ (=arg Z). Each point on the Nyquist plot represents the impedance at a particular frequency. However, the value of that frequency cannot be extracted from the plot. Low frequency data are on the right side of the plot and higher frequencies are on the left;
- another frequently used format is the Bode plot (see Figure A2-6**(b)**). The Bode plot can be separated into a magnitude plot and a phase plot. The data are plotted with the logarithm of frequency on the X-axis and both the logarithm of the absolute value of the impedance, |Z|, and the phase shift, φ, on the Y-axis. These plots provide information on the dependence of impedance to the frequency;

Equivalent electrical circuit fitting

EIS data is commonly analysed by fitting it to an equivalent electrical circuit model. An equivalent electrical circuit is actually a dummy circuit, consisting of some electronic dummy components, that has the same current or potential response, to a small amplitude of potential or current stimulation, as the corrosion system. For the model to be representative of the ongoing electrochemical processes occurring at the interface, the elements in the model should have a basis in the physical electrochemistry of the system (Song and Shayan, 2000; Mohamed, 2009; Gamry, 2010a).

Both the resistance (used in DC theory) and impedance (used in AC theory) are described as a measure of the ability of a circuit element to resist the flow of electrical current or

[r] mathematicians use *i* to stand for $\sqrt{-1}$, but electrochemists use *j* to avoid confusion with *i*, the symbol for current (Poursaee, 2007).

electrons (Gamry, 2010a). In an electrochemical cell, various processes can impede the flow of electrons, such as slow electrode kinetics, slow preceding chemical reactions and diffusion. In an electrical circuit, these processes are considered to be analogous to resistors, capacitors and inductors, respectively. In DC circuits, only resistors produce this effect, while in AC circuits, capacitors and inductors also impede the flow of electrons (PAR, 2010a).

Resistors, capacitors and inductors, each of which stands for some particular process of the corrosion system, are therefore commonly used as electrical elements to compose the equivalent electrical circuit. Table A2-1 lists the common circuit elements, together with the equation for their impedance (Song and Shayan, 2000; Mohamed, 2009; Gamry, 2010a).

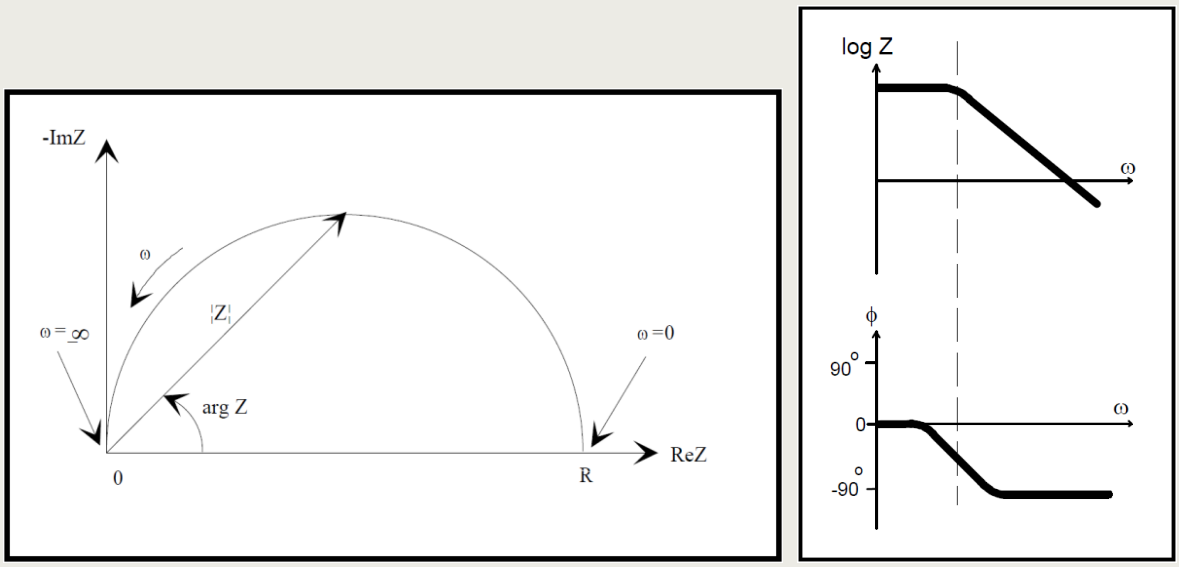

(a) **(b)**

Figure A2-6. Schematic illustration of the response of a simple electrochemical system (GAMRY, 2010a).
(a) Nyquist plot.
(b) Bode plots.

Table A2-1. Circuit elements, together with their impedance expression, used in EIS (Scully, 1995; Kelly, et al, 2003; Poursaee, 2007; Gamry, 2010a).

Component	resistor, *R*	capacitor, *C*	inductor, *L*	Warburg element, *W*	constant phase element, *CPE*
impedance	R	$\frac{-j}{\omega C}$	$j\omega L$	$\frac{1}{Y_0\sqrt{(j\omega)}}$	$\frac{1}{Y_0(j\omega)^{\alpha}}$

The different equivalent circuit models that have been adopted to simulate the electrochemical corrosion processes of steel in concrete are listed in Figure A2-7.

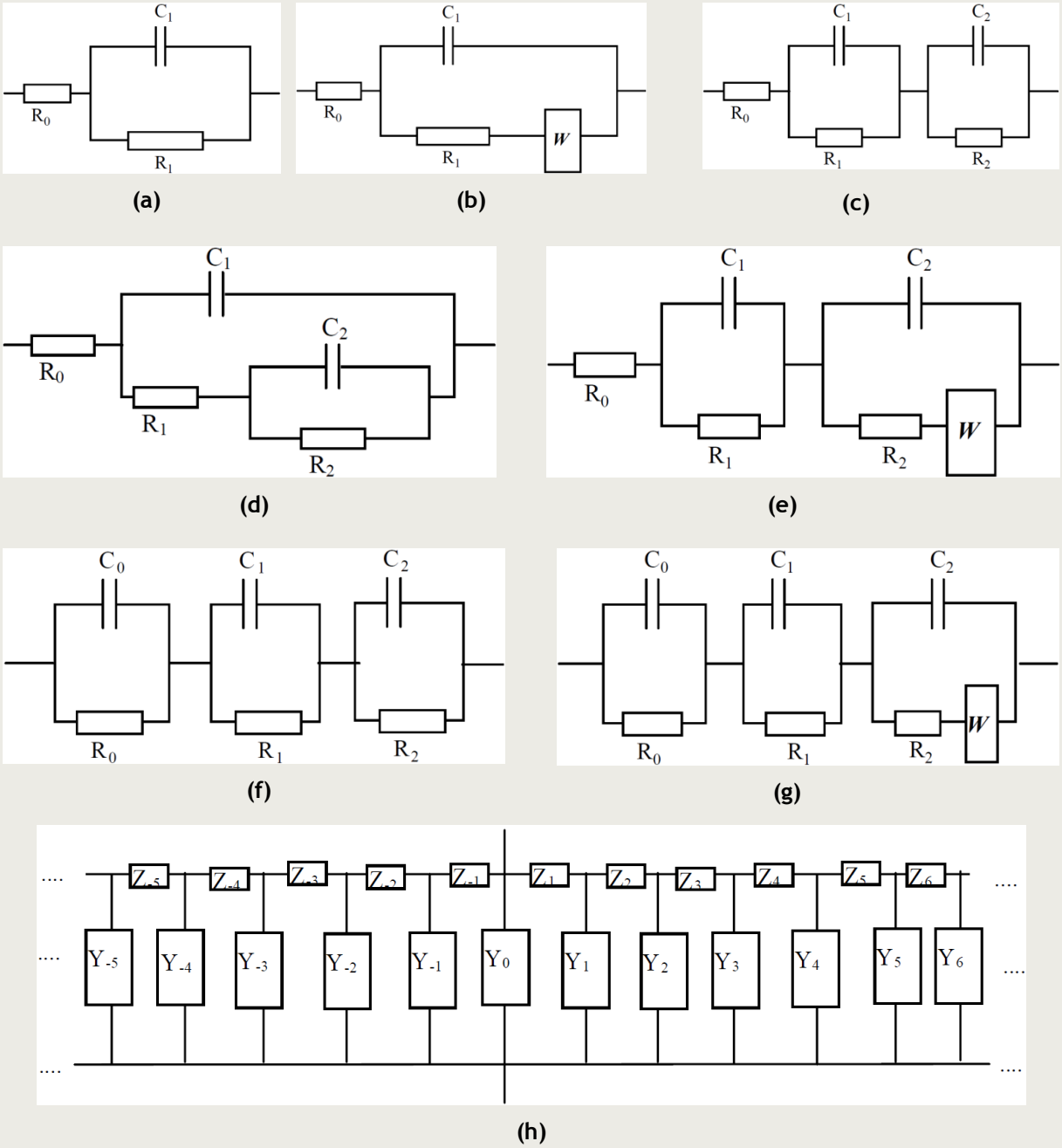

Figure A2-7. Different equivalent circuit models used to simulate the electrochemical corrosion processes of steel in concrete (source: adapted from [Song and Shayan, 2000]).

(a) One-time-constant circuit (McCarter and Brousseau, 1990; Sagues, et al, 1995, Thompson, et al,, 1988; Thompson and Lawson, 1991; Bertocci, 1997);

(b) One-time-constant with a diffusion (Warburg) element (Hope, et al, 1986; Thompson et al, 1988; Thompson and Lawson, 1991; Bertocci, 1997);

(c) Two-time-constant circuit, series connection (Christensen, et al, 1992; Christensen, et al, 1994; Aperador, et al, 2009);

(d) Two-time-constant circuit, inclusive connection (Wenger, et al, 1980; Wenger, et al, 1985; Hachani, et al, 1992; Hachani, et al, 1994; Bertocci, 1997);

(e) Two-time-constant circuit with a diffusion (Warburg) element (McCarter and Brousseau, 1990; John, et al, 1981; Newton, et al, 1988);

(f) Three-time-constant circuit Newton, et al, 1988; Gu, et al, 1996);

(g) Three-time-constant circuit with a diffusion (Warburg) element (Lay, et al, 1985; Sagoe-Crentsil, et al, 1992);

(h) Transmission line model (Macdonald, et al, 1988; Macdonald, et al, 1991; Macdonald, et al, 1994; Feliu, et al, 1988; Feliu, et al, 1989);

In the equivalent circuits described in Figure A2-7, each element has a physical-chemical meaning (Song and Shayan, 2000):

- Figure A2-7**(a)** is the simplest equivalent circuit and it is called the *Simplified Randles Circuit*: R_0-concrete resistance; R_1-polarisation resistance of the reinforcement; C_1-double layer capacitance between the reinforcement and concrete;
- Figure A2-7**(b)** is called the *Randles Circuit*: R_0, R_1 and C_1 have similar meanings to those in Figure A2-7**(a)**; W-Warburg impedance due to diffusion-controlled transport of oxygen in the concrete;
- Figure A2-7**(c)** shows the series connection configuration of a two-time-constant circuit: R_0 has no meaning (only used for the purpose of calculation of other parameters); R_1-concrete resistance; C_1-capacitance of concrete; R_2-polarisation resistance of the reinforcement; C_2-double layer capacitance;
- Figure A2-7**(d)** shows the inclusive connection configuration of a two-time-constant circuit: R_0, R_1 and C_1 have similar meanings to those ion Figure A2-7**(a)**. The part $C_2||R_2$, corresponding to the second time constant, usually becomes significant when the impedance of the reinforcement is low;
- Figure A2-7**(e)**: R_0-concrete resistance; R_1-interfacial resistance; C_1-interfacial capacitance; R_2-polarisation resistance; C_2-double layer capacitance; W-Warburg diffusion impedance;
- Figure A2-7**(f)**: R_0-concrete resistance; C_0-capacitance of concrete; R_1-resistance of the steel/concrete interfacial film; C_1-capacitance of the steel/concrete interfacial film; R_2-polarisation resistance of the steel rebar; C_2-double layer capacitance of the steel surface;
- Figure A2-7**(g)**: R_0, C_0, R_1, C_1, R_2 and C_2 have similar meanings to those in Figure A2-7**(f)**; W-Warburg diffusion impedance;
- Figure A2-7**(h)**: Z_i-the impedance of concrete per unit volume; Y_j-the electrochemical impedance of the interface between the concrete and steel reinforcement per unit length; Y_j is commonly assumed as one of the above equivalent circuits or their combination;

Among all of the above equivalent circuits, it seems that those represented by Figure A2-7**(g)** and Figure A2-7**(h)** are the most reasonable. The former theoretically simulates most of the important processes involved in the reinforced concrete system at a micro-scale. The latter realistically considers the influence of spatial distribution of electrochemical processes in reinforced concrete at a macro-scale (Song and Shayan, 2000).

A2.2.3.4. Electrochemical noise technique (EN)

Electrochemical noise (EN) is a non-destructive technique that has recently emerged as a promising tool for studying a wide variety of corrosion systems, such as active and passive corrosion, pitting and crevice corrosion in passive films, metastable pitting, stress corrosion cracking, as well as for the measurement of uniform corrosion rates, the evaluation of inhibitors and coatings and monitoring of corrosion of reinforced concrete structures (Hladky and Dawson, 1981; Bertocci, et al, 1983; Gabrielli, et al, 1985; Cottis and Loto, 1990; Gabrielli and Keddam, 1992; Legat and Govekar, 1994; Legat and Doleček, 1995; Bertocci, 1996; Bertocci, et al, 1997b; Lee and Mansfeld, 1998; Mansfeld, et al, 1998; Tallman, et al, 1998; Gowers and Millard, 1999; Bierwagen, et al, 2000; Leban, et al, 2000; Mansfeld, et al, 2000; Song and Shayan, 2000; Mansfeld, et al, 2001; Zhou, et al, 2002; Legat, et al., 2004; Mojica, et al., 2004; Pujar, et al., 2007; Song and Saraswathy, 2007; Gamry, 2010b).

The author's intent of this chapter is only to present to the reader a brief description of the measurement method and the different approaches that have been used for the analysis and interpretation of EN data. More detailed information on the EN technique can be found in (Eden and Rothwell, 1992; Bertocci and Huet, 1995; Cottis and Turgoose, 1995; Bertocci, 1996; Dawson, 1983; Dawson, 1996; Bertocci, et al, 1997a; Eden, 1998; Cottis and Turgoose, 1999; Roberge, et al, 2000; Cottis, 2001; Perdomo and Singh, 2002; Huet, 2006; Cottis, 2008).

EN refers to the spontaneous fluctuations in electrochemical potential and corrosion current that occur on a metal's surface during corrosion. Electrochemical potential is related to the driving force (thermodynamics) of the reaction, while corrosion current is related to the rate of reaction (kinetics) of the reaction. The idea behind EN is that random electrochemical events on the surface of a corroding metal generate noise in the overall potential and current signals. The principle of the EN technique is based on measuring this noise (potential and current fluctuations) (Song and Shayan, 2000; Holcomb, et al, 2001; Mendoza, 2003).
In the EN technique, the potential and/or current fluctuations of a working electrode are measured under freely corroding conditions, *i.e.* that no external perturbation of the current or potential is applied. Therefore, the characteristics of electrochemical noise is only influenced by the corrosion process (*e.g.* type and rate of corrosion) (Song and Shayan, 2000; Holcomb, et al, 2001; Mendoza, 2003).

The standard method for measuring the electrochemical potential or current noise generally involves measuring the fluctuation in potential or current difference between a working electrode and a reference electrode or between two nominally identical working electrodes coupled through a zero resistance ammeter (ZRA). By using ZRA, the galvanic coupling current between these two electrodes can be measured while the coupled electrodes are maintained with negligible potential difference (Cottis and Turgoose, 1995; Cottis, 2001).

The output of an EN measurement is a curve of potential or current fluctuation in the time domain. Analysis methods for electrochemical noise data can be separated into three categories (Cottis and Turgoose, 1999; Song and Shayan, 2000; Bullard, et al, 2002; Zhou, et al, 2002; Kelly, et al., 2003; Mendoza, 2003):

- *deterministic*. The simplest approach to data analysis is to examine the time record(s) for features that are characteristic of particular types of corrosion. The shape of the transients can already provide a limited insight in the type of corrosion, *e.g.* when general corrosion is occurring on the metal surface, the electrochemical noise has a relatively smooth appearance, whereas when pits begin to form and propagate, occasional sharp increases and decreases in the amplitude of both the potential and current noise data can be observed (Cottis and Turgoose, 1999; Bullard, et al, 2002].
- *statistical*. The recorded potential or current difference signals (in the time domain) are treated as statistical fluctuations about a mean level. Several statistical parameters can be obtained. Among these parameters are the noise resistance and the localisation index.
  The noise resistance, R_n, is defined as the ratio of the standard deviations of the potential and current noise fluctuations and is given by the following relationship (Zhou, et al, 2002; Mansfeld, 2003; Mendoza, 2003; Song and Saraswathy, 2007]:

  $$R_n = \frac{\sigma V}{\sigma I} \qquad \text{(eq. A2-18)}$$

  where σV and σI are the standard deviation of the potential and current fluctuations, respectively. Eden et al. (Eden, et al, 1986) and Chen and Skerry (Chen and Skerry, 1991) suggested that R_n is related to the polarisation resistance, R_p, that was commonly

determined by linear polarisation techniques or electrochemical impedance spectroscopy (EIS). Initially, R_n was thought to be equivalent to R_p (Cottis, 2001; Mansfeld, 2003) and hence the value of R_n could be used to calculate the corrosion current density (from the Stern-Geary equation (A2-6)) and the corrosion rate (from equation (A2-2), or the simplified equation (A2-4) for the corrosion of steel). It was found later that, in reality, R_n was not always equal to R_p but rather that R_n was related to R_p indirectly (Zhou, et al, 2002). Mansfeld (Mansfeld, et al, 2000) and Lee (Lee, et al, 1998) have determined that for passive systems, R_n can deviate significantly (up to several orders of magnitude) from R_p. Moreover, Mansfeld (Mansfeld, et al, 1998) has found that R_n is close to R_p only in those cases where the impedance is independent of frequency within Δf.
The localisation index, *LI*, which is derived from the ratio of the standard deviation of the current to the root mean square (rms) of the current ($LI = \frac{\sigma I}{I_{rms}}$), is a parameter that can give information on the type of corrosion. *LI* ranges from 10^{-3} for general corrosion to 1 for localised corrosion (Holcomb, et al, 2001; Bullard, et al, 2002; Perdomo and Singh, 2002; Song and Saraswathy, 2007).

- *spectral*. In spectral analysis, first the noise signal is converted from the time domain into a frequency equivalent by means of either a fast Fourier transform (FFT) algorithm or the maximum entropy method (MEM). So, every time domain function has a counterpart in the frequency domain. This counterpart function is called the power spectral density (PSD), that is, the distribution of the power of the signal in the frequency domain. The value of the slope of the amplitude-frequency plots is indicative for the type of corrosion taking place (Perdomo and Singh, 2002; Kelly, et al, 2003; Pujar, et al., 2007; Song and Saraswathy, 2007).

A2.2.4. Corrosion rate calculated from passive current density (i_{PASS}) measurements (PCD)

A2.2.4.1. i_{PASS} determinined from polarisation curves

Figure A2-1 shows a typical polarisation curve for a passivating metal. Such a polarisation curve can yield important information such as

- the potential region over which the metal remains passive;
- the corrosion rate in the passive region;

Carbon steel exposed to high pH environments, such as concrete, is known to passivate (see section 2.2). Under these conditions, carbon steel will adopt an open-circuit potential within the passive region. The passive current density can therefore be used as a measure of its corrosion rate.

Polarisation curves can be obtained potentiodynamically or potentiostatically:

- a potentiodynamic polarisation curve is obtained by continuously changing the potential at a constant rate (a typical scan rate of 0.167 mV/s is used). This technique is described in more detail in section A2.2.1.;
- a potentiostatic polarisation curve is obtained by changing the potential stepwise after the current has reached a steady-state value or after a predetermined time has elapsed. This technique is extremely time-consuming and expensive;

Blackwood et al. (Blackwood, et al, 2002) adopted a variant technique to determine the passive current density. The electrode potential was increased continuously at a constant scan rate such as in the potentiodynamic method up to a holding potential close to the oxygen reduction potential.

A2.2.4.2. i_{PASS} measured potentiostatically under steady-state conditions

In this technique, the current density is continuously recorded while holding the sample at a constant applied potential, which is situated within the passive region. The current density needs to be recorded sufficiently long (typically in the order of several years) to ensure that steady-state conditions have been reached.

A2.3. Quantification of hydrogen gas evolving from the corrosion of steel

The quantification of hydrogen gas evolving from the anaerobic corrosion of steel can be determined in the following ways:

- volumetric gas measurement method (gas cell technique). In this technique, the uniform corrosion rate is correlated with the amount of hydrogen gas evolving from the corrosion of the steel, which is measured through the displacement of a column of liquid;
- gas chromatography/mass spectrometry. This technique requires an inert gas stream to flow through a sealed cell over the test medium that contains the corroding steel. Hydrogen gas, evolving from the corrosion reactions, is entrained in the inert gas, which is then carried to, and quantified in, either a gas chromatograph or a mass spectrometer;
- hydrogen-sensitive probes incorporated in the test cells;

A2.4. Corrosion rate estimated from archaeological artefacts

Neff et al. (Neff, et al, 2006; Neff, et al, 2007) outline a procedure for estimating corrosion rates from archaeological artefacts and report the results of measurements on ~40 objects from five different sites. The minimum corrosion rate was estimated from the amount of precipitated corrosion products by dividing the thickness of the corrosion product layer by the exposure period and a correction factor to account for the difference in density between the underlying metal and corrosion product. The maximum corrosion rate is estimated by adding an amount to account for the advective-diffusive loss of soluble corrosion products estimated by multiplying a fraction of the annual precipitation at the site by the solubility of the corrosion product (King, 2008).

Yoshikawa et al. (Yoshikawa, et al, 2003; Yoshikawa, et al, 2008) reported corrosion rates from a study of ~1,000 artefacts from a 1,500-year-old site in Japan. The authors used an X-ray computer tomography technique to non-destructively map density differences in encrusted corrosion products, from which the location of the metal/oxide interface was estimated and a corrosion layer thickness inferred. The reduction in thickness of the original material is then calculated from the corrosion layer thickness by using a conversion factor that takes into account the ratio of the iron content of the different components present in the rust layer. A 1 mm thickness of rust is considered equal to 0.35 or 0.14 mm thickness of iron metal when the rust component is assumed to be due to magnetite or goethite, respectively (King, 2008).

OPERA
Meer informatie:

Postadres
Postbus 202
4380 AE Vlissingen

T 0113-616 666
F 0113-616 650
E info@covra.nl

www.covra.nl